Roskilde Universitet

Study of Swelling Response Variation in Homopolymer Thin Films during SVA

Jonathan Gow

Master's Thesis Project Report

Roskilde Universitet (RUC)

Project Supervisor: Dorthe Posselt

Contents

Summary

The goal of this project is to find relationships between the properties of homopolymer thin films and the swelling behavior of the films during Solvent Vapor Annealing (SVA). Solvent sorption and desorption in thin films is governed by interaction parameters which are not well determined. Testing of samples which vary over a single parameter is used to determine their correlation with specific features of swelling behavior.

I developed and implemented a simplified program for consistent solvent vapor introduction with precise timings and smooth swelling response for a specific polymer-solvent pair, Polystyrene and Toluene. Evaluation of the program consisted of tests on polymers ranging in molar mass from 1.8 to 6000 kg/mol, and film thicknesses ranging from as low as 40nm up to 260nm. The swelling kinetics and optical properties are recorded as a function of time, and correlated across the range of samples.

Features of the swelling response include identification of the Glass Transition, distinct solvent sorption hysteresis around the Glass Transition, variation in the maximum equilibrium swelling position, and early characterization of signs of de-wetting. Also discussed is the effects of thermal annealing prior to SVA.

The Fresnel equations describing interfaces of optical media are used to characterize the swelling response, and for qualitative description of the film surface uniformity.

The Flory-Huggins model of polymer melts is analyzed and evaluated as a quantitative predictor of thin-film swelling. Deviations from the model are identified, quantified, and given physical interpretations.

Iterative development of the annealing procedure and analysis methods has improved reliability and quantified parameters relevant to the methodology that were previously unknown or misunderstood. This includes demonstration of swelling dependent index of refraction for thin films, and solvent concentration dependent index of refraction for the carrier gas.

It is found that the polymers show no variation in Glass Transition temperature as a result of being confined to thin film geometries in this thickness range. While maximum swelling ratio of the films does vary, it does not show correlation with the thickness.

It is found that the Glass Transition temperature of polymers as a function of their molar mass is not affected by being constrained to a thin film. The same functional relationship to the Fox equation is maintained for all samples.

1 Introduction

Polymers constrained to thin films have the potential for self-assembly into nano-structures with periodic patterns, long-range ordering, mechanical stability, and uniform size and orientation. Increasing effort is being dedicated to apply polymer self-assembly kinetics to form unique materials, beyond the resolution limit of state-of-the-art UV photolithography, and enabling a range of new chemical, optical, and biological functions for nano-manufacturing [Cummins et al., 2020; Efremov and Nealey, 2022; Hulkkonen et al., 2019; Kim et al., 2010; Nelson et al., 2018; Yang et al., 2022]. The nano-structures can be tuned to desirable sizes and orientations by choice of polymer constituents and molecular weight. Directed Self-Assembly of polymers is seen as a promising nano-scale fabrication tool for ultra-small semiconductor devices, both for its high feature density and large area parallel formation, which clearly contrasts the sophisticated processing steps of typical silicon manufacturing. Outside of electronic nanotechnology, implementation of polymer films is also gaining popularity for filtration membranes, protective surface coatings, optical meta-materials and anti-reflective coatings, photovoltaics, and more [Castel et al., 2020; Cummins et al., 2020; Ghori and Conway, 2015; Yang et al., 2022].

When initially cast from solutions, the polymer thin films are frozen in dis-ordered and irregular patterns, trapped far from their equilibrium structure [Efremov and Nealey, 2022]. Annealing of the film is necessary to enable phase separation, formation of regular structures, and minimize defects. Techniques for promoting specific ordering of polymer patterns and elimination of defects include chemical or topographical treatments of the substrate surface [Nelson et al., 2018]. The removal of defects remains a challenging component for implementation in semiconductor processing, but many other emerging polymer technologies have higher defect tolerances [Cummins et al., 2020].

A variety of approaches for ordering polymer thin films have been developed, including thermal annealing, electric field alignment, surface energy/geometry adjustment, and others. But the most promising of these techniques is Solvent Vapor Annealing (SVA), because it is able to avoid the time-intensive and high-cost problems from iterative lithography of substrate priming methods, and avoids any heat degradation or problematic chemical interactions which cause trouble in thermal annealing [Efremov and Nealey, 2022; Hulkkonen et al., 2019; Nelson et al., 2018]. In spite of these benefits, SVA has not yet reached wide-spread implementation due to lack of methodology standardization and reproducibility of results. SVA enables the thin film to anneal by diffusing solvent into the polymer and dramatically increasing its mobility. The solvent molecules cause the film to swell, and the mobility afforded to the polymers enable them to kinetically anneal to their thermodynamic equilibrium configuration. Upon the removal of solvent the polymer de-swells, hardening into place with its annealed structure.

While many of the most intriguing applications apply to block copolymers and other complex polymer types, the number of experimental parameters which affect the annealing results overwhelms the ability to establish reliable methodology [Efremov and Nealey, 2022]. Homo-polymers are

simplistic in comparison, with a far smaller set of parameters. Concurrently, many factors about the SVA process are still not well understood, and more basic investigation on the interaction between Solvent and Polymer in Thin Films should be conducted. This project adds to the field by studying Solvent Vapor Annealing of Homo-Polymers, as a simplified model of the annealing process for co-polymers. The goal is to provide knowledge specific to SVA, without the many complicating aspects of copolymer dynamics.

1.1 Swelling Response Variability - Motivation

Significant variation is observed in the equilibrium swelling thickness of thin-films during Solvent Vapor Annealing; the amount of swelling shows a non-linear dependence on solvent concentration. The observed result is a huge increase in swelling at the maximum concentration of solvent. This behavior has been observed for multiple polymers and with multiple solvents. An example is shown in Figure 1.1 below; a large increase in swelling response occurs at the maximum solvent vapor concentration.

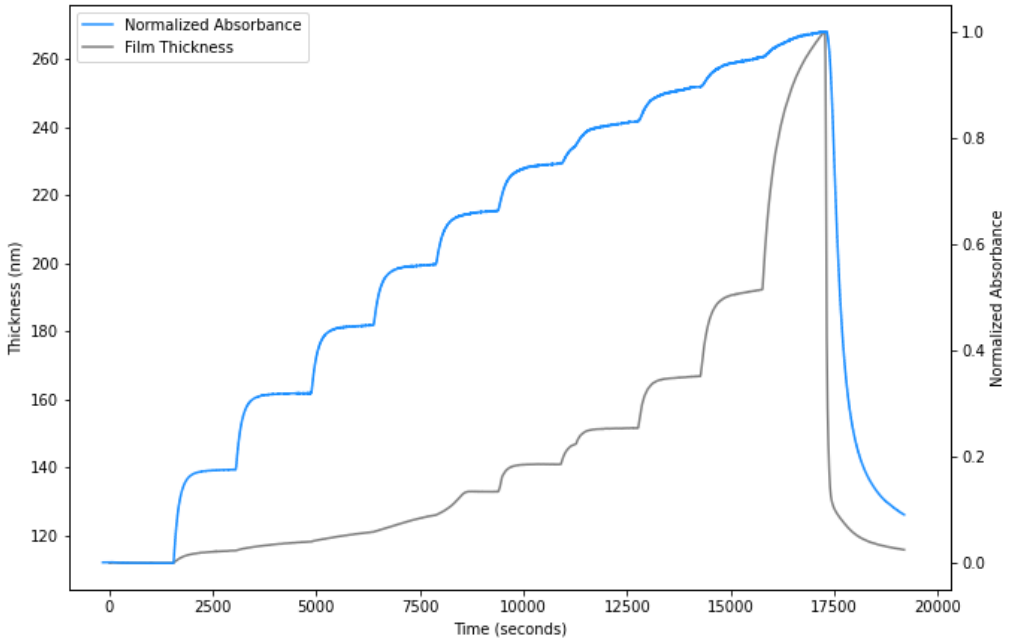

Figure 1.1: Swelling Response of Polystyrene thin film (grey), and Normalized Absorbance (blue). The film thickness data is fitted from the reflectance model, and shows extreme increase at maximum solvent pressure. The Absorbance measurement is based on UV diode transmission through the exhaust gas, and corresponds directly to the solvent vapor concentration.

The initial motivation of this project is to investigate this change in swelling response, and to better understand its dependence on other variable factors of SVA. More specifically, these questions motivate the research for this project:

- How does the initial thickness of the polymer film impact the swelling response during SVA?
- How does the polymer length (or molar mass) impact the swelling response during SVA?
- What is the extent of the swelling/de-swelling hysteresis?

Some additional questions which interest me but are not the main focus of the study are:

- How does the solvent swelling change the film's optical properties, primarily index of refraction? And how might it change the optical properties of the vapor-carrying gas?
- What is the maximum rate of swelling that can be achieved, while maintaining repeatability?
- Can microscope images help us to understand the interaction between polymer film and substrate? (eg. de-wetting)

To investigate these questions I performed 22 SVA tests on thin film samples chosen for their variety in film thickness and molar masses. Each sample was individually fabricated, imaged, annealed, and the data analyzed for a comprehensive approach to all aspects of SVA. Data Analysis tools and fitting methods were specially designed to match the SVA equipment and procedure. The Flory-Huggins solution theory for polymer melts is quantitatively compared with the SVA measurements. Where the model behavior deviates from the measured behavior, I attempt to make reasonable physical interpretations specific to the thin film geometry and annealing choices. I was not able to dedicate much time to understanding the de-wetting of films, but it is mentioned on several occasions and presented as a topic for future research.

2 Theoretical Background

2.1 Glass Transition and other Polymer Dynamics

Polymers constrained to a thin film necessarily exhibit more complex dynamics than those in bulk. However, it is helpful to start with some discussion of polymers in general and some of the very well researched aspects of their bulk properties.

A distinction should be made between homopolymers and copolymers. All polymers are macromolecules formed by covalent bonding of individual molecule specie (monomers) into long chains. The name 'homopolymer' simply indicates that the polymer is comprised of a single species of monomer. Copolymers are then polymers with at least 2 species of monomer, and this difference allows for far more complexity. The sequential arrangement of species in the polymer chain can take many forms. The arrangement may be randomized, or perfectly alternating / periodic. The name 'Block' copolymer indicates a linear arrangement with entire regions (blocks) of a single monomer species. Furthermore, non-linear assemblies with branches, cross-linkages, and star shapes adds new dimensions to the complexity of these polymers [Brandrup et al., 1999]. The interaction energies between regions of polymer chains can influence the bulk material to form semi-crystalline structures. As mentioned in the introduction (Section 1), research on block copolymers is a source of much interest for nanotechnology, and even these linear block arrangements involve complex dynamics because of the many interaction energies between solvent, substrate, and each species of monomer. This project is limited to the use of homopolymers exclusively, because the intended focus is on the polymer-solvent interactions.

The defining characteristic of a polymer is the length. The most notable properties of polymers are direct consequences of the bonding between the monomer units into long chains which have the chance of entanglement one another: the high viscosity, long-range elasticity, high strength [Flory, 1953]. Each of these properties are highly dependent on the length of the polymer. Additionally, the structure of the bonding (linear, branching, or cross-linked) will also have a large influence on the mechanical and thermal properties: heat capacity, thermal expansion coefficient, and modulus [Li and Xiao, 2021].

All polymers also exhibit glass transition behavior, characterized by a range of temperatures over which these thermodynamic and mechanical properties of the polymer can change by many magnitudes. Below the glass transition, the polymers are said to be in a glassy state; hard, brittle, and low mobility. Above the glass transition, the polymers said to be in a rubbery state, having gained mobility and become flexible and soft. The temperature at which the glass transition occurs is denoted T_g, and it is dependent on all aspects of the polymer chemistry: length, bond-structure, added plasticizing agents, and age [Efremov and Nealey, 2022; Li and Xiao, 2021; Yoshioka and Tashiro, 2003].

2.2 Thin Films

When the polymer is cast to a thin-film, there is very little organization to their arrangement. The secondary interaction energies (from Van der Waals forces) between different polymer chains makes it energetically favorable for the polymers in the film to form regular patterns in a semi-crystalline structure [Efremov and Nealey, 2022]. This is true for most polymers, but it is especially true for block copolymers which have an energetic preference for phase separation by block species. Because the polymer is in a glassy state, it is stuck in the un-organized configuration; kinetically trapped from reaching thermodynamic equilibrium.

The nano-technology applications of block copolymers relies on the formation of structures in thin films. Getting the polymer to form and keep the desired structure is achieved by shifting the polymer above and below its glass transition. Manipulating the polymer to a rubbery state above T_g, annealing the polymer to the desired structure, and then returning the polymer to a glassy state with the structure frozen in place. With block copolymers, the nano-structure is realized by removal of a single block, either by a UV laser and photo-resist, or a chemical dissolution which is responsive to a single molecular species.

Producing even simple nano-structures will generally require a careful choice of copolymer, which is made even more complex by frequent use of one or more nano-particle additives. These additives are embedded in the structure of the polymer, often to bolster certain mechanical properties, especially as a guard against age-related degradation [Bhadauriya et al., 2018; Emad et al., 2023]. In other cases, the additives can be metals or non-organics with a distinct electromagnetic response to provide an active optical surface [Alvarez-Fernandez et al., 2021]. For the homopolymers in this project, there are no additives and there is no phase separation. When brought above the glass transition, the homopolymer is not expected to anneal to a new phase. However, some re-arrangement during annealing is still expected, as the configuration of the homopolymers is allowed to reach a thermodynamic equilibrium while in the rubbery state. When the wafer is initially spin-coated with the polymer, the rapid drying (“curing”) freezes the polymer in place without enough time to reach a thermodynamic equilibrium.

Thermal annealing is the most direct method of bringing a polymer above its glass transition, heating the polymer to increase its mobility, and allowing it to cool once it reaches thermodynamic equilibrium in the desired structure. The thermal annealing method is losing favor for most applications, as the heating can cause unintended damage to the polymers, especially for co-polymers where the heat may drive unwanted reactions between specie. Also, for particularly long polymers with extreme molecular mass, thermal annealing is still very slow. Solvent Vapor Annealing was developed as an alternative technique with far fewer defects, and several orders of magnitude faster [Nelson et al., 2018].

2.3 Solvent Vapor

As suggested by the name, in SVA the purpose of the solvent vapor is to act as a plasticizing ("annealing") agent for the otherwise glassy polymer. When introduced to the SVA chamber, the solvent vapor diffuses into the polymer film and dramatically increases the polymer chain mobility, allowing the polymers to re-configure to a thermodynamic equilibrium.

The diffusion behavior of the solvent is crucial for the annealing of the polymer thin films. A typical diffusion coefficient of small molecules in a glassy polymer is on the order of 10^{-14} $m^2\,s^{-1}$ [Castel et al., 2020; Karlsson et al., 2001]. Even with this extremely small diffusion coefficient, diffusion across a characteristic length of 100 nm is calculated to have a characteristic equilibrium time of 500 ms. Even for the thickest of films used in this project (approx. 300nm), the diffusion time scale is less than 5 seconds. These times are much less than the experimental time scale; during SVA measurements are taken every 10 seconds and changes in the solvent flow occur at most every 100 seconds.

The solvent diffusion at the interface of the film depends on the vapor pressure in the SVA chamber. Solvent is introduced to the SVA chamber from a mass flow controller pumping Nitrogen gas through a toluene bubbler. It is assumed that the gas bubbles emerge fully wet with solvent (i.e. 100% relative humidity). Additionally, the temperature control keeps the solvent bubble, gas mixer, and SVA chamber at uniform temperature (24°C), so we don't expect that the solvent vapor pressure changes from heating/cooling of the gas while in the SVA chamber. However, size of the SVA chamber means that changes in the solvent vapor concentration of the input gas flow takes time to reach equilibrium in the larger chamber. More on this in Section 3.3 regarding the measurement equipment. Because of this delay, the solvent vapor pressure of the exhaust gas is measured through other means. I want to emphasize to the reader the temperature dependence of the vapor pressure because it is an important consideration in how to measure this quantity. Even small changes in the gas temperature can affect the vapor pressure significantly. The role of solvent vapor pressure in SVA will elaborated on in Section 2.5, as a variable in Flory-Huggins solution theory.

Once the solvent has adsorbed into the thin film, its presence has several effects. First, the solvent takes up space in the thin film, causing the thickness to increase to accommodate the additional volume. This effect is the 'swelling' which can be detected by the optical reflectometry, and it is the only method of in-situ characterization of the film. The theory regarding the optical reflectometry measurements is detailed is detailed in Section 2.6. It is notable however that the change in thickness of the film is not a direct measurement of the solvent volume uptake. It is likely that the dry film contains empty free space between the long polymer chains which can be filled by the much smaller solvent molecules. For this reason it is expected that the initial diffusion of solvent may cause no change in film thickness at all. Additionally, for any mixture of 2 molecules the volume will depend on the specific packing arrangement. While the actual arrangement is certainly quite

complex, styrene monomers and toluene have similar molar volumes (both being derivatives of a single benzene ring), so I expect that the volume changes of the film will be nearly a 1:1 response to the uptake volume of the solvent.

The second notable effect of the diffused solvent presence in the film is the plasticizing of the polymer. In the context of polymers, a 'plasticizer' refers to a miscible, low molecular weight diluent, which increases the free volume in the polymer [Immergut and Mark, 1965]. By taking up space within the polymer chain, the solvent molecules lower the inter-molecular forces which are responsible for the high elasticity and viscosity of the glassy polymer. In effect, the solvent lowers the glass transition temperature T_g of the film. With sufficient solvent volume fraction, the film will have T_g lowered to room temperature and enter a rubber state, allowing the polymer enough mobility that the film will anneal. Later, when the solvent vapor is replaced with dry N_2 gas, the solvent in the film will desorp and the polymer will harden to a glassy state as the value of T_g returns to its original value. The impact of the solvent on the glass transition temperature T_g of the thin film is detailed in Section 2.4.

For the solvent to be an effective plasticizing agent, it must be well miscible with the polymer. If the relative solubility of the polymer and solvent are mismatched, the solvent vapor will not readily adsorb into the film. With less adsorbed solvent, the film will take longer to rubberize, and the decreased swelling response lowers the resolution of the measurement. For these reasons, the best choice of solvent for this project will be to match the relative solubility of polymer and solvent as closely as possible. The solubility of many materials (especially non-polar materials) is often estimated by the Hildebrand solubility parameter (δ), which compares a material's enthalpy of vaporization and molar volume. This is discussed more thoroughly in Section 3.1.

2.4 Fox Equation

With adsorbed solvent, the Glass Transition Temperature (T_g) of the thin film is no longer determined by the polymer T_g alone. The Fox Equation describes the glass transition temperature of the combined system ($T_{g,P+S}$) as a weighted sum of reciprocals of the transition temperatures of the pure substances ($T_{g,P}$ and $T_{g,S}$), with the weights being the respective mass ratios [Fox and Loshaek, 1955].

$$\frac{1}{T_{g,P+S}} = \left(\frac{\phi\,\rho_P}{\phi\rho_P + (1-\phi)\,\rho_S}\right)\frac{1}{T_{g,P}} + \left(\frac{(1-\phi)\rho_S}{\phi\,\rho_P + (1-\phi)\rho_S}\right)\frac{1}{T_{g,S}} \tag{2.1}$$

In Equation 2.1, the densities ρ, and glass transition temperatures T_g, are have subscripts P for polymer and S for solvent. The glass transition temperature of the thin film (polymer + solvent) is denoted $T_{g,P+S}$. The quantity ϕ is the 'polymer volume fraction' of the thin film, which ranges from 1 (for a film with no solvent), down to 0 (for a film with entirely solvent). The complementary term is $(1-\phi)$, called the 'solvent volume fraction'. In other sections of this report, the quantity of "Swelling Ratio" (SR) is often used instead of polymer volume fraction ϕ, because SR has a

more intuitive relationship to the changing film thickness, which is the actual measured quantity. Assuming that any increase/decrease in volume of the film is a 1:1 response to a volume adsorption/desorption of solvent, then the Swelling Ratio and the polymer volume fraction are simply reciprocals of each other. This assumption will be called into question in a later section of this report, but for now the two variables should be assumed as simple reciprocals of one another (SR $= 1/\phi$).

The solvent and the polymer have similar densities, but very different glass transition temperatures because the solvent is a single monomer and therefore must be cooled to very low temperature before Van der Waals (inter-molecular) forces can cause viscous effects to dominate, (at least in comparison to the polymer with its long chains with strong covalent bonds). Specific use of the Fox equation with the chosen polymer and solvent will be shown in Section 3.1 with the rest of the material properties.

2.5 Flory-Huggins Solution Theory

Above the glass transition, the sorption process of solvent, and consequently the swelling behavior of thin films, is typically described using Flory-Huggins solution theory [Efremov and Nealey, 2022; Laschitsch et al., 1999]. Flory-Huggins is a statistical mechanical approach to a lattice model of polymer solutions, which predicts a free energy of mixing given by Equation 2.2, where N_S and N_P are the number of molecules of Solvent and Polymer, and ϕ is the polymer volume fraction [Flory, 1953; Sheehan and Bisio, 1966].

$$\Delta G_m = k_B T \Big[N_S \ln(1-\phi) + N_P \ln(\phi) + \chi N_S \phi \Big] \tag{2.2}$$

The first two terms in the sum are the standard formula for Entropy of Mixing, and the final term is the Enthalpy change, which accounts for the energy difference from each monomer-solvent interaction. χ is the Flory-Huggins interaction parameter, and is the only material-dependent part of the model. If $\Delta G_m < 0$, then the polymer and solvent prefer to form a solution. If $\Delta G_m > 0$, then they prefer to separate.

The chemical potential of the solvent in the film is given by the derivative of ΔG_m with respect to the number of solvent particles N_S. Note that the polymer volume fraction (ϕ) is not independent of N_S.

$$\phi = \frac{V_{m,P}\ N_P}{V_{m,S}\ N_S\ +\ V_{m,P}\ N_P} \qquad \frac{\partial\,\phi}{\partial\,N_S} = \frac{-\phi^2\,V_{m,S}}{N_P\ V_{m,P}} \tag{2.3}$$

$$\mu_{\text{film}} = \left(\frac{\partial}{\partial N_S} \Delta G_m \right)_{T,P,N_2} = k_B T \left[\ln(1-\phi) + \phi + \frac{N_P}{N_S}(\phi - 1) + \chi(\phi - \phi[1-\phi]) \right] \tag{2.4}$$

$$\mu_{\text{film}} = k_B T \left[\ln(1-\phi) + \left(1 - \frac{V_{m,S}}{V_{m,P}}\right)\phi + \chi\,\phi^2 \right] \tag{2.5}$$

A plot of the solvent chemical potential μ_{film} divided by k_BT is provided in Figure 2.1. Each line in the figure shows a different value of the interaction parameter χ, and in each the assumption is made that the polymer is much much larger than the solvent ($V_{m,S} << V_{m,P}$).

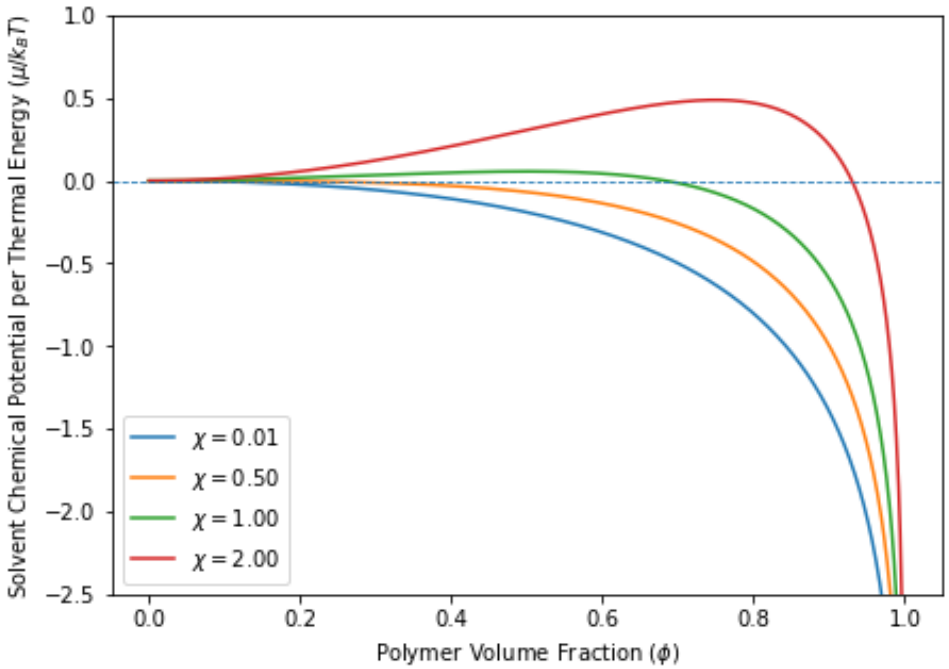

Figure 2.1: Plot of Flory-Huggins theory calculated solvent chemical potential μ_{film}, divided by k_BT, using Equation 2.5, with infinite polymer molar volume. Horizontal axis is Polymer Volume fraction ϕ, and each line is a different value of interaction parameter χ. The horizontal dashed line is $\mu_{\text{film}} = 0$. If $\chi \leq 0.5$, then the value of μ_{film} is always negative.

The thin film will adsorb or desorb solvent molecules as needed to maintain equilibrium between the chemical potential of the solvent in the film (μ_{film}) and the chemical potential of the solvent in the vapor phase (μ_{vap}). The vapor phase chemical potential depends on the relative humidity, and is given by Equation 2.6, where p is the solvent vapor pressure, and p_{sat} is the Saturation vapor pressure of the solvent (solvent vapor pressure when fully wet) [Hulkkonen et al., 2019; Laschitsch et al., 1999]. The ratio of vapor pressure to saturation vapor pressure is sometimes called 'activity', and is denoted a. Except for over-saturated vapor, the value of μ_{vap} will always be less than or equal to 0.

$$\mu_{\text{vap}} = k_BT \ln\left(\frac{p}{p_{\text{sat}}}\right) = k_BT \ln(a) \tag{2.6}$$

Equating the 2 chemical potentials gives a relationship between the solvent vapor pressure and the equilibrium polymer volume fraction of the thin film.

$$k_BT \ln\left(\frac{p}{p_{\text{sat}}}\right) = k_BT\left[\ln(1-\phi) + \left(1 - \frac{V_{m,S}}{V_{m,P}}\right)\phi + \chi\,\phi^2\right] \tag{2.7}$$

$$\frac{p}{p_{\text{sat}}} = (1-\phi)\ \exp\left[\chi\,\phi^2 + \left(1 - \frac{V_{m,S}}{V_{m,P}}\right)\phi\right] \tag{2.8}$$

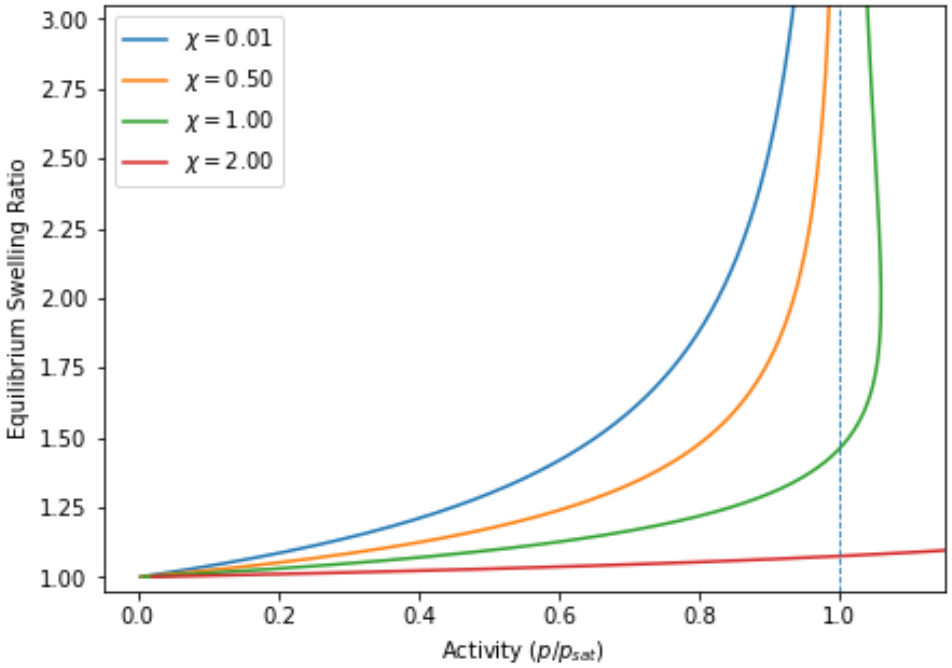

Figure 2.2: Plot of Flory-Huggins theory calculated Swelling Ratio for a thin film in equilibrium with solvent vapor pressure p, and with infinite polymer molar volume. Horizontal axis is Solvent Activity p/p_{sat}, and each line is a different interaction parameter χ. The vertical dashed line is Solvent Activity of 1, ($p = p_{\text{sat}}$). All the functions converge to the dashed line of Solvent Activity of 1, as swelling ratio approaches $+\infty$, which is of course non-physical.

Figure 2.2 shows a few plots of Equation 2.8, with different values of interaction parameter χ. The vertical axis shows the Swelling Ratio (SR), instead of the polymer volume fraction. In the context of SVA, the more natural representation of the film thickness changing from adsorption of solvent is a increase in swelling, rather than as a decrease in the reciprocal value. It should be noted that in this project, no swelling ratio has exceeded 2.5. It is obviously a non-physical result of the model that swelling ratios can reach arbitrarily large values.

2.6 Optical Reflectometry

The optical model of the thin film system is based on the Fresnel equations for reflection and transmission. Light incident on an interface between two different optical media observes the following equations for reflectance and transmission.

$$\begin{aligned} r_\perp &= \frac{n_I \cos\theta_I - n_T \cos\theta_T}{n_I \cos\theta_I + n_T \cos\theta_T} & r_\parallel &= \frac{n_I \cos\theta_T - n_T \cos\theta_I}{n_I \cos\theta_T + n_T \cos\theta_I} \\ t_\perp &= \frac{2n_I \cos\theta_I}{n_I \cos\theta_I + n_T \cos\theta_T} & t_\parallel &= \frac{2n_I \cos\theta_T}{n_I \cos\theta_I + n_T \cos\theta_I} \end{aligned} \tag{2.9}$$

The equations are separated for the orthogonal polarization directions of the Electric Field. The subscripts I (incident) and T (transmission) refer to the 2 media separated by the interface. In

most literature, the symbols for polarization directions are instead given by 's' (for perpendicular) and 'p' (for parallel), referring to the orientation to the plane of incidence. A major simplification for this project is that the light is assumed to have normal incidence to the sample wafer, and thus $\theta_I = \theta_T = 0$. The physics will then be independent of polarization, and only 2 equations are needed to describe the interface.

$$r = \frac{n_I - n_T}{n_I + n_T} \tag{2.10}$$

$$t = \frac{2n_I}{n_I + n_T} \tag{2.11}$$

These reflection and transmission coefficients refer to the electric field strength. The measurements of intensity will correspond to the value of these coefficients squared. Equation 2.13 simply reminds us that the power at the media interface is conserved.

$$R = |r|^2 \tag{2.12}$$

$$T = 1 - R \tag{2.13}$$

The equations above refer to the behavior at a single interface between optical media. With thin film reflectometry, the model must account for each of these interfaces, as well as the changing phase as the light propagates. The phase change is a function of the thickness of the layer with a simple proportionality of $\frac{2\pi n}{\lambda}$. The phase change induced by propagation through a layer in the model is given the symbol β. In Equation 2.14 below, the subscript j is the layering index; n_j and d_j are respectively the index of refraction and the thickness of the j-th layer.

$$\beta_j = \frac{2\pi}{\lambda} n_j d_j \tag{2.14}$$

Tracking the phase change is crucial because it is the only part of the model which is dependent on the thickness of the layers. The interference effects which arise from the accumulation of phase difference between the rays is the primary contributor to the chromaticity of the reflection response, and the key to recovering the thicknesses of the layers.

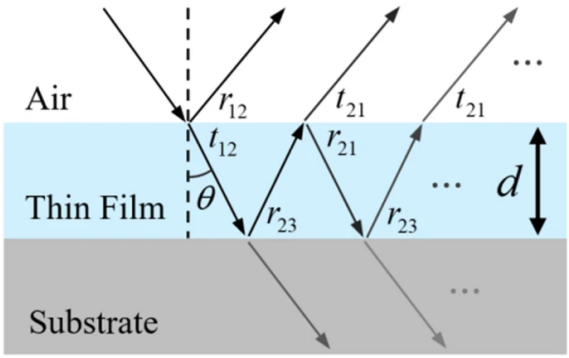

Figure 2.3: Schematic diagram of the Layer Model of Thin Film on Substrate, showing incident light from the air, and cascading reflections and transmission rays. Image from *Nature*, [Lee and Jin, 2022]

For the single layer model depicted in Figure 2.3, the total amplitude reflection coefficient is the sum of each of the outgoing rays. The result is an infinite geometric series, which has a convenient formula.

$$r_{123} = r_{12} + (t_{12}t_{21}r_{23}e^{(-i2\beta)}) + (t_{12}t_{21}r_{23}e^{(-i2\beta)})(r_{23}r_{21}e^{(-i2\beta)}) + ... \tag{2.15}$$

$$r_{123} = r_{12} + \frac{t_{12}t_{21}r_{23}e^{(-i2\beta)}}{1 - r_{21}r_{23}e^{(-i2\beta)}} = \frac{r_{12} + r_{23}e^{(-i2\beta)}}{1 + r_{12}r_{23}e^{(-i2\beta)}} \tag{2.16}$$

Notice that the phase change β is multiplied by 2 because the rays travel twice the thickness of a layer during an internal reflection. The phase change is then applied in the familiar manner; $e^{(-i\,\Delta\phi)}$ multiplied as a coefficient to the Electric field vector.

Any higher order layer model behaves identically, with the above Equation 2.16 applied recursively from the lowest interface outwards to the highest. In this project, a 2-layer model is sufficient: the polymer thin film layer of course, plus a very thin layer of silicon oxide at the surface of the substrate. Well before the polymer is added, the silicon substrate wafer is exposed the air and oxidizes. For the remainder of this report, the reflection coefficients, phase thicknesses, indexes of refraction and other related terms will be indexed as: 0 - Ambient (air / solvent vapor), 1 - Polymer Film, 2 - Silicon Oxide Layer, 3 - Silicon Substrate.

$$r_{0123} = \frac{r_{01} + r_{123}e^{(-i2\beta_1)}}{1 + r_{01}r_{123}e^{(-i2\beta_1)}} \tag{2.17}$$

$$r_{123} = \frac{r_{12} + r_{23}e^{(-i2\beta_2)}}{1 + r_{12}r_{23}e^{(-i2\beta_2)}} \tag{2.18}$$

$$r_{jk} = \frac{n_k - n_j}{n_k + n_j} \tag{2.19}$$

These 3 equations form the model for the reflectivity of a thin film. In Section 3.5, more information is given regarding the use of this model for quantifying the thickness of a sample.

3 Experimental Method and Data Analysis

3.1 Material Choices - Polystyrene and Toluene

The only polymer used in this project is Polystyrene (PS). I wanted to focus as much as I could on the SVA process, so I decided to only test a single type of polymer. Polystyrene was the best candidate for this as a variety of samples were already available in the lab. Most of the Polystyrene samples are part of an ISO Certified Reference Material kit from Polymer Source, Inc. The samples range in molar mass from 0.8 to 6000 g/mol. The polydispersity index of the samples ranges from 1.02 to 1.12 [Polymer Source, Inc., n.d.]. The only exception is a Polystyrene sample with molar mass of 20k g/mol, which was sourced from the Kristoffer Almdal Lab, at DTU.

Polystyrene has a glass transition temperature of approximately 100 °C, but some dependence based on the length. For shorter samples with molar mass of less than 15k g/mol, the value of T_g begins to decrease rather quickly, and T_g is about room temperature for PS of molar mass just below 1k g/mol [Abiad et al., 2009].

The solvent used in this project is exclusively Toluene. There are several options for a choice of solvent, considering that Polystyrene is soluble in all aromatic hydrocarbons, as well as ketones and esters [Flory, 1953]. The best choice for the solvent in this project will be to maximize the thin-film swelling response during the vapor annealing. Relative solvency between solvent and solute is generally judged with Hildebrand solubility parameter (δ) [Lin and Nash, 1993; Venkatram et al., 2019]. In Equation 3.1 below, the variables are Enthapy of Vaporization (ΔH_v), Ideal Gas Constant (R), Temperature (T), and the Molar Volume in the condensed phase (V_m).

$$\delta = \sqrt{\frac{(\Delta H_v - RT)}{V_m}} \tag{3.1}$$

Materials of with similar values of δ can be expected to be miscible, because there would be a relatively small enthalpy difference between the mixed and the separated states (referred to as 'solution' and 'separation' phases). The minimization of the Gibbs Free Energy is dominated by the change in Entropy, which obviously favors the solution phase over the separated phase.

The solubility parameter for Polystyrene ($\delta_{PS} = 18.7\,\text{MPa}^{1/2}$) is very close to the value for Toluene ($\delta_T = 18.2\,\text{MPa}^{1/2}$), especially compared to the other readily-available option: Acetone ($\delta_A = 20.3\,\text{MPa}^{1/2}$) [Brandrup et al., 1999; Mark, 2007]. Previously collected data confirms that SVA of Polystyrene with Toluene results in over 5 times the swelling response as with Acetone.

The shift in Glass Transition Temperature of a polymer in response to diffused solvent molecules was described in Section 2.4 using the Fox Equation. With the choice of Polystyrene polymer and Toluene solvent, the Fox equation can estimate the amount of solvent which will induce the glass transition. Polystyrene has a density of $\rho_P = 1.05$g/mL. Toluene has a density of $\rho_S = 0.866$g/mL, and the temperature of the glass transition for Toluene is $T_{g,S}$ =117 K [Angell et al., 1978; Hinze et al., 1995]. Like all polymers, the glass transition for polystyrene depends on the length of the

polymer chain. Longer chains are prone to more entanglement, more viscosity, and must be heated to higher temperatures before rubberizing. In general, $T_{g,P+S}$ =100°, or 373 K, but this begins to drop off as the polymer molar mass drops below 20kg/mol.

During SVA, the thin film will enter the rubbery state once enough solvent has absorbed into it that the glass transition temperature is equal to the temperature in the SVA chamber. Thermal control of the SVA chamber and related equipment is set to 24°C, so the Fox equation should be solved for $T_{g,P+S} = 297\text{K}$.

$$\frac{1}{297\text{ K}} = \left(\frac{\phi}{0.825 + 0.175\phi}\right)\frac{1}{T_{g,P}} + \left(\frac{1-\phi}{1 + 0.211\phi}\right)\frac{1}{117\text{ K}} \tag{3.2}$$

Figure 3.1, shows the lowering of $T_{g,P+S}$ as polymer volume fraction decreases. The plotted lines are for different values of $T_{g,P}$, one for each of the polymer types. The horizontal dashed line is the is 24°C, so during SVA the film will be in a glassy state when above the dashed line, in a rubbery state when below the dashed line. Table 3.1 lists the relevant numbers, and relates each to the varying molar mass of Polystyrene which determines the glass transition temperature. The values for $T_{g,P}$ accompany each source of polymer [Polymer Source, Inc., n.d.].

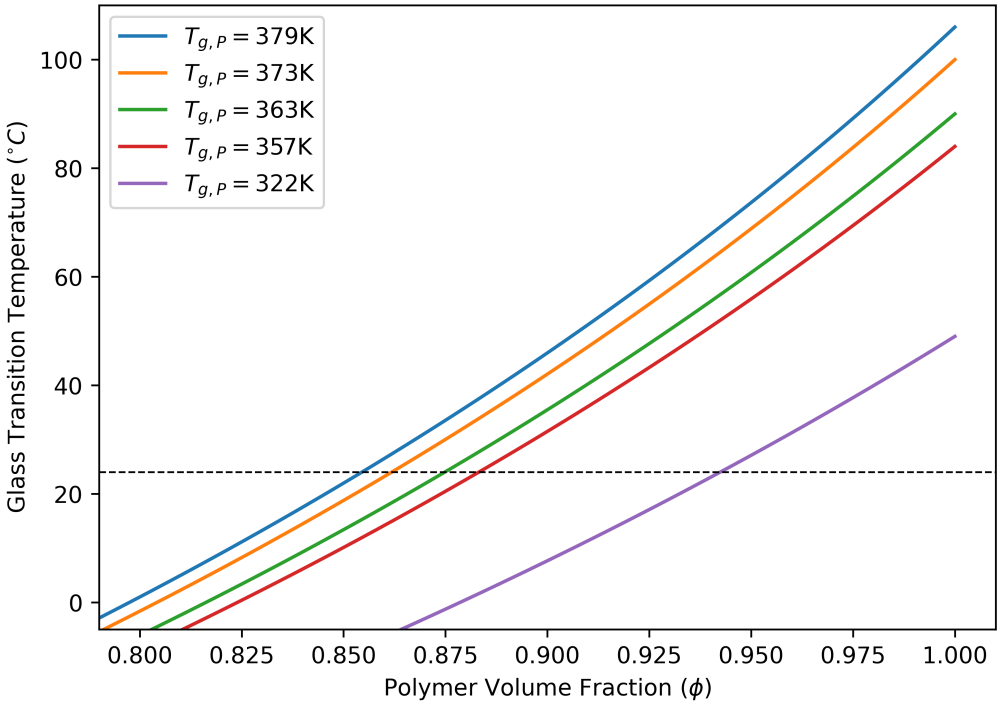

Figure 3.1: Plot of single-term Sellmeier model of Chromatic Dispersion of Polystyrene, Toluene, and Silicon Di-Oxide. See Table 3.2 for more dispersion model parameters.

Molar Mass (kg/mol)	$T_{g,P}$ (K)	ϕ for $T_{g,P}$ =24°C
6000	379	0.8545
105	373	0.8618
20	373	0.8618
11	363	0.8748
5.5	357	0.8832
1.8	322	0.9424

Table 3.1: Table of Glass Transition Temperatures for each of the Polymers used in this project, separated by their Molar Mass. These values are provided directly from the source, Polymer Source, Inc. [Polymer Source, Inc., n.d.]. Also listed is the Polymer volume fraction ϕ (when mixed with Toluene) for which the film is expected to have its Glass Transition Temperature T_g lowered to 24°C, as predicted by fox Equation, 3.2

The data above will be revisited in later sections when analyzing the SVA data. For now, the reader should notice two results from Table 3.1 above: First, the glass transition is expected to occur for 20kg/mol polystyrene when $\phi = 0.86$, or a Swelling Ratio of SR $= 1.16$. Secondly, that the lower molar mass polymers are expected to have their glass transition occur with much less diffused solvent. Both of these insights will be compared with the experimental data is Section 5.

The final material parameter to discuss in this section is the Flory-Huggins interaction parameter χ. Typically, χ is an empirically determined quantity, but can be estimated from the Hildebrand solubility parameters, and the molar volume of the solvent and monomer units. This approach has been adopted for estimation only, and requires a constant β with a commonly used value of 0.34 [Nistane et al., 2022; Sheehan and Bisio, 1966].

$$\chi_{\text{Hildebrand}} = \sqrt{V_P V_S}\,\frac{(\delta_P - \delta_S)^2}{RT} + \beta \tag{3.3}$$

For simplicity, I will assume the geometric mean of the molar volumes of styrene monomer units and toluene is 100 mL/mol, which is accurate enough for estimation. Using the Hildebrand solubility parameters listed above ($\delta_{PS} = 18.7\,\text{MPa}^{1/2}$ and $\delta_T = 18.2\,\text{MPa}^{1/2}$).

$$\chi = \frac{(100\ \text{mL mol}^{-1})(0.25\,\text{MPa})}{(8.314\,\text{J mol}^{-1}\,\text{K}^{-1})(297.15\text{K})} + 0.34 = 0.35 \tag{3.4}$$

This estimation method is not terribly convincing because the formulation makes it impossible to have a value less than the parameter β, and our calculation is extremely close to β. Other literature sources give empirically determined values from 0.45 to 0.31 at the same temperatures [Mark, 2007; Plastic Technology, n.d.]. This is a relatively large range of values, and there is no customary method for determining the value of χ more precisely, so a rough estimation will suffice. Of the many values I have seen reported, I will use a reasonable average value of $\chi = 0.42$ for the remainder of this report, but the reader should keep in mind that estimations made from

Flory Huggins theory might deviate from measured data because of this parameter uncertainty. Additionally, the interaction parameter χ is known to depend on temperature, but also depend on solvent concentration (i.e. polymer dilution). This means that the value of χ is subject to variation throughout the SVA process, so choosing the "right" number for χ is not possible with only a single value.

3.2 Sample Preparation

The thin films are formed by spin-coating a polymer solution deposited onto diced silicon wafer chips of approximately 2cm on a side. The polymer is prepared by first dissolving it in a solution of Toluene. The solutions vary from 1.5% to 3% polymer by weight; enough solvent that the polymer can dissolve completely. The solution is agitated for at least a few hours and kept at 40°C to ensure that the polymers are fully mixed with solvent and does not form any clumps. The heaviest polymer used in this project has molar mass of 6000 kg/mol. Even in toluene solution with only 1.5% polymer by weight, this solution remained significantly more viscous than pure toluene (like an oil or light syrup). All other polymer samples have much lower molar mass, and showed no signs of increased viscosity.

The Silicon wafer that serves as the substrate for the polymer films is diced and cleaned before coating. Wafers are plasma cleaned in a low-pressure environment to improve the adhesion of polymer film. The plasma cleaning is said to 'activate' the surface by removing loosely bound organic matter exposing chemically reactive sites near the wafer surface. This dramatically increases the surface energy of the silicon wafer and improves the wetting of the thin film. It should be noted that the Plasma Cleaning is done only to improve the wetting of the film, and reflectometry tests show no discernible change in the reflectance of the substrate wafers as a result of plasma cleaning. Below are images from 2 different wafers, one which has not been plasma cleaned (Figure 3.2), and another which had been cleaned earlier that day (Figure 3.3). The difference is noticeable, but the reflectance profiles will be mostly identical. Small bits of dust are not enough to effect the reflection measurement, but will definitely affect the wetting of the film to the wafer surface.

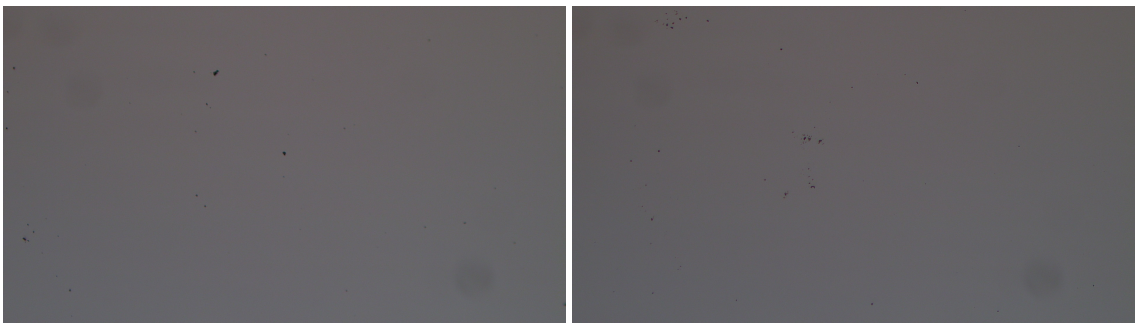

Figure 3.2: Images of a wafer which has not been plasma cleaned. There is some noticeable dust or other artefacts on the surface. Images are 10X magnified.

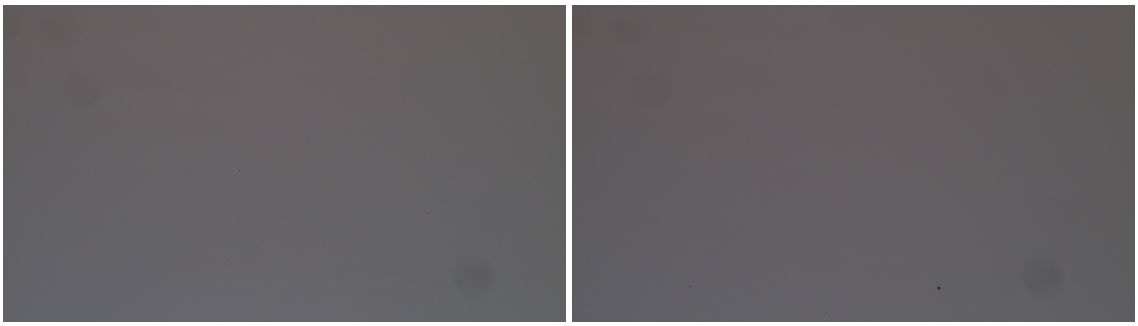

Figure 3.3: Images of a wafer which was been plasma cleaned about an hour before being imaged. There are few, if any, visible artefacts on the surface. Images are 10X magnified.

With both the silicon wafer and the polymer solution prepared, about 100-200μL of the solution is placed on top of the wafer with a micro-pipette. The thin film is fabricated by spin coating at a few thousand rpm, which removes excess solution and "cures" (evaporates) any remaining solvent. The speed of the spin-coating is adjusted to influence the thickness of the samples. Rotation speed ranged from 2000rpm up to 6000rpm, with acceleration fixed at 4000rpm/s.

The plasma cleaning and spin-coating processes are not the main subject of investigation for this project, but a few images of the films after spin-coating is useful to understand the film surface.

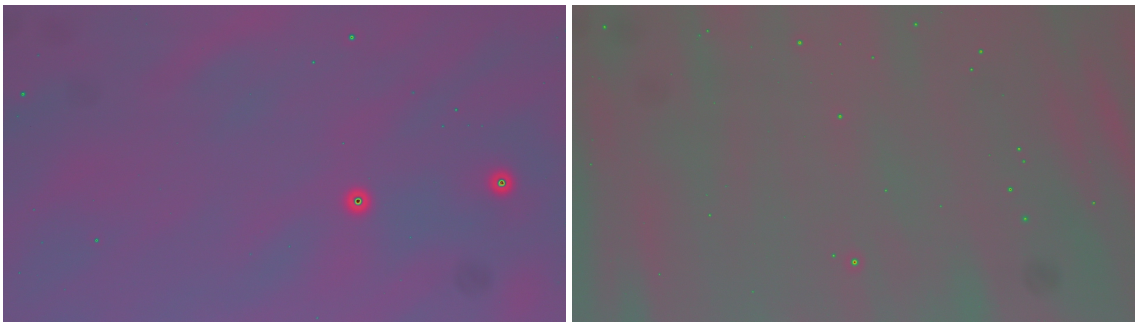

Figure 3.4: Images of 2 wafers after spin-coating. The thickness of the polymer film can be seen to change with the changing color. Uniform coloring shows where the film is uniformly thick. Small artefacts are visible which distort the color of the film, but only in small area. The artefacts are different sizes, but none large enough to impact overall reflectance.

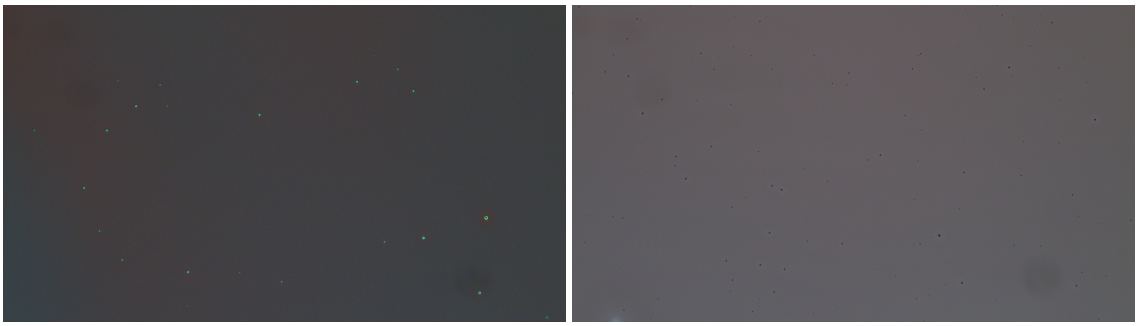

Figure 3.5: Images of 2 wafers after spin-coating. The polymer film is quite thin, and there is not much color in the reflections. Small artefacts are visible as either bright or dark spots, but are very small. The artefacts are different sizes, but none large enough to impact overall reflectance.

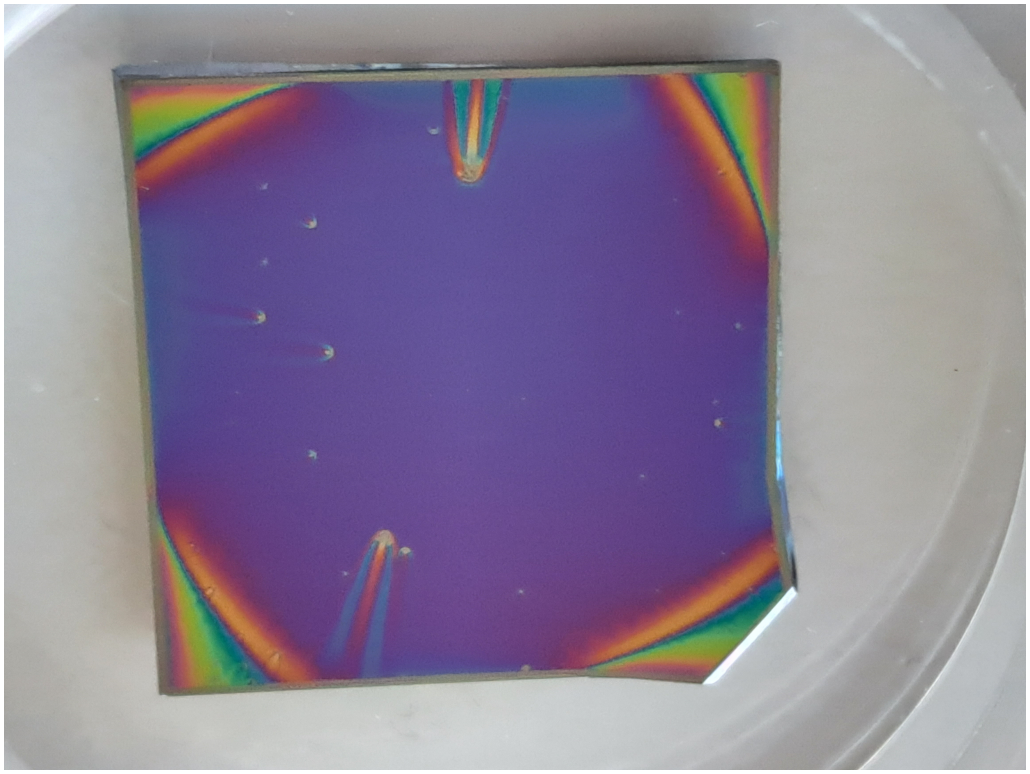

Figure 3.6: Camera Phone Image of Sample (J18) just after spin-coating and before SVA.

Figure 3.6 shows sample J18, a wafer with a film of polystyrene of molar mass 20kg/mol, about 250nm thick. Streaks have formed around dust particles or other artefacts on the wafer, which emanate outwards. Clearly these result from the spin coating. The corners of the wafer also have chromatic difference due to change in film thickness there. The reflectometery measurements of SVA only illuminate the center portion of the wafer, where the surface is clean and uniform.

3.3 SVA Chamber and Equipment

The thin-film samples must be placed in a sealed chamber for the solvent vapor annealing process. Figure 3.7 shows the SVA chamber with the relevant equipment. The computer sends commands to the gas flow controllers to adjust the solvent vapor in the chamber. The data received by the computer is from 2 sources: a) the spectrometer measuring the reflected light, and b) the solvent vapor concentration (SVC) sensor, which measures the UV transmittance of the exhaust gas. Even though the computer controls the input gas flow, the composition of the gas in the chamber needs to be measured separately by the SVC sensor. Due to the physical size of the SVA chamber, possible temperature differences, and the inherent risk of formation of solvent condensate within the chamber/tubing, the composition of the exhaust gas is often different than the composition of the input gas.

The light source is provided by a Halogen Lamp (HL-2000-HP-FHSA), with connected fiber optics. The Spectrometer device is NanoCalc Thin Film Reflectometry System (NanoCalc-XR), which includes a bifurcated UV fiber with metal jacketing. Both halogen lamp and NanoCalc are products from Ocean Optics, Inc. [Ocean Insight, n.d.].

The wavelength range of the halogen lamp output is specified as 360nm - 2400nm, but I think most of the longer wavelengths are attenuated by the fiber which is listed as a UV fiber. The NanoCalc has a spectral range of 250nm-1050nm. For all measurements in this project, the wavelength range is 400nm - 900nm. Future improvements could be made by extending the wavelength range to lower values, where the reflectance has increased chromatic dependence and therefore has more features for better fitting of thickness.

The fiber enters the SVA chamber from above through the lid, and the illumination enters through a small lens system which collimates the light. The sample rests in the SVA chamber on a stage which is normal to the incident light, and about 2cm below the end of the fiber. The reflected light re-enters the UV fiber and from the bifurcation arrives at the NanoCalc where the spectrum is measured.

The gas flow and direction is shown in Figure 3.7 with red arrows, starting from the N_2 tank on the left, and emerging as exhaust on the right. The solvent vapor is added to the N_2 gas in the Bubbler. The submerged gas forms many small bubbles with a low enough surface area to volume ratio that they very quickly become saturated with solvent vapor. For now, an assumption is made that the gas leaving the bubbler is fully saturated, (100% relative humidity), but this assumption is investigated later in Section 5.5. The solvent vapor concentration is adjusted using the mass flow controllers (MFCs), which set the rate of flow of N_2 gas between 0 and 200 sccm (standard cubic centimeters per minute). The total flow from both MFCs together is kept fixed at 200sccm, and solvent vapor pressure is controlled by adjusting the portion which passes through MFC2 (and therefore the solvent bubbler), and the portion which passes through MFC1 (and remains 'dry' N_2 gas). The gas from both MFCs combine in the mixing chamber to equilibrate the solvent vapor

concentration, and then flows to the SVA chamber through a gas distribution tube which equally disperses throughout the chamber to reduce concentration gradients.

The gas leaves the SVA chamber through additional tubing and after a few centimeters enters the SVC sensor, before finally being vented to the chemical fume hood/exhaust system. This sensor has both a UV photodiode, and a Mercury lamp, with stabilized output at 254nm. The toluene solvent, unlike the N_2 carrier gas, absorb in the UV range, so the transmission through the SVC chamber will be modulated by the concentration of solvent vapor molecules. The UV photo-diode measures the transmittance (T) of the gas, which is converted to absorbance (A) following the Beer-Lambert Law [Beer, 1852]. Equation 3.5 shows this law, with a quantity T_0 to represent full transmission, (photo-diode measurement with fully no solvent, only N_2 gas).

$$A = \log_{10}(T_0/T) \tag{3.5}$$

With pure N_2 gas flowing for at more than an hour to empty out any solvent, the SVC sensor gives a transmission value of about 90, and differs only very slightly from day to day. With full flow through the bubbler, (i.e. maximum solvent concentration), the SVC sensor transmission value drops to approximately 10. To normalize the value the Absorbance, the Beer-Lambert equation is scaled according to the range of values of data collected. Notice in Equation 3.6 that because of the scaling, the logarithm base is arbitrary.

$$A_{\text{normed}} = \frac{\log_{10}(T/T_{\text{max}})}{\log_{10}(T_{\text{min}}/T_{\text{max}})} = \frac{\ln(T) \ - \ln(T_{\text{max}})}{\ln(T_{\text{min}}) - \ln(T_{\text{max}})} \tag{3.6}$$

The SVA chamber (and mixing box) is approximately 400cm^3, and with a flow rate of 200sccm, the relaxation time for the solvent concentration to come to equilibrium ($1/e^2$) is approximately a full 2 minutes. There will be more discussion about this in the next section.

The bubbler, mixer, and SVA chamber are in thermal equilibrium with one another, and temperature controlled to 24°C, so the saturation vapor pressure should be constant through that part of the system. The heating element is Polyimide Thermo-foil Heater, 28V, 12W from Minco Products, Inc. [Minco Products, Inc., n.d.]. The SVC sensor chamber is also thermally controlled to 24°C, but as part of a different thermal system, so the actual temperature may change between the SVA chamber and SVC chamber.

Not shown in the diagram are 4 screws which fasten the lid of the SVA chamber, and the O-ring which seals the chamber of any vapor leakage.

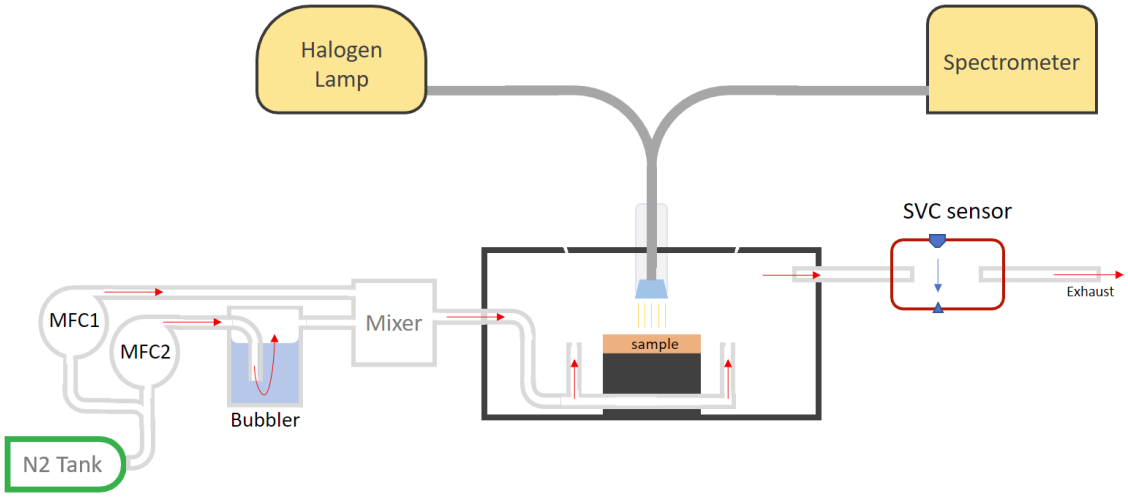

Figure 3.7: Schematic Diagram of the solvent vapor annealing chamber and associated equipment. The solid gray connecting the halogen lamp, sample chamber, and spectrometer is the optical fiber. The flow of Nitrogen gas is depicted with red arrows, with rates controlled by the MFC (Mass Flow Controller) devices, and which also carries solvent vapor when passing through the bubbler. The liquid toluene is represented by the light blue substance in the bubbler tank. The SVC (Solvent Vapor Concentration) sensor includes a UV lamp and a photo-diode, with UV light shown as a blue arrow. The computer collects data from the spectrometer and SVC sensor, and gives commands to the MFCs.

3.4 Annealing Procedure

The SVA procedure is simple, but deserves some explanation. As explained in a later section (Section 3.6), the measurement of thickness of samples requires both a reference spectrum measurement (a blank wafer with no thin film), and a 'dark' or background spectrum measurement (no reflected light). At least 2 measurements of the reference and background intensities are made both before SVA begins and after it is finished. Each measurement is performed more than once to make sure that the light source has properly warmed up and reached a steady-state emission.

Once the sample under test has been placed in the SVA chamber and the lid fastened, the flow of N_2 gas at the exhaust is checked to be sure that the gas system is fully sealed.

The SVC sensor runs continuously, and makes measurements 4 times every second. This gives very good resolution for changes in the solvent vapor, but a 4Hz sampling rate is definitely faster than necessary for most of the SVA tests. Usually the solvent vapor concentration only changes in small amounts, but some SVA methods for copolymers use 'quenching' to rapidly dry the sample and remove solvent as quickly as possible. In those cases the 4Hz sampling rate of the SVC can be very useful. However, for most applications, this rate should be re-considered. Very high sampling rate may be the cause of timing errors, and certainly generates data files with unreasonable size. The SVC sensor also has a built-in digital display of its most recent measurement value, which is

useful for the experimenter to consult.

The NanoCalc spectrometer makes measurements every 10 seconds. Each measurement is fitted immediately to a thickness value so that the experimenter can observe changes in swelling in real-time. Plots of both the most recent reflectance data and all the fitted thicknesses are shown in the GUI for the spectrometer measurements. Additionally, the mean squared error of the fitting procedure is shown, which allows the experimenter to anticipate deterioration of the sample. When a thin film de-wets from the wafer surface, it does so in a nucleation and growth process from defect points in the film. This means that small sections of the film are destroyed first, and gradually grow larger. By paying attention to the error of the fitting procedure, de-wetting can be seen (and stopped) before it advances to complete film destruction.

The gas flow lines are also controlled through the computer, and commands can be sent to the Mass Flow Controllers (MFCs) either by user input, or through a timed script. The SVA tests are almost always performed by scripted gas flow. The most important flow scripts are included in full in Appendix A, but I will explain them here. Commands are sent to each MFC device separately, first to the MFC with 'dry' N_2 gas, and then 1 second later to the MFC with the solvent bubbler. The total gas flow is kept steady at 200sccm, except for the 1 second interval between these commands.

The Flow Script that I use most often is shown in the figure below. For the purposes if this project, it is given the name 'FS_swell_deswell_linear'. This Flow Script changes solvent vapor concentration with steps of 1%, which allows for good resolution regarding specific swelling response changes in the film.

After an initial period of 1000 seconds with pure N_2 gas flow to establish a basis for the sample before any swelling, the script increases the flow through the solvent bubbler by 2sccm (1% of total), every 100 seconds. 100 seconds was chosen as the interval between steps because testing showed that after 100 seconds, thin films will have swollen more than 90% of the way to the equilibrium swelling position. In the previous section it was estimated that the SVA chamber has a relaxation time of 120 seconds, and that was for large step sizes. I am confident that at 1% steps, 100 seconds produces a steady rate of swelling. I did not check the same relaxation time for de-swelling, but I assume it is not significantly different. Once the flow script reaches 100% flow rate through the bubbler, it stays at this maximum position for 1500 seconds. This is to allow the film to continue additional swelling to equilibrium thickness, but in practice allowing the film to swell until a complete stop would take a very long time. Then the flow script begins decreasing the flow rate through the bubbler with the same 1% steps. Upon reaching 0% flow through the bubbler, the flow script has given its last command. The measurement can continue as long as I please, and I usually wait at least another 15000 seconds before ending the measurement.

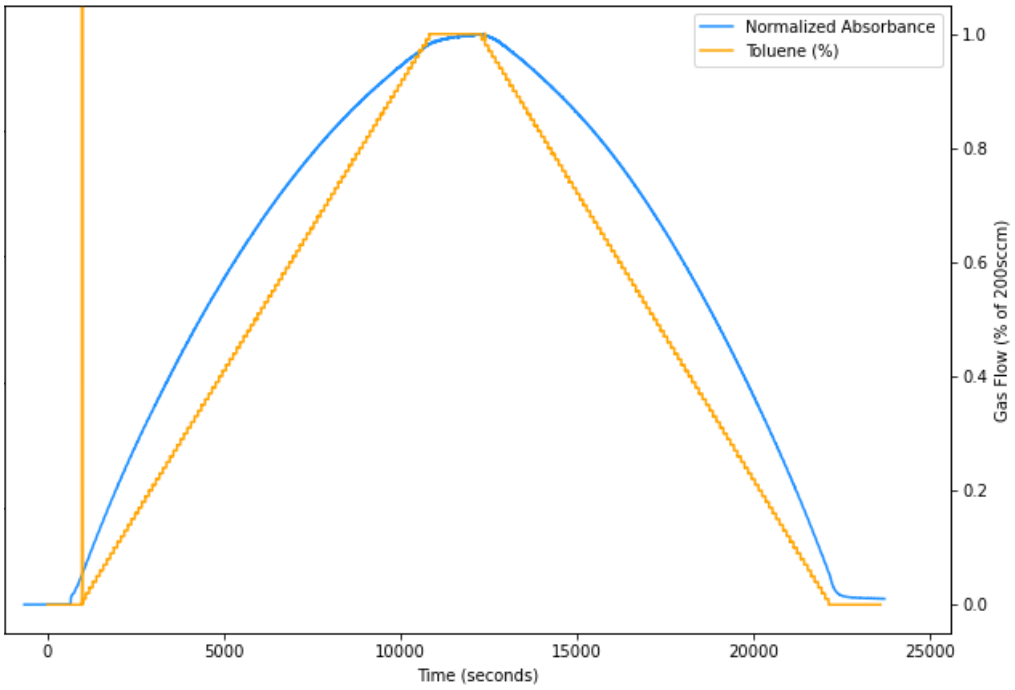

Figure 3.8: Plot of the measured values from the Mass Flow Controller leading to the solvent bubbler, as scripted by SVA Flow Script 'FS_swell_deswell_linear'. Timing discrepancies are visible.

Figure 3.8 shows both the gas flow measured by the MFC (as a fraction of the total 200sccm), and also the Normalized Absorbance measured by the SVC sensor. A spike in the measurement occurs when the toluene is first introduced, but this is just a measurement artefact of the MFC turning on. The spike produces no resultant change in the SVC sensor. There are 2 important things to notice in this plot. First, the Absorbance measurement by the SVC sensor follows a non-linear path. Meaning either the SVC photo-diode response is inaccurate, or the solvent bubbler does not work linearly. The Absorbance starts off with a linear rate of change, but as the Absorbance gets closer and closer to 1, the rate quickly slows down. Recall that the SVC makes transmission measurements, which are converted with a logarithm function to absorbance. I am not sure if the UV photo-diode is intended to work over such a large range of intensities ('dynamic range'). However, if I had to guess, I think solvent bubbler inefficiencies is a more likely candidate for causing this. More details on that in a later section of the report.

The second important result to notice from the plot is the time correlation between the data sets is inaccurate. I have shifted the data sets such that the maximum absorbance value occurs at the last second before the Flow Script begins reducing the solvent concentration. However, in the first 1000 seconds, the SVC data clearly increases before any solvent is introduced. This is not a flow script error but rather a timing error. The clock on one of these systems is not counting at the same pace as the others, so there is no way to get all simultaneously measured data points to match one another. I am pretty sure it is the SVC sensor, controlled by MATLAB, which has a separate clock and is somehow *over*-counting the seconds. A few dozen extra seconds or so over the course

of several hours may not seem like much, but it can make a difference when trying to correlate swelling and absorbance data together.

Before future research is conducted, these two issues should be better understood and appropriately addressed. It is crucial that the data collection methods are corrected, because even well thought out and organized experiments risk have their results made unreliable or even unusable from inaccurate data collection.

3.5 Optical Model

As mentioned in Section 2.6, the optical reflectometry model depends only the thickness and index of refraction of each layer. The thicknesses are unknowns, but the indexes of refraction must be given. With a few exceptions which are explored further on in this report (5.8), the values of the index of refraction for each media is collected from available literature and remains the same for all samples.

I will briefly mention the extinction coefficient κ, which is not used in this project and requires justification. Absorption within an optical medium is always non-zero, and an extinction coefficient κ is often included as an imaginary component in the otherwise real value of the index of refraction.

$$\underline{n} = n - i\,\kappa \tag{3.7}$$

This complex index of refraction is included in calculations of electric field propagation in the identical manner of a change in phase, with the familiar multiplication by $e^{(-i\,\Delta\phi)}$ where $\Delta\phi$ is the phase difference.

$$E = E_0\ \exp[-i\Delta\phi] = E_0\ \exp\left[-i\ \frac{2\pi\underline{n}}{\lambda}\ x\right] = E_0\ \exp\left[-i\ \frac{2\pi(n - i\,\kappa)}{\lambda}\ x\right] \tag{3.8}$$

$$E = E_0\ \exp\left[-i\ \frac{2\pi n}{\lambda}\ x\right]\ \exp\left[-\ \frac{2\pi\kappa}{\lambda}\ x\right] \tag{3.9}$$

The result is an exponential decay factor with scale factor of $2\pi\kappa/\lambda$. For this term to have any appreciable ($\geq 1\%$) effect on the intensity of the measured reflectance, with propagation distance through the optical medium on the order of 1μm, the value of the extinction coefficient κ would have to exceed a magnitude of 6×10^{-4}. Recent literature gives values of the extinction coefficient for Polystyrene of less than 10^{-6} in the relevant range of wavelengths [Zhang et al., 2020]. It is clear that the extinction has no measurable effect on the reflectometry results. For this reason, it is ignored for the remainder of this project.

The indexes of refraction for all of the materials in the thin-film system exhibit some chromatic dispersion, so a constant value is not sufficient for the modelling. However, I want to keep the required number of parameters for the model as low as possible. I have used a single-term Sellmeier

equation for the model of dispersion.

$$n^2 = 1 + \frac{A\lambda^2}{\lambda^2 - B} \tag{3.10}$$

The literature sources where I obtained the Sellmeier coefficients often give two-terms or three-terms in the Sellmeier model. In some cases, these additional terms are negligible at the relevant wavelengths and everything except the first term can be ignored without affecting the modeling outcome. In the other cases, I simply took the full model and fitted it to the simpler one-term model, with very close agreement to the original data points.

Table 3.2 gives the values I used for the single term Sellmeier parameters A and B, and lists the literature source of either the values directly, or the raw data points which I fitted to the Sellmeier model myself to find the parameter values. Also included is the value of the refractive index at $\lambda = 600$ nm; a wavelength which is near the center of the range of the laboratory spectrometer, and is also near the maximum intensity output of the halogen lamp used as a light source. I used the popular database "RefractiveIndex.INFO" as a way of finding these various sources [Polyanskiy, n.d.].

Material	A	B	n($\lambda = 600$nm)	Source
Ambient (Air)	0.0006	0.0000	1.0003	Ciddor, 1996
Polystyrene	1.4435	0.0202	1.5904	Sultanova et al., 2009
Toluene	1.1748	0.0183	1.4959	Kedenburg et al., 2012
Silicon Di-Oxide	1.1530	0.0088	1.4771	Gao et al., 2013
Silicon Substrate	10.3260	0.1039	3.9389	Schinke et al., 2015

Table 3.2: Table of Sellmeier coefficients for modelling chromatic dispersion of each material in the reflectometry set-up. In most cases the literature sources refer to a data set from which I fitted to the Sellmeier model to determine the coefficients.

A visualization of the chromatic dispersion as modelled by the Sellmeier equation is given in Figure 3.9 below, which plots the changing index of refraction for Polystyrene, Toluene, and Silicon Di-Oxide over the range of wavelengths from 400nm to 900nm.

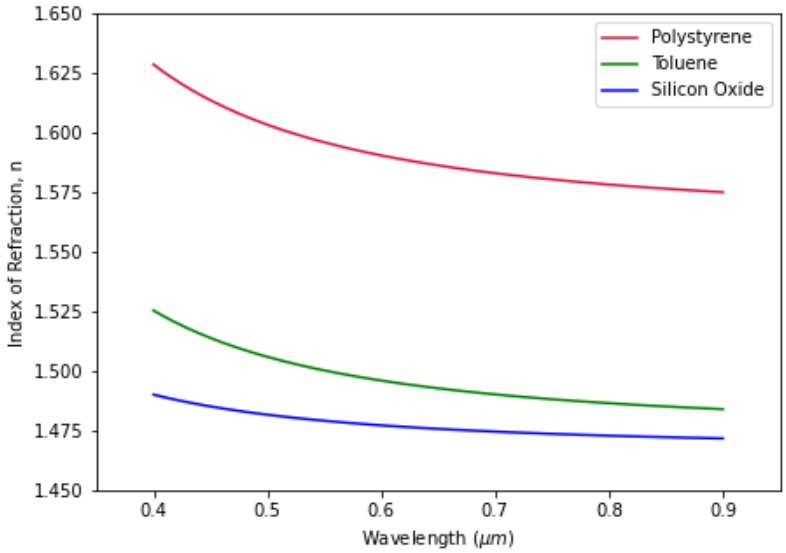

Figure 3.9: Plot of single-term Sellmeier model of Chromatic Dispersion of Polystyrene, Toluene, and Silicon Di-Oxide. See Table 3.2 for more dispersion model parameters.

It is worth noting here that Table 3.2 and Figure 3.9 refer to Silicon Di-Oxide (SiO_2), but it is not immediately clear that the silicon substrate should be modelled as having reached this level of oxidation. The pure silicon exposed to O_2 will oxidize, but away from the interface with the air it is not clear how the composition changes. While I am not able to find an exact relationship between oxygen content and index of refraction, some studies suggest that increasing valence x in SiO_x (from 0.98, to 1.74), decreases the index of refraction (from 1.85 to 1.48) measured at 633nm [Miyazaki, 2010; Salazar et al., 2016]. This amounts to a change of more than 20%. For the sake of this project, because the oxide layer is extremely thin ($\sim$1nm), these differences in index of refraction will not have a huge impact on the reflectivity of the samples. However, future researchers should consider ellipsometric measurements or other methods to accurately determine the composition of the oxide layer.

3.6 Measuring Thickness

The spectrometer measures the reflected intensities, but to compare this to a model of reflection requires knowledge of the incident beam intensity. Because the incident beam and the reflected light travel through the same bifurcated optical fiber, the incident beam cannot be characterized by an equivalent measurement system as reflected light. Instead, the reflected intensities of a sample are compared to a reference system which is has a simple, well-known reflectance profile. Equation 3.11 shows the relationship between the measured intensities and the reflectance models.

$$R_{(\text{Sample})} = \frac{\text{Sample Spectrum}}{\cancel{\text{Incident Spectrum}}} = \frac{\text{Sample Spectrum}}{\text{Reference Spectrum}} \times R_{(\text{Reference})} \tag{3.11}$$

The best choice for the ‘reference’ is a Silicon wafer without any polymer film. The model of this

reference system is extremely simple; just a very thin layer of silicon oxide. The exact thickness of the SiOx layer is not well-known, but a collection of measurements discussed later in this report suggest a thickness of 0.5nm is accurate. Differences of $\pm$2nm effect the model of reflectance by less than 1%, so while the SiOx layer thickness should not be ignored, extreme precision is not necessary.

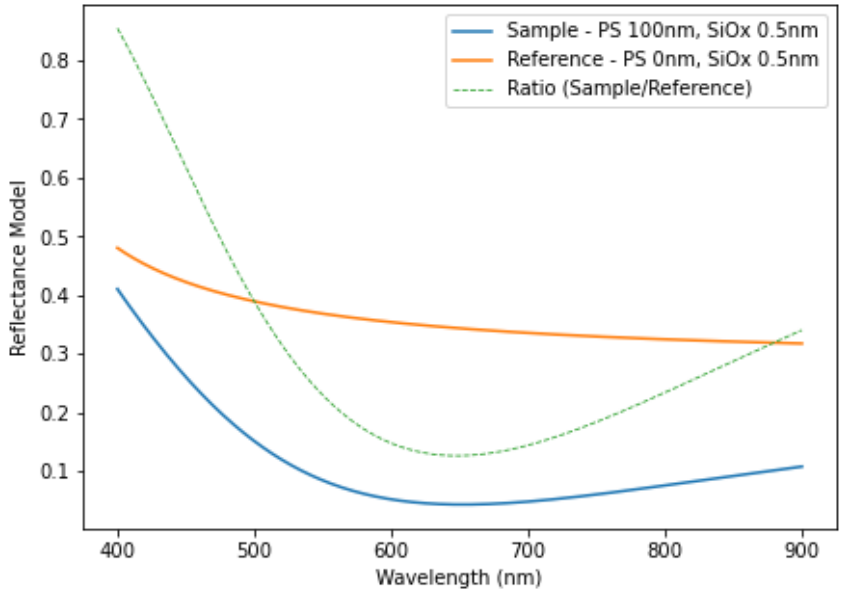

Figure 3.10: Plot of Reflectance Models for Reference and Sample systems, as a function of wavelength. The Reference is a 1 layer system of only SiOx (d = 0.5nm). The Sample is a 2 layer system with Polystyrene (PS) of thickness 100nm, then SiOx (d = 0.5nm). The ratio of Sample reflectance to Reference reflectance is also plotted with a dashed green line.

Using this method, the only difference between the sample and the reference wafers is the addition of the polymer thin-film. This means that the ratio of the reflectance of the 2 systems only depends on the thickness of the Polystyrene. Figure 3.11 below shows a few ratios of the sample reflectance and reference reflectance. It is clear that for the thinnest of Polystyrene films, the reflectance ratio is near 1, because the Sample and Reference systems have little deviation. With increased film thickness, the accumulated phase from propagation through the film is eventually enough that destructive interference reduces reflection intensity to nearly 0 for some wavelengths. Destructive interference resulting from the polystyrene layer would be expected at wavelengths of $\lambda = 4\text{n}d/(2m+1)$, where d is the thickness of the layer, n the index of refraction, and m is any integer. The largest of these wavelengths will be $\lambda = 4\text{n}d$, when $m = 0$. For a PS layer of 100nm, and index of refraction estimated as n(633nm) = 1.59, the largest wavelength with destructive interference would be expected at 636nm. Notice that Figure 3.11 shows a minima very near to that wavelength. Even at these minima, the result is not complete destructive interference because light transmitted past the polystyrene layer is still able to reflect on the later interfaces and return to the detector.

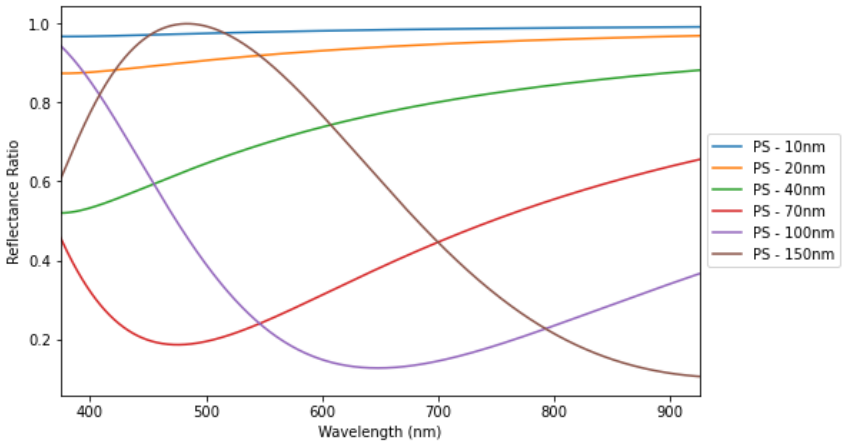

Figure 3.11: Plot of Reflectance Ratios for systems with different thickness of the PS film layer, ranging from 10nm up to 150nm, as a function of wavelength. The modelled reflectance of the Sample system is divided by that of the Reference system, and both have a SiOx layer with thickness of 0.5nm.

With the values of the indexes of the refraction and the SiOx layer thickness fixed, the reflectance ratio is a function of a single variable: The Polystyrene thickness. Once a set of data is collected, all that remains to calculate the thickness is using a least-squares method to fit this single parameter function to the data. Examples are shown in Section 4.1, with the discussion on the accuracy of this method.

4 Data

This section will give an overview of the collected data.

The first section will show some of the raw reflectance data from the spectrometer, and discuss the amount of error present in the measurement. This is to convince the reader of the accuracy of the equipment and the data collection method, as well as the reflectance model.

The second section will show the data taken during an SVA test, and discuss the repeatability and accuracy of the fitted values. Because the thickness of the films is not able to be measured directly, it is necessary to establish the veracity of the fitting procedure.

4.1 Reflectance Data

The measured intensity values from the spectrometer have to be compared with a reference wafer because the incident intensity is unknown, as discussed in Section 3.6

When comparing to the measured data, the background measurement through the optical fiber without any reflection (termed 'Dark Spectrum') is removed from both sample and reference measurements. For measurement of the Dark Spectrum, the lid of the SVA chamber is removed, and the UV fiber with it, and pointed towards a matte black cloth a few centimeters away.

$$\frac{R_{(\text{Sample})}(d_{\text{SiOx}}, d_{\text{PS}})}{R_{(\text{Reference})}(d_{\text{SiOx}})} = \frac{\text{Sample Spectrum - Dark Spectrum}}{\text{Reference Spectrum - Dark Spectrum}} \tag{4.1}$$

Equation 4.1 above shows how the collected spectrometer data sets are related to the models of Reflectance, ($R_{(\text{Sample})}$ and $R_{(\text{Reference})}$). The ratio of modelled reflectances is a function of only 2 variables; the thicknesses of the silicon oxide layer and the polymer layer.

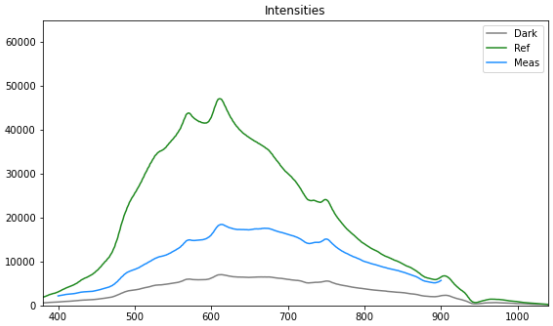

(a) Intensities measured by the Spectrometer. Each data set is a separate measurement. The sample measurement only goes from 400nm to 900nm, where the intensities are measurable.

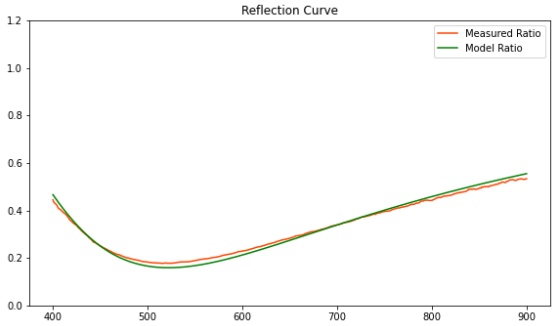

(b) The reflectance ratio curves (sample/reference) of both the measured data in a), and a fitted model. The model uses 0.5nm as the thickness of the SiOx layer, and 78.5nm for the polymer film layer thickness.

Figure 4.1: Example of a) the measured intensities, and b) the reflectance ratio of both the collected data and the model. Good agreement is seen in the reflectance curves. In both, the horizontal axis is the wavelength, measured in nanometers.

An example of the measured spectrum values and corresponding reflectance model is shown in Figure 4.1. The intensities plot shows the reference data has significantly larger values than at some wavelengths more than others. This spectrum distribution is mostly a product of the lamp output and the range of the UV fiber. The material of the reference wafer is pure silicon, and is obviously very reflective. The range of wavelength data used in this project is from 400nm to 900nm, although it can be seen that the intensities become quite small at those limits. Future researchers with a focus on removing noise from the reflectance modelling should consider either reducing the wavelength range to avoid regions with limited intensity, or extend the range of the light source equipment.

The reflectance ratio plot in Figure 4.1 b) shows the calculated values from the data and from the model. The 2 curves show good agreement, but with some variation in amplitude. Notice that shifting the model reflectance left or right will only make the deviation worse. Deviations from the model of this form and magnitude are typical, and repeatable (not noise level). It is not enough error to meaningfully impact the fitted thickness of the film by more than $\pm$2nm, and the form of the deviation stays constant over several hours of SVA testing. For these reasons, this discrepancy between data and model is ignored, but the source should still be discussed.

The best explanation for the source of error in the model is that the surface of the film is not a single uniform thickness. Some sections of the film are thicker or thinner than others, and the measured reflection intensity is just an average of all of the reflections from each illuminated section of the film. Microscope images of the film surface (such as Figure 3.4) show small sections where the film thickness deviates from the surroundings, likely caused by dust particulates or damage on the silicon wafer surface before spin coating. Errors like this are not enough to effect a major portion of the reflectance profile, but can ‘smear’ the reflectance curve and effectively smooth out the chromatic response in the reflected intensities slightly (lower the high points, and raise the low points), as seen in Figure 4.1 b).

Alternatively, it is possible that the model shows deviation from the data because the values for the index of refraction of the materials have not been chosen correctly. In a later section of this report (Section 5.8), the effects of slight variations of the indexes of refraction are shown.

Lastly, I want to mention that handling optical fibers can be really tricky and even small movements can effect the intensity of their output. After measuring the reference wafer, the lid of the SVA chamber has to be fully removed (and along with it the optical fiber is moved), in order to replace the reference wafer with the sample wafer. If the lid is not handled carefully the fiber will shake or be pulled. To show just how much change this can cause, Figure 4.2 is a plot of 6 reference measurements, all with the same reference wafer, taken over the course of about an hour. I am not certain if these differences account for the deviation from the model seen in Figure 4.1 b), but it could be a contributing factor.

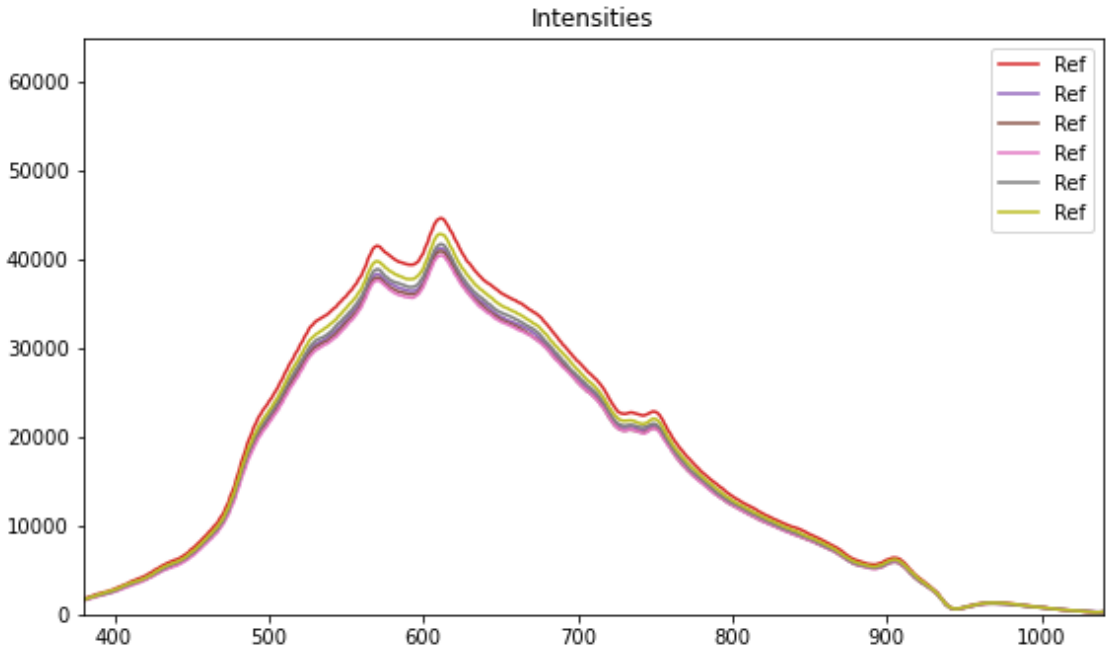

Figure 4.2: A plot of 6 reference measurements, each made consecutively over the course of about an hour. 4 of the 6 are nearly indistinguishable, but 2 others show increased intensity. The changes are the result of removing and replacing the lid of the SVA chamber, which changes the position and direction of the optical fiber.

Further illustration of this can be seen in Table 4.1 of fitted thickness values from sample J3. The first 2 measurements are taken without touching the setup at all, just waiting about 60 seconds. After the first 2 measurements, the SVA lid is removed, the sample taken out, and a new reference measurement taken. Then the same sample is put back in the SVA chamber for the third measurement. The third measurement only changes by about 1nm, but this is still more then 10 times larger than the 'noise' level differences between measurement 1 and 2.

Measurement	Fitted Thickness (nm)
1	91.324
2	91.235
3	90.380

Table 4.1: Sample J3 thickness measurements tested multiple times, with the same configuration. Between test 1 and 2, nothing was changed except to wait about 60 seconds. After the second measurement, the sample wafer was removed, and a new reference and dark measurement are taken, and the same sample is placed back in the SVA chamber for the third measurement.

This should convince the reader of 2 things. First, that the measurements of thickness are likely accurate to within a few nanometers ($\pm$2nm) of the true thickness of the film. And second, that while the SVA chamber remains sealed and the optical fiber un-moved, the thickness measurements are very precise relative to one another. During SVA measurements the equipment is unperturbed,

so changes in the fitted thickness over time can be trusted to correspond to actual swelling of the film, not noise.

4.2 SVA Test Data

The reflectance measurements from an SVA test are all fitted individually, so there is not much difference in the analysis of the spectrometer data from an SVA test and the single measurements discussed in the previous section. However, the fitting procedures for SVA measurements do use the most recent fitted thickness value as a initial guess for the subsequent fitting. It was suggested to me that this might make the results biased based on timing direction, especially for very thin films where noise is more prominent. But I have tested this multiple times by fitting the same data set both backwards and forwards, and the results are always equal.

An additional tool which is helpful during SVA is to track the sum of squared residuals (RSS) of the reflectance ratio data. This can be useful for single thickness measurements as well, but RSS is a relative value, and is not very revealing on its own. During an SVA test, tracking the real-time value of the RSS can indicate to the researcher very early on if the thin film is degrading. Small but consistent increases in the RSS value over time suggest that the surface profile of the film is becoming less and less flat. If this phenomenon is observed in co-polymers, it can often be explained as buckling or wrinkling of the film surface from in-plane swelling or uneven swelling across separated phases [Castel et al., 2020]. However, those swelling behaviors are not expected for homopolymers so in the context of this project, increasing RSS is an indicator of de-wetting. Following the trend of the RSS value can allow an experimenter to anticipate de-wetting a few minutes before the film is significantly degraded, and potentially keep it mostly preserved.

The interpretation of the SVA data involves not just the fitted thicknesses, but also the SVC sensor measurements of transmittance through the solvent carrier gas. Section 3.3 introduced the Beer-Lambert Law and the conversion from Transmittance to Absorbance, with a normalization. The normalized absorbance correlates directly with the solvent 'activity' ($a = p/p_{\text{sat}}$), the ratio of solvent vapor pressure to saturation vapor pressure.

Unfortunately, due to the fact that the SVA chamber and the SVC sensor are separated by a length of tubing, the absorbance data has a tendency to have a delayed response to solvent changes. This is in addition to the non-linearity and timing errors discussed in Section 3.4. An example is shown in the Figure 4.3; the value of the Absorbance reaches an upper limit and has a flat top. The film clearly begins to de-swell around 13000 seconds, but the Absorbance line doesn't begin to drop until past 15000 seconds. The Flow Script stays at maximum solvent vapor concentration for 1500 seconds, but the Absorbance measurement is fixed at this upper limit for nearly 4000 seconds. In this example, the cause is visible, condensation in the exhaust line (Figure 4.4).

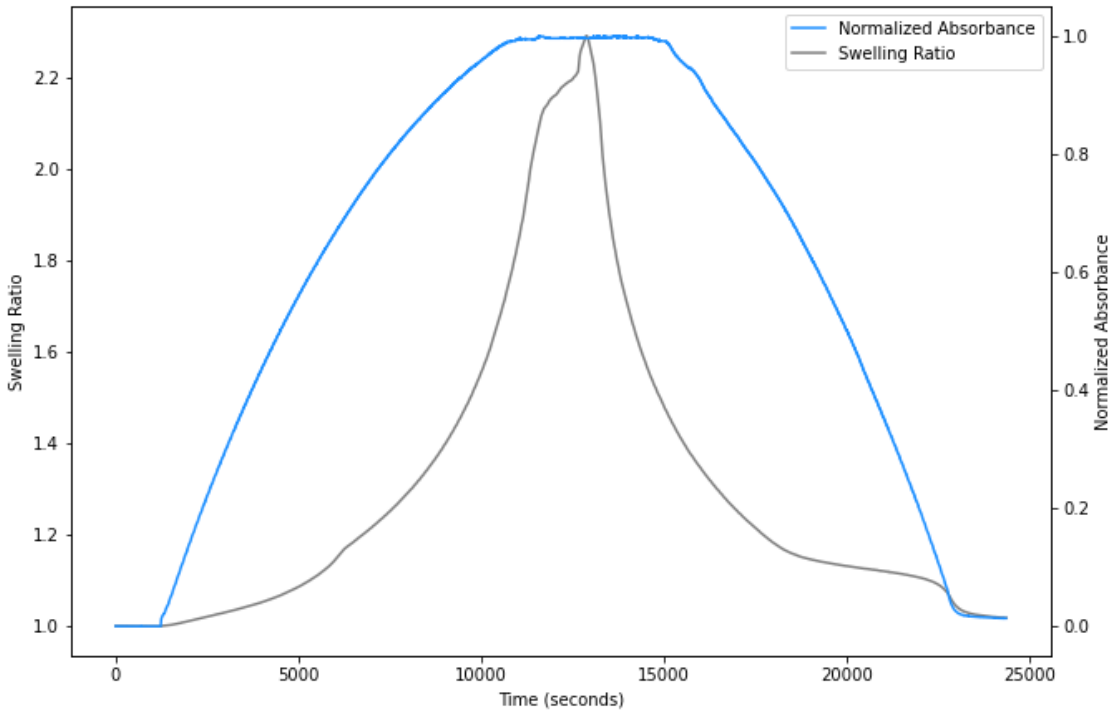

Figure 4.3: Swelling Ratio of sample J18 during SVA, plotted with the Normalized Absorbance measured by SVC sensor. The flat top of the Normalized Absorbance is attributed to reaching saturation vapor pressure inside SVC chamber.

Figure 4.4: Images of Condensation forming in the exhaust tube and beginning to pool at a low point in the tubing, after exiting the SVC chamber. This indicates that the solvent has exceeded the saturation pressure.

Condensation in the system is a problem for SVA, because condensed solvent will quickly destroy the polymer film [Castel et al., 2020]. However, this sample was not damaged, and it can be seen that the swelling ratio responded immediately to the reduction in solvent vapor concentration by the Flow Script. In Figure 4.3, only the Absorbance data has been affected by the condensation. After leaving the SVA chamber but before leaving the SVC chamber, the saturation vapor pressure

of toluene in the carrier gas dropped lower and allowed the condensation to form. This must be the result of a temperature drop, probably in the tubing which carries the gas from one chamber to the other.

The excess solvent condensate forming the in the SVC chamber means that we cannot correlate the swelling ratio with the absorbance for this sample. It is clear that the solvent activity in the SVA chamber is not the same as in the SVC chamber. When using absorbance data in later sections of this report, I have made sure to check that the data does not reach a flat-top upper limit which indicates the chamber has reached saturation and might be condensing. Consider that this means a normalized absorbance of 1 is almost certainly NOT equivalent to a solvent activity of 1. The two variables are closely related, but we should not assume they are equivalent.

4.3 Data Analysis GUI Tool

Data analysis of SVA tests was performed in a custom GUI tool which I made. The NanoCalc spectrometer has its own fitting procedure which enables the experimenter to view the swelling behavior of the samples in real-time, but for later comparison of different fitting procedures and model parameters, a separate fitting software is needed.

Full Python code for the fitting procedure is visible in Appendix B. The figure below is meant to give the reader an impression of the careful monitoring of reflection and intensities at every step in the analysis of SVA data.

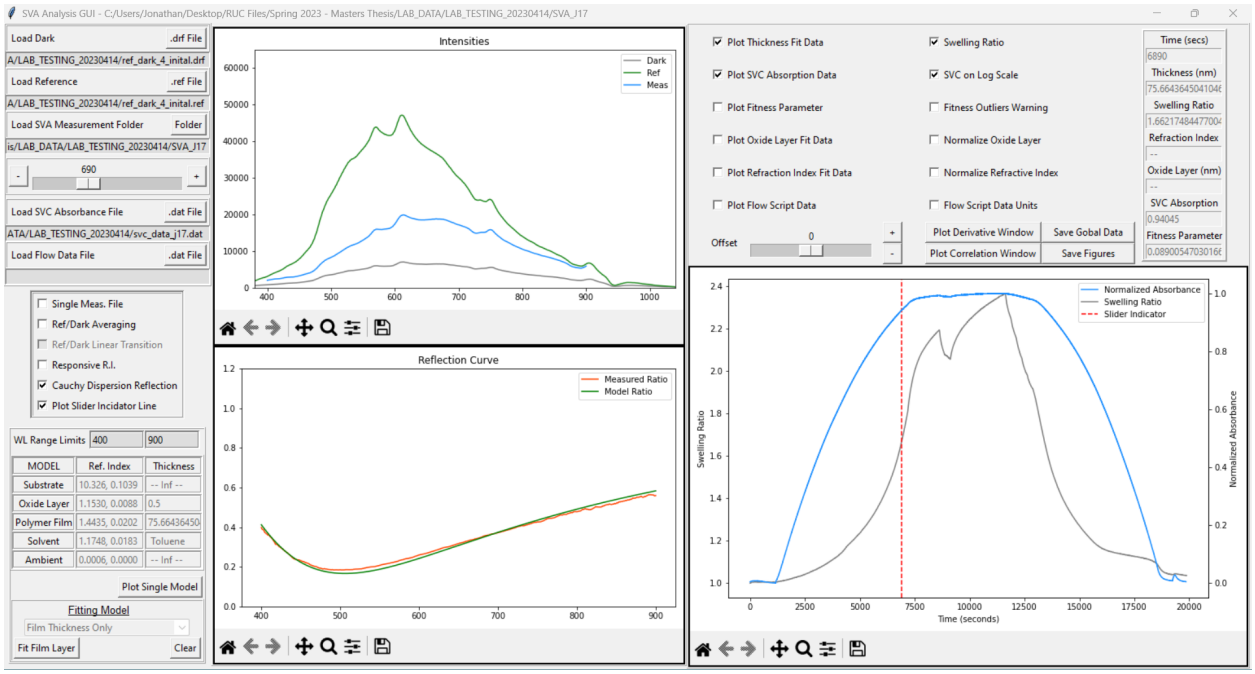

Figure 4.5: Screenshot of the SVA data analysis GUI tool that I made for rapid and efficient comparison of measured data, modelling parameters, and fitting procedures.

5 Results

Nearly 2 dozen SVA tests were performed, and a lot of data collected. The following sections show the notable and relevant results which appear once the data has been analyzed. Most of the analysis is very standard, but some of the later sections (5.7, 5.8, 6.3) discuss something completely different.

5.1 Swelling Behavior

In all SVA tests, the swelling of the polystyrene thin-films show the extreme swelling response at the largest solvent concentration, which is the behavior that initially motivated this project. The first SVA tests were performed to try to reproduce this effect as the first step in investigating the reason for this behavior. Figure 5.1 below shows the results from one of these early tests which shows this very large swelling increase.

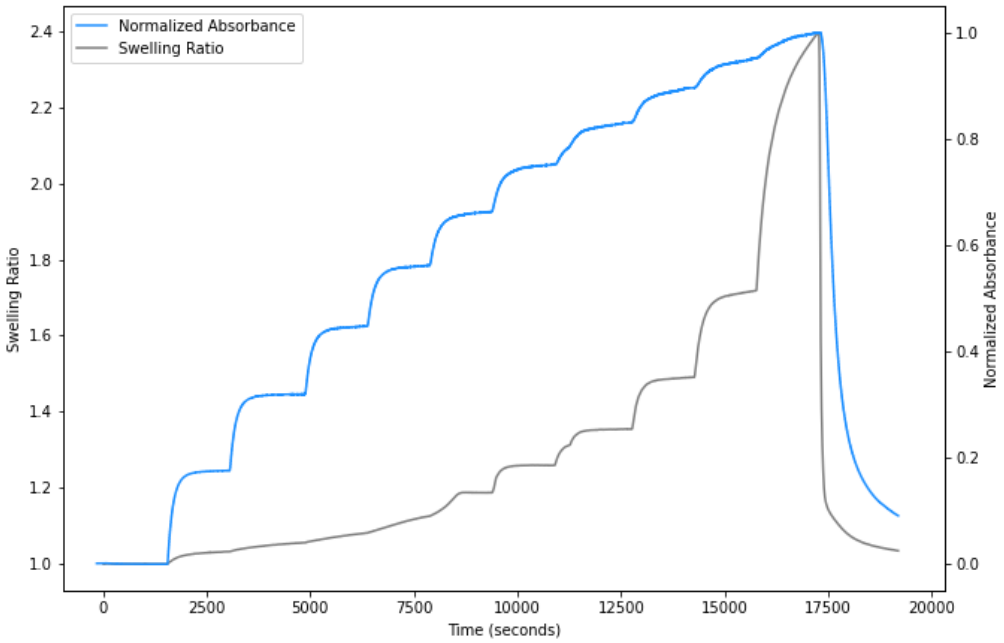

Figure 5.1: Swelling behavior of Polystyrene thin film. The fitted values of the Polystyrene swelling is shown in gray (left vertical axis), and the Normalized Absorbance of the SVC sensor is shown in blue (right vertical axis).

In the example above, the thin film (initial thickness measurement of 111.8nm) is Polystyrene with molar mass of 20K g/mol, and the solvent is introduced in steps of 10%. With the flow rate of the solvent bubbler at 90%, the swelling ratio only reaches 1.719. However, when the solvent bubbler flow rate increases to 100%, the swelling ratio dramatically increases up to 2.397.

Also, the final step in the SVA swelling in this plot seems to be continuing to swell, up until the

programmed flow script quenches all solvent flow and begins to clear the SVA chamber with only N_2 gas. At each previous step in the solvent introduction, the thin film reaches an equilibrium swelling ratio. But when the bubbler is at the full flow rate, the swelling ratio continues to increase for the entire 1500 seconds (25 minutes) and had not reached equilibrium at the time of quenching. This observation raises questions about the SVA procedure. If allowed more time, would the film thickness reach equilibrium at an even larger swelling ratio? Or has the polymer gained so much mobility from the addition of solvent that the film has become unstable, and is beginning to de-wet? More detail on this is given in Section 6.3, which discusses surface energy and the attempts to keep the film wetted to the substrate.

In order to investigate these behaviors and also the other research questions, I experimented with a few different Flow Scripts for the SVA process. The Flow Scripts were explained in more detail in Section 3.4, and the full text of the flow script files are included in the Appendix A. In general, the changes made to the flow scripts were: decreased step size to 1% for better measurement resolution of the solvent vapor concentration, longer time spent at maximum solvent concentration, and also mirroring the flow script by having decreasing steps to slowly 'de-swell' the film instead of the rapid quenching of solvent seen in Figure 5.1. I tried to keep the Flow Script consistent for the remaining tests, but due to both my own errors and computer glitches, some SVA tests still vary in the timing of toluene vapor introduction.

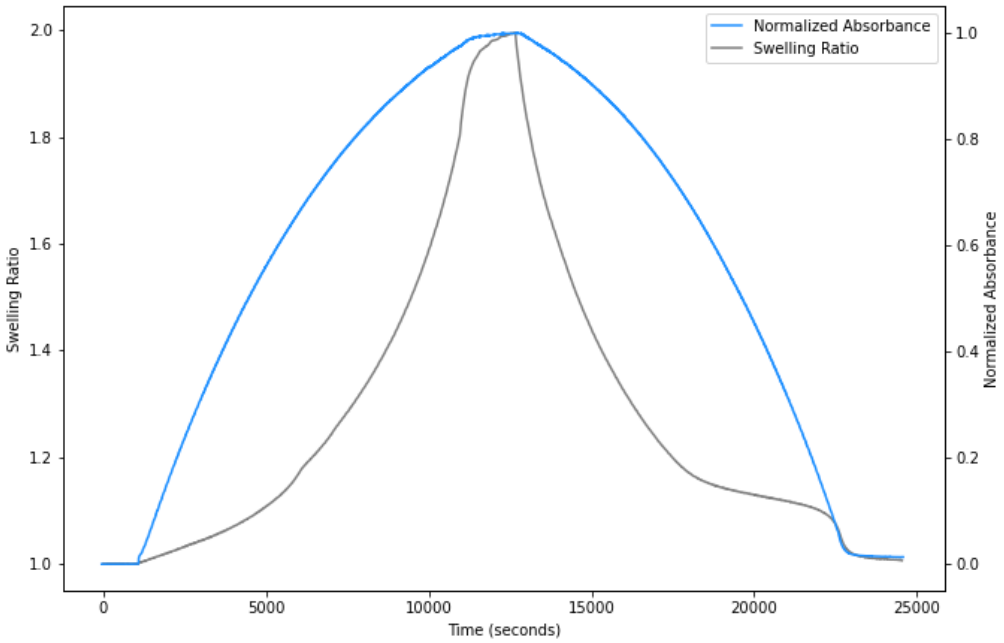

Figure 5.2: Swelling behavior of Polystyrene thin film. The fitted values of the Polystyrene swelling is shown in gray (left vertical axis), and the Normalized Absorbance of the SVC sensor is shown in blue (right vertical axis).

An example of the SVA tests with smaller increments of solvent vapor concentration is shown in Figure 5.2. In particular it is data from sample J26 (Polystyrene, 20 kg/mol, initial thickness 94nm).

The swelling appears as a smoothly varying line for most of the SVA, but at approximately 6000 seconds (SR = 1.18), there is an abrupt change in the rate of swelling. This position represents the glass transition of the thin film: enough solvent has entered the film that the value of T_g is reduced to 24°C and the film enters the rubbery state [Efremov and Nealey, 2022; Laschitsch et al., 1999]. Below this swelling threshold the annealing process has yet to begin, because the polymer remains in the glassy state. The shift of the Glass Transition Temperature was predicted in Section 3.1, using the known density and glass transition temperatures for pure Polystyrene and pure Toluene. Referring to Table 3.1, for molar mass of 20 kg/mol the Glass Transition is expected at a polymer volume fraction of 0.8618, or a Swelling Ratio of SR $= 1.16$. This estimation is remarkably close to the observed glass transition in the data which occurs at SR = 1.18.

$$\frac{1}{297\text{ K}} = \left(\frac{\phi}{0.825 + 0.175\phi}\right)\frac{1}{373\text{ K}} + \left(\frac{1-\phi}{1 + 0.211\phi}\right)\frac{1}{117\text{ K}} \quad \rightarrow \quad \phi = 0.8618 \tag{5.1}$$

The SVA test in Figure 5.2 also includes the film de-swelling, with the solvent vapor reduced in small increments. Significant differences can be observed between the swelling and deswelling thickness behavior, especially below the glass transition. During de-swelling, the film thickness decreases until the glass transition threshold, and then almost completely stops. As soon as the film is returned to a glassy state, the deswelling slows down dramatically, and remains that way until the SVA chamber is almost fully dried of solvent vapor. Surprisingly, another rapid drop in film thickness occurs as the last bit of solvent is removed from the chamber. It seems as though there is 2 transitions for the de-swelling film: the first is the familiar glass transition which returns the film to a glass state, and a second transition which comes much later to drive out any remaining solvent and return the film to its original thickness. Additional data regarding the behavior changes from swelling to de-swelling are in Section 5.6.

5.2 Film Thickness

This section compares the swelling response of thin films which differ in initial condition in only one manner: the film thickness. All samples are made from the same polystyrene polymer source, with molar mass of 20 kg/mol. More samples of this polymer type were made and tested, but many of the early tests failed due to de-wetting.

Sample Name	Initial Thickness (nm)
J6	112
J12	155
J17	43
J18	265
J26	92

Table 5.1: Table of Samples consisting of the same polymer: Polystyrene with molar mass 20 kg/mol. The initial thicknesses of the samples will be used to compare their behavior during SVA.

Figure 5.3 shows the SVA tests for each of these samples, but the solvent flow scripts are not consistent for each test, so not much can be learned from comparing them in this way. This figure is meant to illustrate the range of thickness being tests.

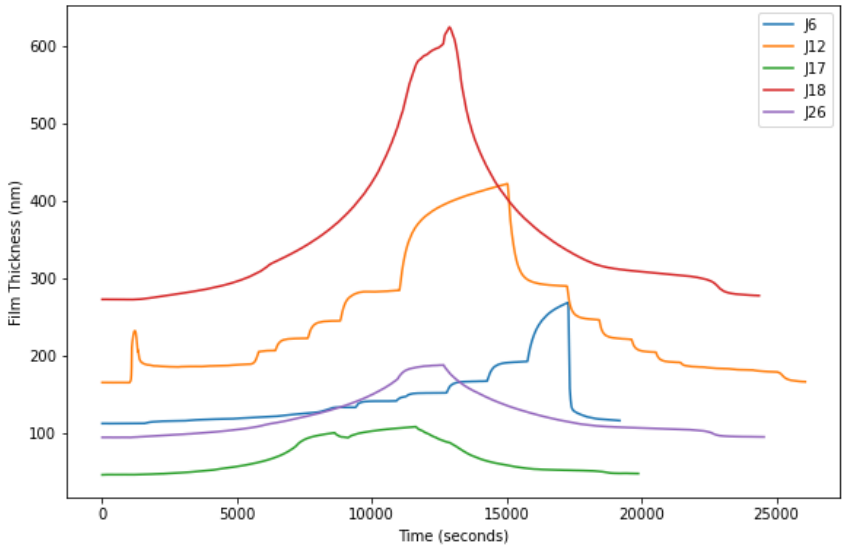

Figure 5.3: Plot of Fitted Thickness values during SVA of samples J6, J12, J17, J18, and J26. The initial thickness vary over the range of 40nm - 260nm. All of the samples are made with Polystyrene with molar mass of 20 kg/mol.

Plotting the fitted values of the Swelling Ratio (instead of film thickness) will scale the data vertically. The swelling response of the same samples is shown in Figure 5.4. While all of the plots start from the same position (SR $= 1$), the maximum value of SR differs across each sample.

Notice that J12 has an accidental swelling spike in swelling at the start of SVA caused by a brief but significant bubble of solvent. A bubble like that always happens after starting the solvent bubbler for the first time since the tank has been re-filled with toluene, but I did not know that at the time.

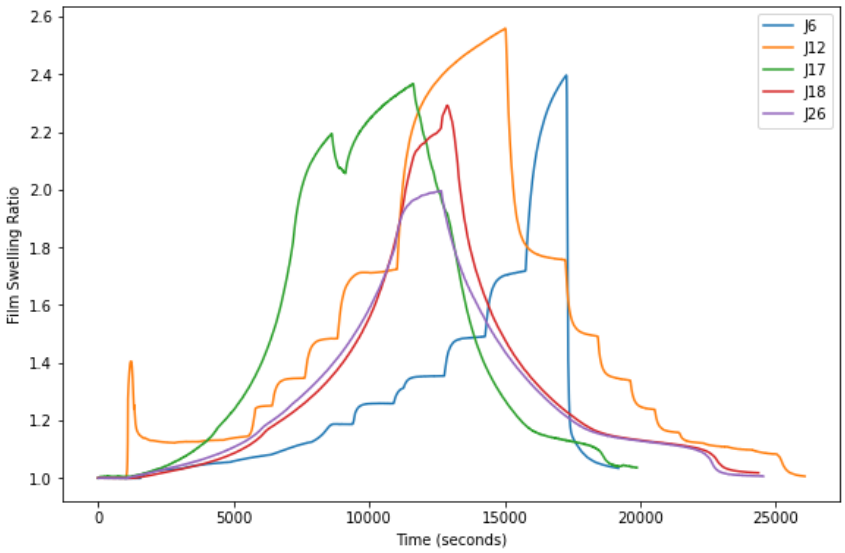

Figure 5.4: Plot of Fitted Swelling Ratio values during SVA of samples J6, J12, J17, J18, and J26. The initial thickness vary over the range of 40nm - 260nm. All of the samples are made with Polystyrene with molar mass of 20 kg/mol.

In the previous 2 figures, the SVA tests have not used the same Flow Scripts, so it is difficult to compare swelling response. For the next figure, I scaled the horizontal axis for some of the data sets such that the time at which the SVA chamber reaches 90% gas flow through the bubbler always occurs at 10,000 seconds.

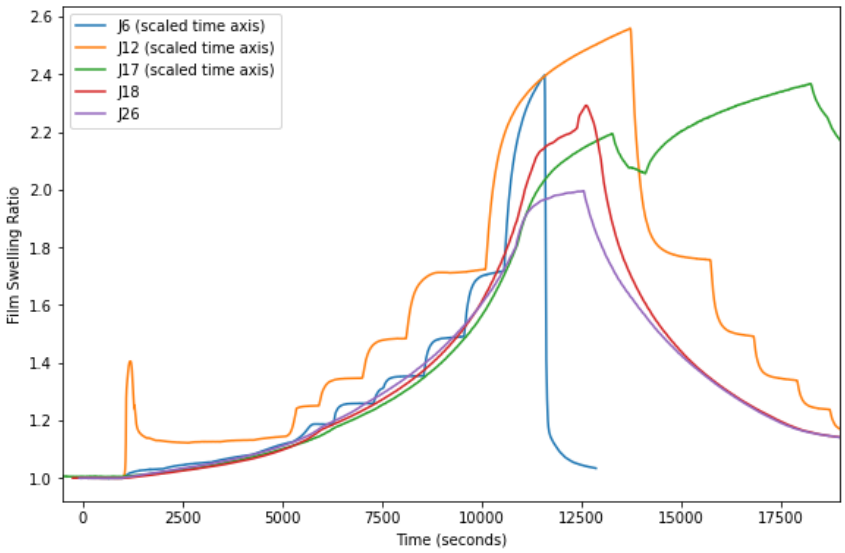

Figure 5.5: Plot of Fitted Swelling Ratio values during SVA of samples J6, J12, J17, J18, and J26. The initial thickness vary over the range of 40nm - 260nm. All of the samples are made with Polystyrene with molar mass of 20 kg/mol. The horizontal axis has been scaled for the data sets of J6, J12, and J17 such that they match the toluene introduction rate of J18 and J26.

With the exception of the over-swelling of J12 caused by the initial solvent bubble, the swelling

responses of each sample appear to all follow the same path. However, the maximum swelling ratio reached is different for each sample. Figure 5.6 is a scatter plot of the maximum SR, plotted against initial film thickness, for each of the samples. The plot does not show any correlation between the initial film thickness and the maximum SR achieved during SVA.

Sample Name	Initial Thickness (nm)	Maximum SR
J6	112	2.397
J12	155	2.559
J17	43	2.367
J18	265	2.292
J26	92	1.996

Table 5.2: Table of Samples consisting of the same polymer: Polystyrene with molar mass 20 kg/mol. Their initial thickness and the maximum Swelling Ratio during SVA are listed for comparison.

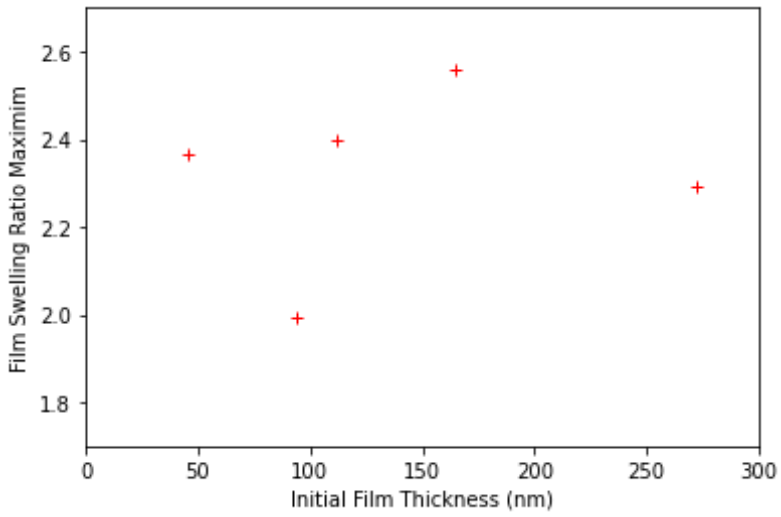

Figure 5.6: Scatter plot of the maximum Swelling Ratio measured during SVA as a function of initial film thickness, for samples J17, J26, J6, J12, and J18 (from left to right). All of the samples are made with Polystyrene with molar mass of 20 kg/mol.

Although the initial thickness does not seem to be correlated with the maximum SR, the SVA tests have other features worth investigating. Figure 5.7 is a plot of the 3 'linearized' (small solvent concentration increments) SVA tests from the 20kg/mol samples. The time axis is shortened to the early swelling section of the SVA test, such that the glass transition behavior is more easily visible. With the larger increments of solvent vapor increase, the glass transition is not discernible.

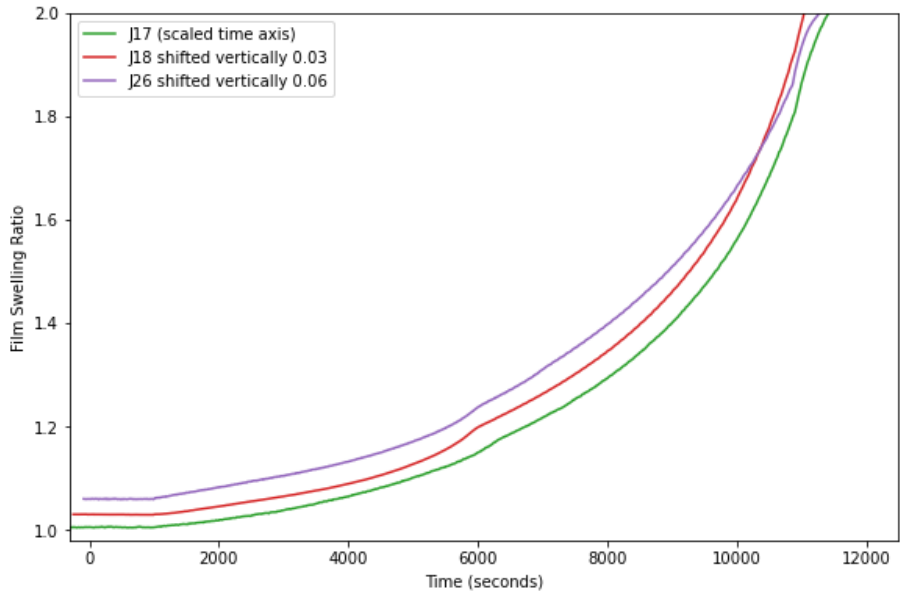

Figure 5.7: Plot of Fitted Swelling Ratio values during SVA of samples J17, J18, and J26. The initial thickness of the samples vary over the range of 40nm - 260nm. All of the samples are made with Polystyrene with molar mass of 20 kg/mol. The horizontal axis has been scaled for the data set of J17 such that it matches the toluene introduction rate of J18 and J26. A vertical shift has been to J18 and J26 for visual clarity.

The swelling ratio curves follow one another quite closely. Close the region of maximum solvent concentration, the thickness of the J26 sample begins to deviate from the other 2 samples, and it will eventually reach a maximum SR value lower than the others (1.99 compared to 2.36 and 2.29). For each sample, the glass transition occurs at nearly the same position. By plotting the derivative of the Swelling Ratio, the phase transition can be seen as a sudden decrease in the swelling rate.

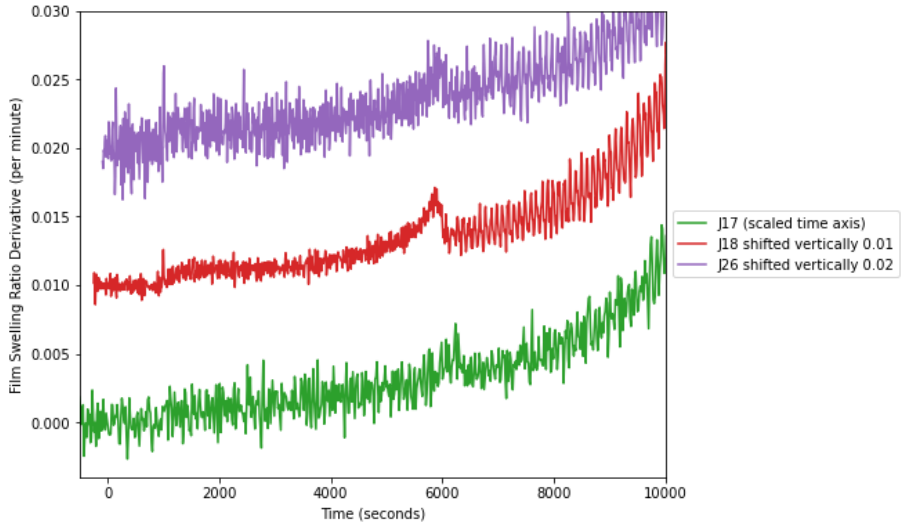

Figure 5.8: Plot of Gradient of the Fitted Swelling Ratio values during SVA of samples J17, J18, and J26. The initial thickness of the samples vary over the range of 40nm - 260nm. All of the samples are made with Polystyrene with molar mass of 20 kg/mol. The horizontal axis has been scaled for the data set of J17 such that it matches the toluene introduction rate of J18 and J26. A vertical shift has been to J18 and J26 for visual clarity. The vertical axis is the rate of change of SR, per minute.

Sample Name	Initial Thickness (nm)	Maximum SR	SR at Glass Transition
J6	112	2.397	N/A
J12	155	2.559	N/A
J17	43	2.367	1.172
J18	265	2.292	1.158
J26	92	1.996	1.181

Table 5.3: Table of Samples consisting of the same polymer: Polystyrene with molar mass 20 kg/mol. Their initial thickness, maximum Swelling Ratio during SVA, and Swelling Ratio at the point of Glass Transition are listed for comparison.

While only 3 data points is not enough to make conclusions, there doesn't seem to be any correlation at all between the initial thickness of the thin film and the glass transition behavior.

5.3 Polymer Molar Mass

Many aspects of polymer dynamics are determined by the molar mass, (as determined by the number of monomer units). Varying the molar mass of the polymer in the thin film will be useful to characterize how these different polymer properties affect the sorption and desorption.

Entanglement of the polymer chains causes a dramatic increase in viscosity of the melt state, and the thickness of the films has been shown to effect the amount of entanglement [Wang et al., 2021].

Entanglement is directly related to the length of the polymers (and thus their molar mass). To understand the effects of entanglement on the SVA process, we will compare the results of swelling and deswelling samples with different molar mass.

Additionally, the glass transition temperature is highly dependent on the polymer length. Below the entanglement length, the polymer glass transition temperature drops off very quickly [Singh et al., 2020]. Because the SVA process functions by shifting the Glass Transition temperature, polymers with low molar mass are expected to have noticeably different swelling behavior during SVA. It should be possible to determine the value of T_g from our SVA data, which can be used to find the relationship between T_g and the molar mass of the polymer.

The maximum swelling response might also be affected by changing molar mass. One explanation for this is χ, the interaction parameter between the polymer and the solvent, is very important in determining the maximum swelling ratio, and exhibits dependence on most aspects of the film composition. I think this would be very interesting, and might indicate that the polymer prefers to form some secondary structures when its length allows. If the secondary structures inhibit or encourage the solvent-polymer interactions, then the maximum swelling ratio will be similarly raised or lowered.

Table 5.4 gives the samples which will be compared, and their molar masses. All samples are Polystyrene, and most vary in initial thickness between 85nm and 100nm. The exception is J20 with molar mass of 6000 kg/mol, which had an initial thickness of approximately 250nm.

Samples	Molar Masses (kg/mol)	De-wetting?
J24	1.8	✓
J25	5.5	✓
J27	11	✓
J26	20	
J22	105	
J20	6000	

Table 5.4: Table of Samples of different molar mass, for comparison of the effect this value has on SVA response.

The 3 shortest of these samples de-wetted from the substrate surface during SVA. For the sake of comparison of the glass transition behavior, I have included truncated versions of the data sets for these samples which excludes the de-wetted portions. The SVA data is plotted below in Figure 5.9.

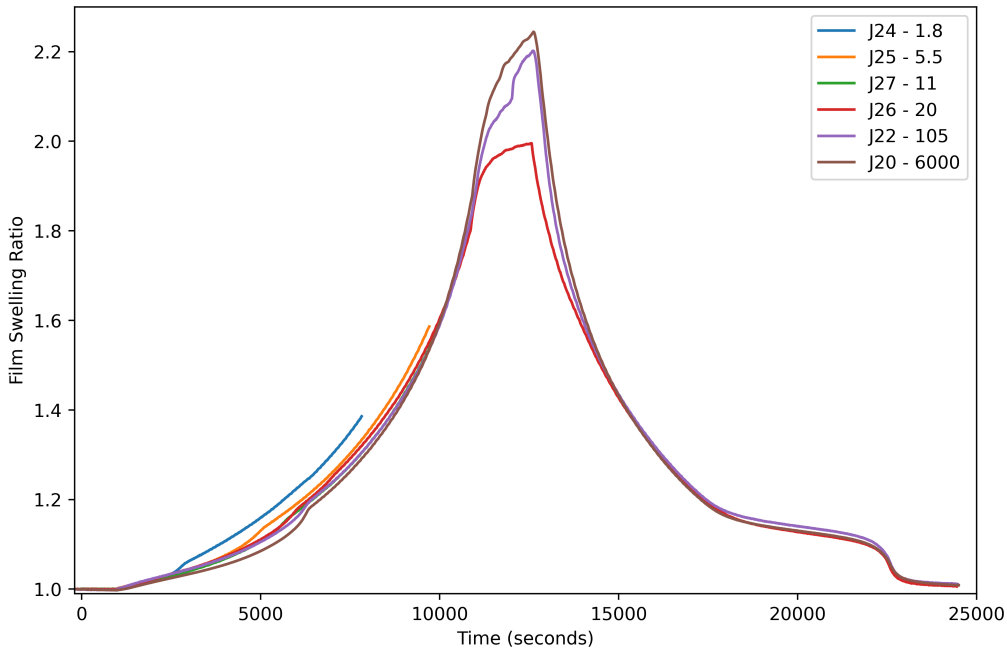

Figure 5.9: Plot of Fitted Swelling Ratio values during SVA of samples J24, J25, J27, J26, J22, and J20. The samples are made with Polystyrene of different molar mass, as listed in the legend with units of kg/mol.

Referring to Figure above, for the first 10,000 seconds the swelling curves show very little variation, with maybe a slight decrease in SR as the molar mass of the sample increases. Near the maximum solvent concentration regime the opposite relationship is seen, as J20 has the largest SR, followed closely by J22 and then J26. However, these 3 data points alone don't amount to a convincing argument for correlation.

Notice the raised portion of sample J24 (and to a lesser extent J25), which is clearly the glass transition occurring much sooner in these low molar mass samples. It was expected that the shortest polymers would transition to a rubbery state the earliest because of the lower glass transition temperature. However, the SR of J24 remains larger than that of the other samples well after all of them have reached a rubbery state. This means that the polymer with lowest molar mass has an equilibrium solvent fraction that is significantly larger than the heavier polymers.

Figure 5.10 below shows the gradient (in units of SR per minute) of the Swelling Ratio for each of these samples. The 'spike', or rather the sudden decreasing rate of change is evidence of the film entering the rubbery state as T_g reaches the temperature of the SVA chamber. The expected relationship is visible: the lowest length polymers enter a rubbery state much sooner than the other samples.

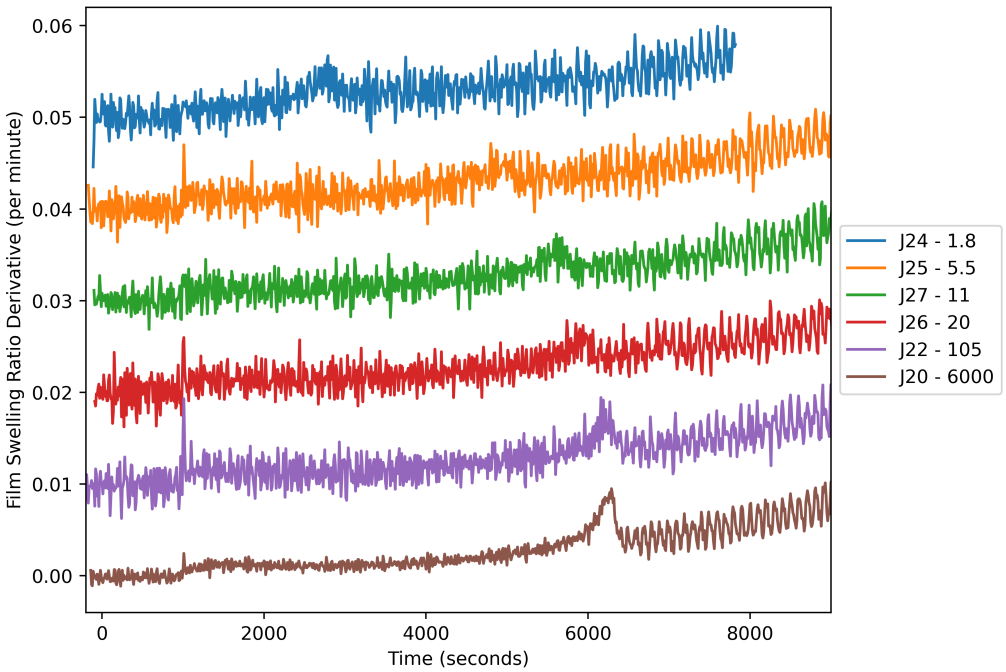

Figure 5.10: Plot of Gradient of the Fitted Swelling Ratio values during SVA of samples J24, J25, J27, J26, J22, and J20. The samples are made with Polystyrene of different molar mass, as listed in the legend with units of kg/mol. The data has been shifted vertically for clarity. The vertical axis is the rate of change of SR, per minute.

Samples	Molar Masses (kg/mol)	De-wetting?	SR at Glass Transition
J24	1.8	✓	1.0536
J25	5.5	✓	1.1395
J27	11	✓	1.1602
J26	20		1.1839
J22	105		1.1892
J20	6000		1.1823

Table 5.5: Table of Samples of different molar mass, for comparison of the effect this value has on SVA response. Also listed is the SR at the Glass Transition, as estimated by the sharp decrease seen in the value of the SR gradient.

Having used the gradient plot to obtain to values of SR at Glass Transition for each sample, these can be compared to the estimated relationship suggested by the Fox equation (Equation 2.1). Figure 5.11 shows both the Fox equation estimate of the Swelling Ratio at the Glass Transition, as a function of the pure polymer glass transition temperature, and the equivalently plotted data points from Table 5.5 above. The variables show obvious correlation, with a slight shift towards higher SR than expected by the Fox equation. The difference is slight, so it could be that counting the SR values from the gradient plots has a tendency to overestimate them. Or, it is also possible that the

assumed Glass Transition Temperature of Toluene ($T_{g,S} = 117$K) doesn't appropriately describe its behavior in a low concentration solution. Toluene crystallizes easily and is a poor glass-former.

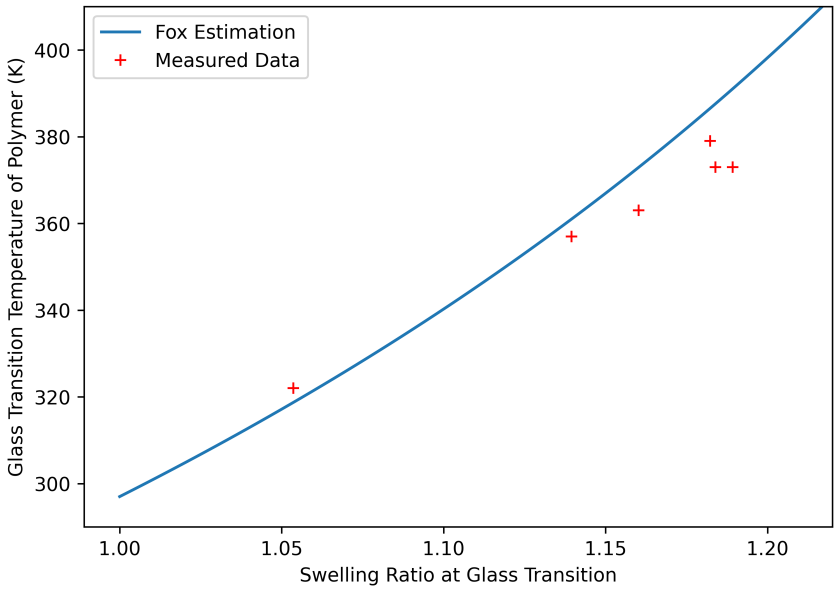

Figure 5.11: Plot of the Fox Equation as shown in Equation 3.2, with $T_{g,S} = 117$K, and the data collected from samples of different molar masses. The vertical axis is the Glass Transition temperature of the pure polymer in Kelvin. The horizontal axis is the Swelling Ratio at which the Film has its glass transition.

Returning to the swelling behavior of the samples, I want to focus on a particular section of the data in Figure 5.9. In the region where all of the samples have entered the rubbery state, but before any of them have de-wetted, the distribution of their Swelling Ratios indicates a significant difference for the smallest length polymer. Figure 5.12 is a zoomed in version of the full SVA thickness data. It is obvious that sample J24 (1.8 kg/mol) is significantly more swollen than the other samples. This is not simply because it has a lower glass transition, because all of the other samples have been rubberized as well. At the listed test time of 7500 seconds, J24 has swollen at least 10% more than all the other samples. This might suggest that the interaction parameter χ, which quantifies the enthalpy of mixing solvent and polymer, might be significantly lowered in low molar-mass polystyrene. Recall from Section 3.1 that literature sources have a range of different values for χ.

Before continuing further with this idea of variable interaction parameter, it is necessary to make a direct comparison of the collected SVA data and the Flory-Huggins solution theory.

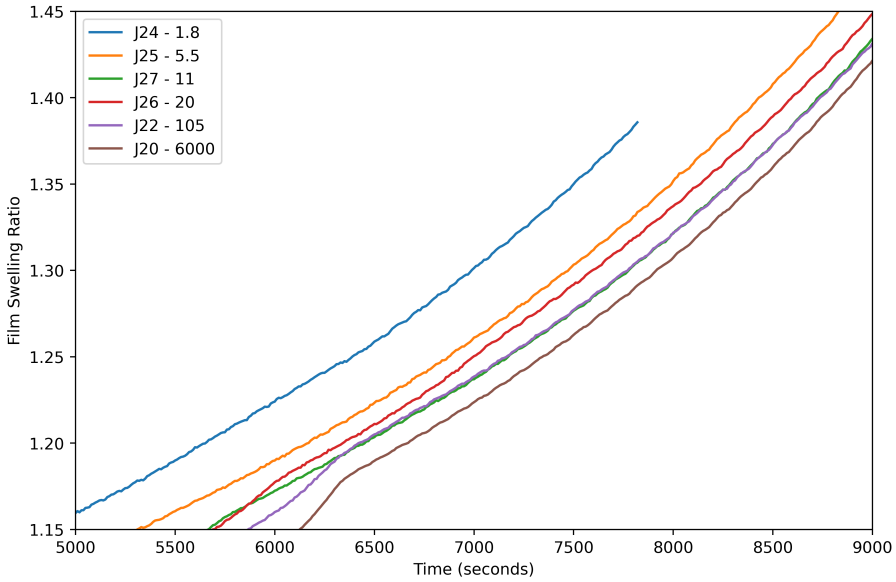

Figure 5.12: Plot of Fitted Swelling Ratio values during SVA of samples J24, J25, J27, J26, J22, and J20. The samples are made with Polystyrene of different molar mass, as listed in the legend with units of kg/mol. The image is looking at a small section of the full SVA plot to show deviation of SR between the samples in the rubbery state.

5.4 Fitness to the Model

Previously in this report, the Flory-Huggins (F-H) solution theory was shown to act as a model of SR as a function of solvent activity. At this time, it is worth comparing the measured swelling response to the expected response based on Flory-Huggins.

$$\frac{p}{p_{\text{sat}}} = (1-\phi)\ \exp\left[(0.42)\,\phi^2+\phi\right] \tag{5.2}$$

The expected relationship between polymer volume fraction (ϕ) and solvent activity ($a = p/p_{sat}$) was given in Equation 2.8. Using an interaction parameter for Polystyrene and Toluene of $\chi = 0.42$, and an assumed polymer molar volume much larger than toluene molar volume ($V_{m,\text{P}} >> V_{m,\text{S}}$), the variables in the model can be compared to the collected SVA data, provided that 2 crucial assumptions are made:

1) The swelling ratio is the reciprocal of the polymer volume fraction. This is only true if sorption of a certain volume of solvent produces an equivalent increase in the volume of the thin film. (i.e. no free space in the film before solvent is added)

2) The normalized absorbance is equivalent to the solvent activity. This is only true if the SVC measurement of minimum transmittance corresponds to completely wet gas (100% relative humidity), and a maximum transmittance corresponds to fully dry gas (no solvent vapor at all)

Looking at Figure 5.13, the curves for the Flory-Huggins (F-H) prediction clearly doesn't follow the data. The glass transition behavior of the sample is seen near $A_{\text{normed}} = 0.7$, and $SR = 1.2$. It is expected that above the glass transition, the F-H theory should match the measured SR value of the thin film.

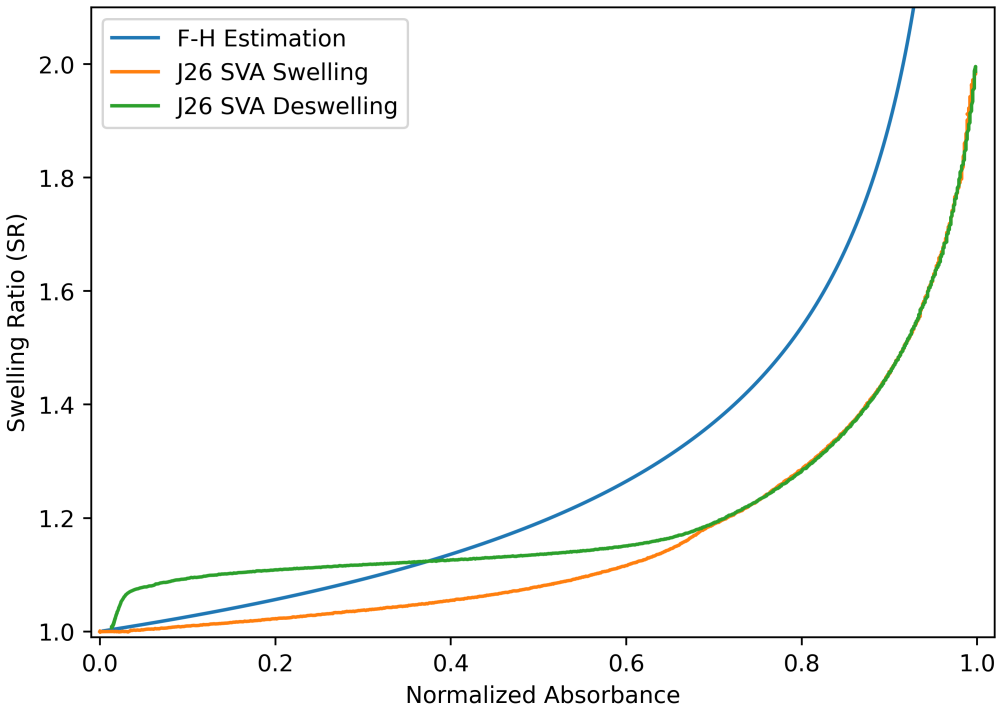

Figure 5.13: Plot of Swelling Ratio as function of Normalized Absorbance. The Flory-Huggins estimation assuming volume conservation and perfect absorbance is shown in Blue. The value of the interaction parameter for PS and Toluene is $\chi = 0.42$. The ratio of molar volumes is assumed to be negligible, ($V_{m,S}/V_{m,P} = 0$). The SVA swelling and de-swelling curves for sample J26 are also plotted. J26 is thin film with PS 20K molar mass, and initial thickness of 92nm.

This discrepancy between the theory prediction and the measured data suggests that the assumptions need to be reconsidered.

1) If there is free space in the polymer film, even before the solvent vapor is introduced, then some of the absorbed solvent will *not* contribute to increasing the thickness of the film. In other words, the volume of the system is not conserved, because some of the original volume of the dry film was empty space. The relationship between SR and ϕ must be updated:

$$\text{SR} = \frac{1}{\phi} \qquad \longrightarrow \qquad \text{SR} = \frac{1}{\phi} - \text{SR}_{\text{holes}} \tag{5.3}$$

With this new expression, the value of SR_{holes} is an unknown parameter which represents the portion of the full SR which comes from holes. Given the same value of ϕ, the value of SR is less than before, because some of the adsorbed solvent which *does* contribute to lowering ϕ, does *not* contribute to increasing SR. This will present as a very non-physical effect when there is very little solvent, because the predicted value of SR is less than 1. However, F-H theory is only supposed

to describe the film when already swollen and above the glass transition, and we can confidently claim that in a rubbery state the film will not have any holes.

2) If the absorbance is not properly normalized, then we might expect that the scale of the horizontal axis is incorrect. The most obvious possibility for causing this is that the Solvent Bubbler does not provide full saturation (100% humidity) to the N_2 bubbles passing through it. As a result, the solvent activity never reaches a value of 1 inside the SVA chamber. This same effect might instead be caused by a temperature difference of the SVC chamber, or maybe an electronic limitation of the internal UV photo-diode, but the solvent bubbler having less than fully wetted bubbles makes the most immediate sense. Recall that the F-H equation has asymptotic behavior at solvent activity of 1, so without this under-scaling of horizontal axis, the only way for the data to match the theory at maximum solvent concentration is to have infinite SR. The relationship between Normalized Absorbance and Solvent activity is re-defined:

$$A_{\text{normed}} = a = \frac{p}{p_{\text{sat}}} \qquad \longrightarrow \qquad A_{\text{normed}} = \frac{a}{\text{H}_{\text{Bubbler}}} = \frac{p}{p_{\text{sat}}} \times \frac{1}{\text{H}_{\text{Bubbler}}} \tag{5.4}$$

The added parameter is $\text{H}_{\text{Bubbler}}$, the effective solvent humidity of the gas when leaving the bubbler. If the bubbler only produces bubbles with 90% humidity, then even at maximum producible solvent vapor concentration ($A_{\text{normed}} = 1$), the solvent activity will only reach a value of 0.9

With these two changes to our assumptions, the Flory-Huggins prediction for the relationship between SR and A_{normed} must be updated:

$$(A_{\text{normed}})\,(\text{H}_{\text{Bubbler}}) = \left(\frac{\text{SR} + \text{SR}_{\text{holes}} - 1}{\text{SR} + \text{SR}_{\text{holes}}}\right) \exp\left[\frac{\text{SR} + \text{SR}_{\text{holes}} + 0.42}{(\,\text{SR} + \text{SR}_{\text{holes}}\,)^2}\right] \tag{5.5}$$

With this new formulation, SR_{holes} and $\text{H}_{\text{Bubbler}}$ are unknown parameters. Notice that one of these parameters depends on the sample (SR_{holes}), and the other does not ($\text{H}_{\text{Bubbler}}$).

Using the same data set presented in Figure 5.13 from sample J26, least-squares fitting of the 2 parameter F-H equation. The range of data selected for the fitting was $0.7 < A_{\text{normed}} < 0.99$. The lower limit of this range was chosen because below 0.7, the swelling and de-swelling curves of the SVA data separate, which indicates the glass transition of the film. Fitting was performed for both swelling and deswelling data, and Table 5.6 below shows the results of the fitting, and also the average.

Fitting Data	$H_{Bubbler}$	SR_{holes}
Swelling	0.90468	0.11327
Deswelling	0.90521	0.11292
Average	0.90495	0.11310

Table 5.6: Table of Parameters for the Flory-Huggins approximation which has been adapted to match the SVA results. Values of the parameters were obtained from fitting to J26 SVA data in the region from $0.7 < A_{normed} < 0.99$. Both swelling and de-swelling curves were fitted, and the average of these parameters is given.

The Fitting result shows very good agreement between the Swelling and De-swelling data, which is encouraging. The physical interpretation of the results is worth re-iterating. The value $H_{Bubbler} = 0.905$ means that when leaving the bubbler the N_2 gas only has humidity of 90.5%. The value of $SR_{holes} = 0.113$ suggests that the dry polymer film (no solvent), has holes which account for 11.3% of the volume of the film.

More the 10% of volume being free space holes seems like an overestimation, but it is of a reasonable order of magnitude. Holes in the film can be quite common, and will release to the surface causing the speckled pattern seen in some microscope images like Figure 5.14 [Zha et al., 2021]. However, I cannot be certain that the release of free space holes is what I am looking at in this image.

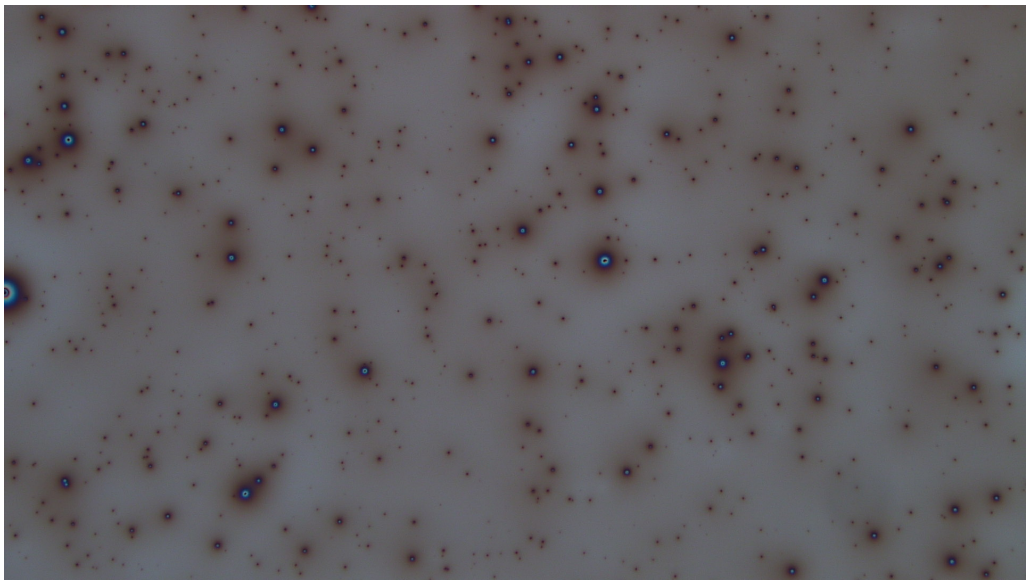

Figure 5.14: Microscope image showing a the surface of a film with many small defects.

The fitted parameters for the F-H equation are used to plot the blue line in Figure 5.15. The result can be seen to still slightly deviate from the data set. Both near the glass transition, and the maximum absorbance, the F-H estimate is below the measured SR of the sample. Improving

the fit in these regions would require either changing the value of the interaction parameter χ, or adding an additional free parameters in the F-H model. I have tried a few options for a third parameter to improve the fitness, and I encourage future researchers to add parameters as they please, but I cannot find a physical justification to make further parameter changes to my model. Additionally, every attempt that I made to add a third free parameter without physical justification, the resulting parameter values show large deviation between the swelling and de-swelling data, which certainly should not occur.

Adjusting the value of χ from the chosen value of 0.42, up to a much higher value of 0.7 allows the F-H prediction to quite closely follow the SVA data. $\chi = 0.7$ is far beyond the range mentioned in any literature I have found regarding Polystyrene and Toluene in this temperature range.

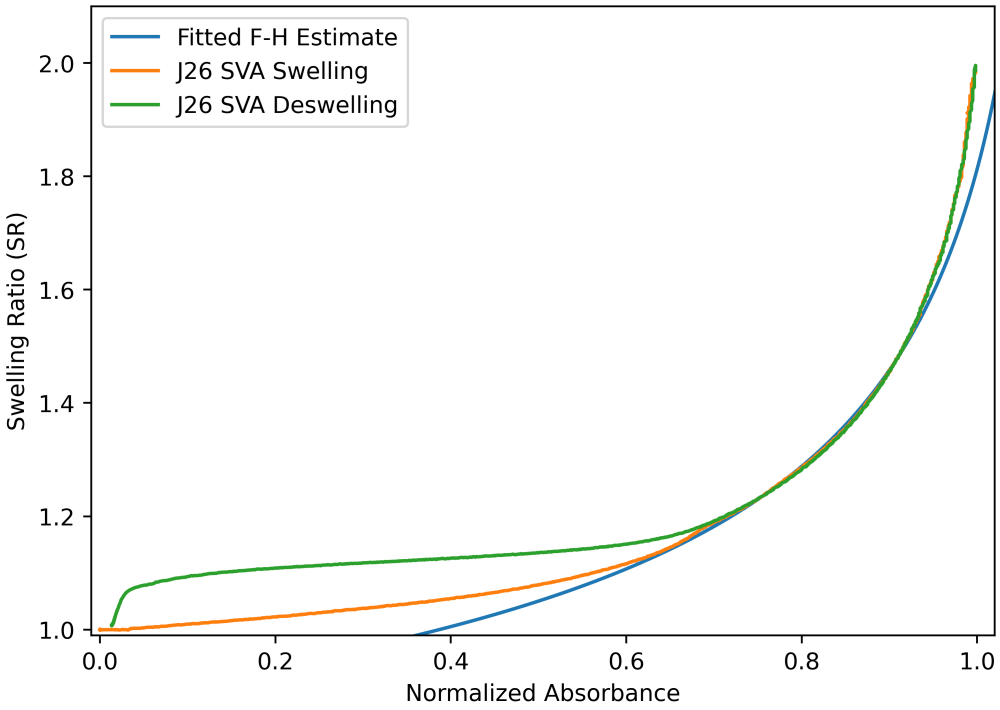

Figure 5.15: Plot of Swelling Ratio as function of Normalized Absorbance. The SVA swelling and de-swelling curves for sample J26 are plotted. J26 is thin film with PS 20K molar mass, and initial thickness of 92nm. The Flory-Huggins estimation from Equation 5.5 is fitted to the sample data, and resulting parameters are used to plot the Blue line. ($\chi = 0.42$, $V_{m,S}/V_{m,P} = 0$).

5.5 Another look at the Bubbler

We have seen that in order to match the collected SVA data, the Flory-Huggins model equation has to be modified with free parameters which can scale both the Normalized Absorbance variable and the Swelling Ratio variable. In this section I will explore the parameter which determines the Absorbance scale, $H_{Bubbler}$. I previously suggested that the physical reason for this scaling is the performance of the solvent bubbler. If the bubbler doesn't produce gas with full solvent saturation,

then the activity and absorbance will not be matched.

The performance of the Bubbler is likely to depend very highly on the fill level of the solvent tank. In my experience, the amount of solvent depleted from the bubbler is generally quite low. After using the bubbler for multiple SVA tests, I went to re-fill the tank only to find that the tank was still nearly 80% filled. Because of this, most days I paid little attention to the solvent bubbler, only bothering to re-fill it every couple of weeks.

To better understand the effect of the bubbler, I went back through my notes and counted the days when the tank was being used and when it was re-filled. I then plotted the maximum swelling ratio of each sample as a function of the number of days since the bubbler had bee refilled. This plotting is shown in Figure 5.16. There is a clear correlation between these 2 variables, and linear regression produces a fitted line with this form:

$$\mathrm{SR}_{\mathrm{max}} = 2.4203 - 0.04737 \times (\text{SVA tests since last refill}) \tag{5.6}$$

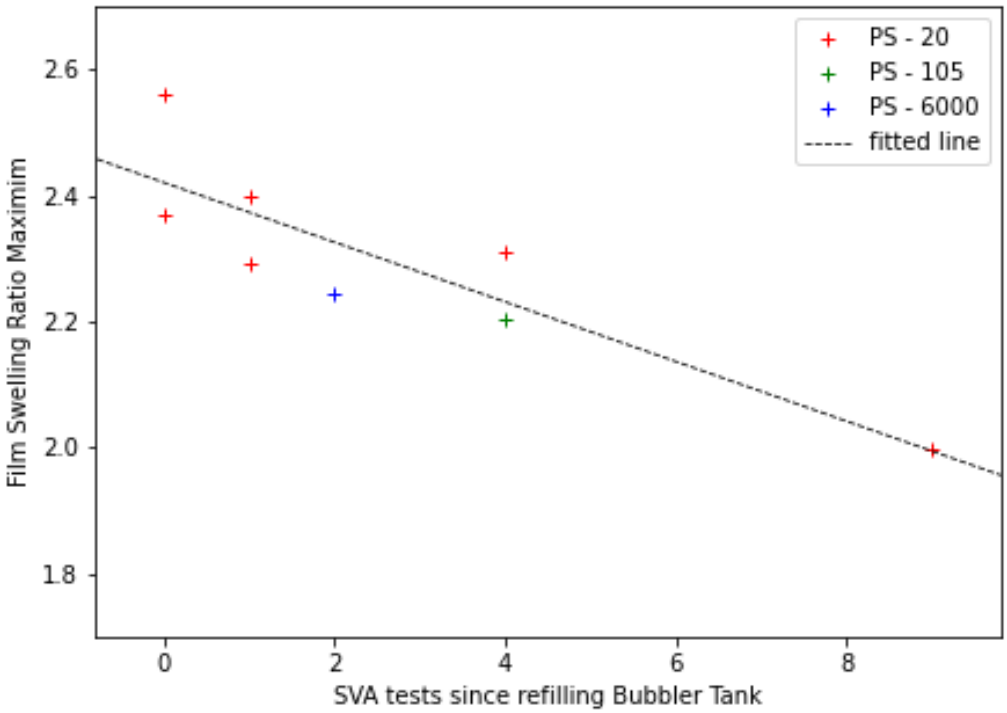

Figure 5.16: Scatter plot of the maximum Swelling Ratio during SVA, as a function of the number of SVA tests since the Solvent Bubbler was re-filled. The data is separated by color to distinguish the molar mass of Polystyrene used in the sample. 0 days indicates that the bubbler was re-filled immediately before stating the SVA test. The fitted line follows $y = (-0.0474)x + 2.42$, for x plotted on the horizontal axis and y on the vertical axis. R^2 value is 0.77, and p-value is < 0.005.

The correlation in this plot is quite striking. Even without the outlier data point on the far right of the Figure, the fitted line has approximately the same parameters, albeit with a larger p-value.

While this is still not a definitive explanation for the variation in maximum swelling ratio, it

strongly suggests that the fill level in the solvent bubbler tank should be more closely controlled.

5.6 Swelling vs. De-Swelling

In this section, I would have liked to apply the same adjusted Flory-Huggins model to additional sets of SVA data, and try to establish a relationship between the value of SR_{holes} and the polymer molar mass. Unfortunately, I am not able to do that because the correlation data for many of the SVA tests is too distorted to be usable. I will explain why that happened, and also talk about the hysteresis around the glass transition that can be seen in the SVA of every sample.

The parameters in the Flory-Huggins model are obtained by fitting the model to the data in the region above the glass transition. Below the glass transition, the F-H theory does not apply. In order to have usable data that F-H can be fitted to, each fitted swelling ratio value must be matched to a corresponding value of absorbance. As an example, Figure 5.17 shows a plot of the swelling ratios and normalized absorbance of sample J22 (105 kg/mol). The correlation plot shown beside it has obvious distortions that result from condensate affecting the normalized absorbance value. But the condensate is only part of the problem. As mentioned in Section 3.3, the SVC sensor functions on a separate clock than rest of the equipment, and the improper timing of the data collection means that precise correlation of these 2 variables is not possible. Neither for the swelling nor the de-swelling curves can the values of SR be mapped onto values for the Absorbance.

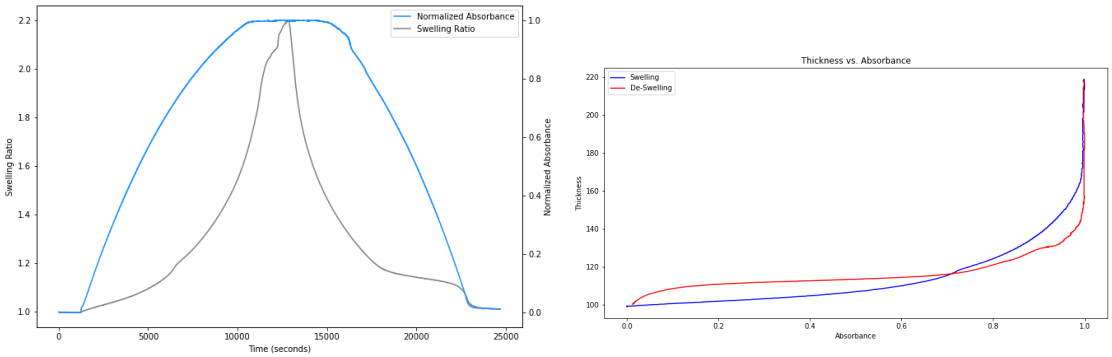

Figure 5.17: Swelling Ratio and Normalized Absorbance plots for sample J22, Polystyrene with molar mass 105kg/mol, and initial thickness 92nm. On the left, the variables are plotted against time, and on the right against themselves.

I was able to partially ignore this problem in the previous section, because the swelling and de-swelling curves for Sample J26 followed the same shape. All that I had to do was to center the SVC data between them so that the correlation curves matched. In this way, the correlation data from the J26 sample is also incorrect (because the SVC timing cannot be relied upon), but the swelling and de-swelling curves have been made equally incorrect. For all of the other SVA tests, the de-swelling data has been at least partially distorted by condensate. Because of this, I will have to leave further attempts to quantify these parameters for a separate project.

Instead, I would like to discuss another interesting feature of correlation plots, the hysteresis around the glass transition. When swelling out of the glassy state, the thin film has a sudden decrease in its swelling rate. This 'kink' is described as being determined by solvent hole filing. When the polymer is returned to the glassy state by the desorption of solvent, some the free sites (which had be empty hole), retain their bonded solvent molecules following Langmuir statistics [Efremov and Nealey, 2022; Laschitsch et al., 1999]. The SVA data shown in Figure 5.18 demonstrates the significant swelling hysteresis of the glassy state. The sample shown in this image is J17 (PS, 20kg/mol, and thickness approximately 43nm) The area between the two curves in the low Absorbance region if referred to as having excess solvent uptake: The thin film is retaining more solvent molecules than predicted. In this regime, the Flory-Huggins solution theory predicts that the polymer is will have a solvent volume fraction that changes linearly with absorbance. Instead, because the polymer is in a glassy state, free sites within the polymer chain have become populated with solvent, and require additional effort to be broken from their bonds.

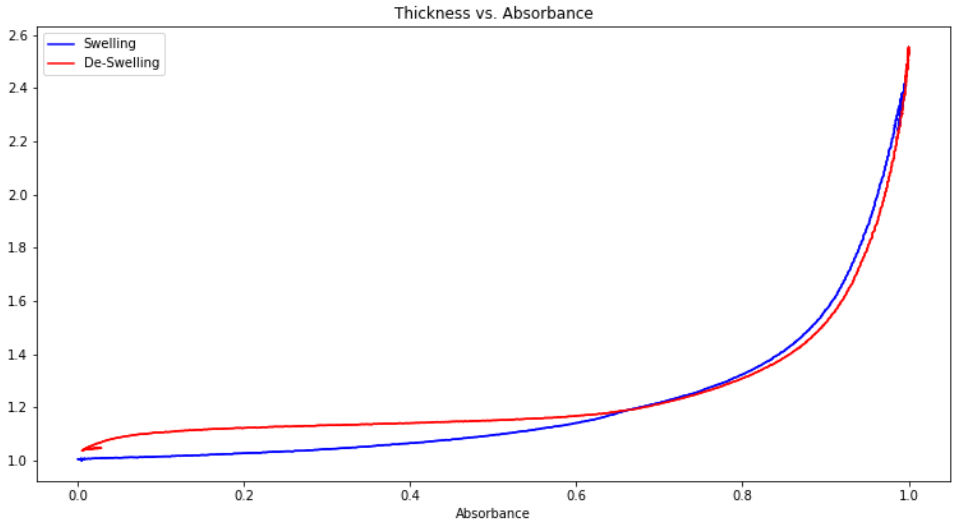

Figure 5.18: Correlation plot showing the change in different behavior between swelling and de-swelling. Sample is J17, (Polystyrene with 20kg/mol molar mass and approximately 43nm thickness)

Another sample (J19) was made to match J17 in almost every way (PS, 20kg/mol, thickness 45nm). With J19 the wafer was first thermally annealed in a vacuum oven at 80°C for a full day. After being removed, J19 was tested in SVA just like J17. Figure 5.19 shows the correlation plots for both J17 and J19; the Swelling Ratio plotted against the Absorbance data. There is a major difference in the swelling ratios of the 2 films. J19 has a very pronounced glass transition behavior. The 'kink' which separates the glassy and rubbery state is much sharper in J19 than in J17. This suggests that maybe the thermal annealing process trapped more of the free sites of the sample J19, such that the sample must be subject to relatively large solvent vapor pressures before the solvent is able to adsorb into those free sites of the polymer chain.

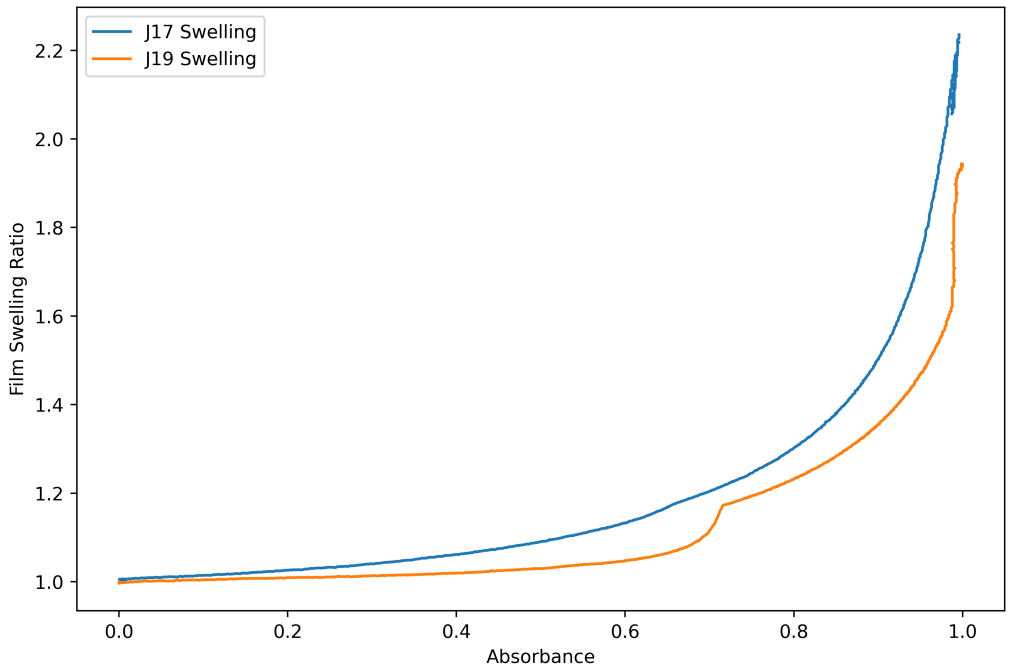

Figure 5.19: SVA correlation data for J17 and J19. The Swelling Ratio is plotted over the Absorbance. Notice that J19 has a much more pronounced Glass Transition.

5.7 Effects of Thermal Annealing

The previous section identified swelling ratio hysteresis as the thin films are swelled and de-swelled. Even with very low solvent concentrations the thin film remains noticeably swollen above its initial thickness.

One reasonable explanation for this observation is that the polymer film had been strained by the rapid spin-coating process, and after the solvent annealing, the film's slightly larger thickness was a more energetically favorable configuration than the initial strained configuration. This explanation would suggest that before the solvent annealing, the thin film is not able to reach an equilibrium state because the film is kept well below the glass transition temperature and the polymers are unable to 'relax'. The polymers experienced horizontal (relative to the film normal) mechanical tensile stress from the centrifugal force of the spin-coating, causing them to contract vertically. These stresses cannot be relieved until the polymers are brought to their rubbery state. The rubbery state is achieved during the solvent vapor annealing process, and the increased mobility of the polymers allows them reach an equilibrium configuration by contracting horizontally and expanding vertically. When the film is de-swelled at the end of the annealing process, there is no application of stress to the polymers, so the film remains in the thicker configuration even when fully dried.

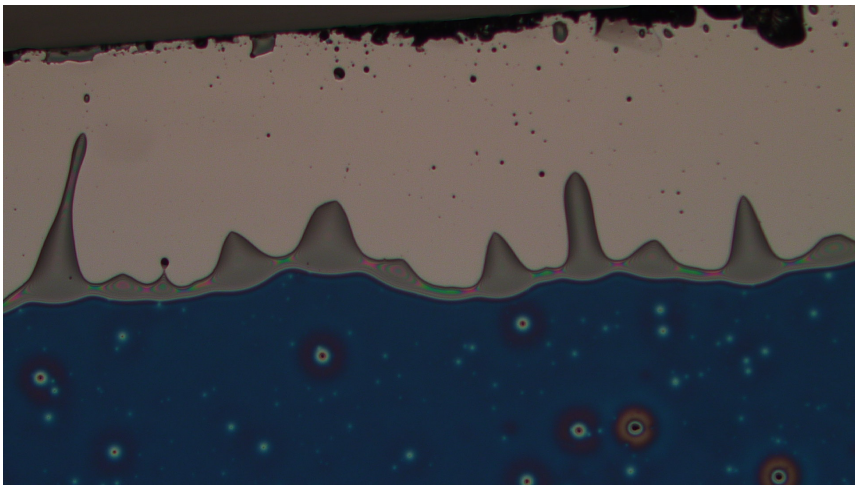

Figure 5.20: Microscope Image (5X) showing the edge of a Silicon wafer (top), with the polymer thin film receding away from the edge. The polymer is Polystyrene with molar mass 105K g/mol, with thickness of about 100nm.

Some physical evidence which may support this first explanation is the microscope images of samples after SVA. In Figure 5.20, the film can be seen to have receded away from the edge of the wafer, although the current state is clearly an effect of de-wetting. The polymer is collecting along a line which runs parallel to the wafer edge, where it is not only much thicker than the remaining thin-film (bottom), but also forms 'spikes' which extend back over the substrate. The spikes have some variety in length and thickness. The de-wetting may be a result of the same relaxation which enabled polymers in the center of the film to expand vertically. For polymers at the edge of the wafer, the mechanical stresses from spin coating kept them fixed while only being pulled in one direction. Once rubberized, their relaxation is directed in-plane, and reduces surface area. More about de-wetting is shown in Section 6.3.

A second explanation for the thickness increase after SVA is that some toluene is not fully removed during the drying process. The solvent diffusion and later desorption is slowed as the polymer film is dried and returns to the glassy state. More importantly, the annealing likely exposed binding sites of the polymer that had been kinetically trapped previously. The toluene molecules are able to form strong bonds at these sites which enables them to remain in the film after the SVA has finished [Efremov and Nealey, 2022].

To investigate these explanations, 2 wafers were *thermally* annealed, with thickness measurements taken before and after. The thermal annealing will take place in a vacuum chamber, such that no oxygen will react with the film, and anything desorbed from the film will be pumped out. For the first of the wafers (J17), Solvent Vapor annealing was performed *before* the later thermal annealing. And for the second of the wafers (J19), the wafer was first thermally annealed, and then *afterwards* was Solvent Vapor annealed.

According to the first explanation for the hysteresis (mechanical tension), the effect of thermal an-

nealing should have no effect at all on the thickness of a thin-film which has already been annealed with solvent vapor. However, a thin-film which has not yet been solvent annealed should release its horizontal tension and expand vertically during the thermal annealing, at which point the later solvent annealing should show no hysteresis.

Alternatively, the second explanation for the hysteresis (trapped solvent) would suggest that the thin-film which is first solvent vapor annealed should become thinner during the later thermal annealing, as the heat raises the polymer mobility and encourages desorption of the now loosened solvent molecules, and then the vacuum is able to pump them away. With the solvent no longer trapped, the polymer film can become thinner, likely returning to its pre-SVA thickness and erasing the hysteresis. However, according to this explanation the polymer film which is first thermally annealed would not change its thickness at all while in the vacuum oven. Only later during the SVA will the film absorb and trap some solvent which will induce the increase the thickness.

The two proposed explanations predict opposite results from the Vacuum Oven annealing, so this test should provide evidence regarding which phenomena is occurring and causing the hysteresis.

The thermal annealing method was quite simple. With the 2 samples inside, the vacuum chamber was evacuated to a pressure of 0.1 mbar, and then the heating element was turned on, raising the temperature from approximately 20°C up to 80°C. The wafers were left to anneal overnight, and the next morning the heat was turned off. After a few hours of cooling, the air-inlet valve is opened and the chamber returned to room temperature and pressure.

The following data was collected. The values listed here are for the polymer film layer thickness, based on the Nano-Calc model. The silicon oxide layer thickness was variable, but remained between 0nm and 2nm.

Wafer	J17 Thickness (nm)	J19 Thickness (nm)
Meas. 1	42.5	–
SVA Test	43.7 $\rightarrow$ 45.0	–
Meas. 2	41.9 42.6	44.2 44.5
Meas. 3	40.3 38.7 38.2	43.7 45.7 44.3
Vacuum Oven	✓	✓
Meas. 4	41.9 41.0 43.4	42.0 45.4 44.8
Meas. 5	–	45.7
SVA Test	–	47.5 $\rightarrow$ 48.4

Table 5.7: Thickness measurements for samples J17 and J19, which indications about the order and timing of the measurements. All values are in nanometers. Thickness modelling is performed by the NanoCalc.

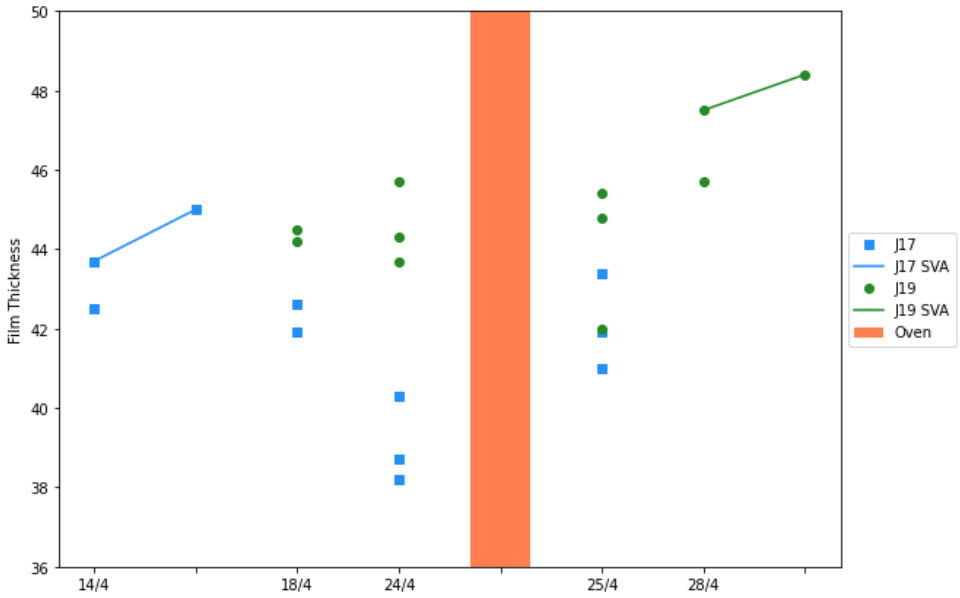

Figure 5.21: Plot of Fitted Thickness values for samples J17 and J19. The data is collected over several days, including a thermal annealing session in a vacuum oven (orange bar). Each measurement is represented by a single data point, and the SVA tests are represented by the line segments. The end-points of the line segments indicate the initial and final thicknesses of the sample during the SVA test, and are meant to help visualize the hysteresis.

The thermal annealing test and the reflectometry measurements defy both of the proposed explanations for the dry film thickness changes before and after SVA. There is no clear trend in the data, and the uncertainty in the measurements is quite large.

In Figure 5.21, the line segments represent the SVA tests, and the endpoints show the initial and final measurements of the thickness. In both cases, the samples have a larger thickness at the end of SVA than at the beginning, and by approximately the same amount (1nm). It does not appear that the thermal annealing in the vacuum oven has changed the dry film hysteresis at all.

The most prominent change in the data is between $18/4$ and $24/4$. The thickness of J17 seems to have dropped about 2.5nm. The change is not much more than the statistically expected measurement deviation. If drop in thickness is to be believed, I cannot find explanation for it. Nothing happened to the samples between $18/4$ and $24/4$, except for sitting on a counter top. Moreover, the 2 samples were directly next to each other, so any ambient effects such as temperature should have effected both equally. The J19 sample does not show any change in the same time period, so if there is some damage or similar effect it would have to have happened to J17 alone. More than 12 microscope images were taken of each sample before and after the thermal annealing, and the entire surface of each wafer was checked for damage.

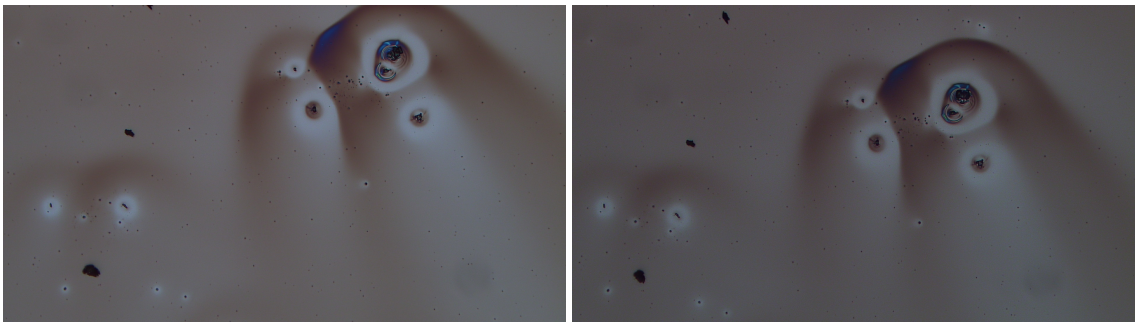

Figure 5.22: Microscope images of the surface of wafer J19, showing some artefacts which have distorted the film surface slightly. The image on the left is from before thermal annealing, and the image on the right is from after thermal annealing.

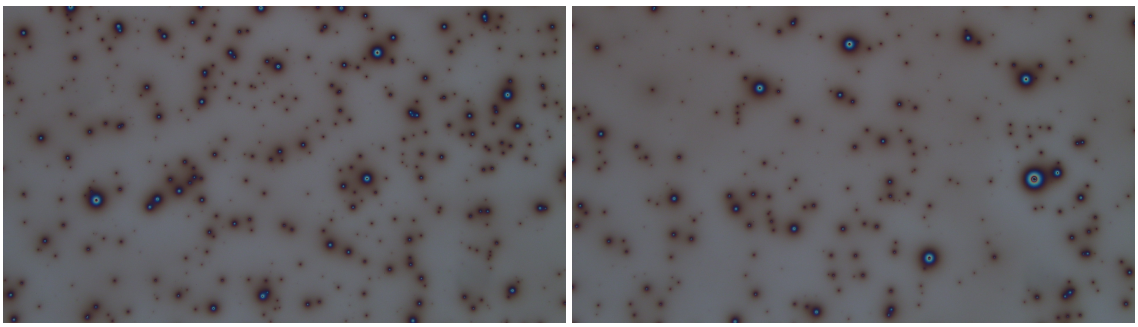

Figure 5.23: Microscope images of the surface of wafer J17, showing some artefacts which have distorted the film surface slightly. This is pretty typical for a wafer which has already been solvent vapor annealed. The image on the left is from before thermal annealing, and the image on the right is from after thermal annealing.

While some small damage, or at least surface defects are visible, nothing in the images accounts for the film thickness decrease. Lastly, after the thermal annealing, the thickness of J17 seems to return to its initial thickness from the previous week. It is unlikely that the thermal annealing would have 'healed' any damage that J17 may have sustained, and this is certainly not suggested in the microscope images.

Returning to the proposed explanations for the hysteresis, the thermal annealing test shows that the dry film hysteresis from the SVA tests is not removed, (and not appreciably diminished) by the vacuum oven. J19 shows just the same discrepancy between initial and final thickness as J17, despite having been thermally annealed prior to the solvent annealing. This means it is unlikely that the film had been vertically contracted due to tension stress during spin coating. Additionally, the explanation involving solvent trapped in the polymer film does not explain the results. Trapped solvent would have been released in the vacuum oven and removed, and this would suggest J17 should have shrunk to a smaller thickness after the thermal annealing; the data shows the opposite of this.

Careful readers will already have noticed an apparent flaw in my methodology: The thermal

annealing vacuum chamber was only raised to 80°C, while the glass transition temperature for Polystyrene is 100°C. It may then be reasoned that the polymer film never reached a rubbery state, so it is not expected to have any change. I think I agree with this critique, because I don't even see any small hints of de-wetting in the microscope images of J19. If the film had been rubberized even slightly, I think the film surface around the defects in Figure 5.22 would have begun to de-wet. However, I will provide a small defense for my choice of annealing temperature: the J19 sample clearly had a more distinct glass transition (seen in Figure 5.19), so the thermal annealing definitely had an effect on the thin film. But whatever effect it had was erased by SVA, because the film once again was retaining excess solvent. But yes, this critique might be valid, and unfortunately the time limitations for this project does not allow for me to conduct additional thermal annealing tests to investigate that.

5.8 Variation of Index of Refraction

The optical properties of any media are subject to change as its chemical composition is changed. This applies to 2 of the media during SVA: the flowing Nitrogen gas and the Polymer Thin Film, both of which have varying solvent content. Testing has been performed to determine if either of these materials have significant changes to their indexes of refraction as a result of the diffused solvent.

The polystyrene and toluene have somewhat similar indexes of refraction, as shown in Figure 5.24, which plots the single term Sellmeier model of their chromatic dispersion. To approximate the changes in the index of refraction of the thin film, a simple weighted average of the Sellmeier parameter A will suffice. The weights are determined by their respective weight percentage of each substance. The two substances have very similar Sellmeier parameter B, so I just use a common value of 0.02 for the approximation. Equation 5.7 shows the formulation for calculating the index of refraction for a mixture with a swelling ratio of SR.

$$n^2 = 1 + \left(\frac{\lambda^2}{\lambda^2 - 0.02}\right)\left(\frac{1.1748(SR) + 0.2687}{SR}\right) \tag{5.7}$$

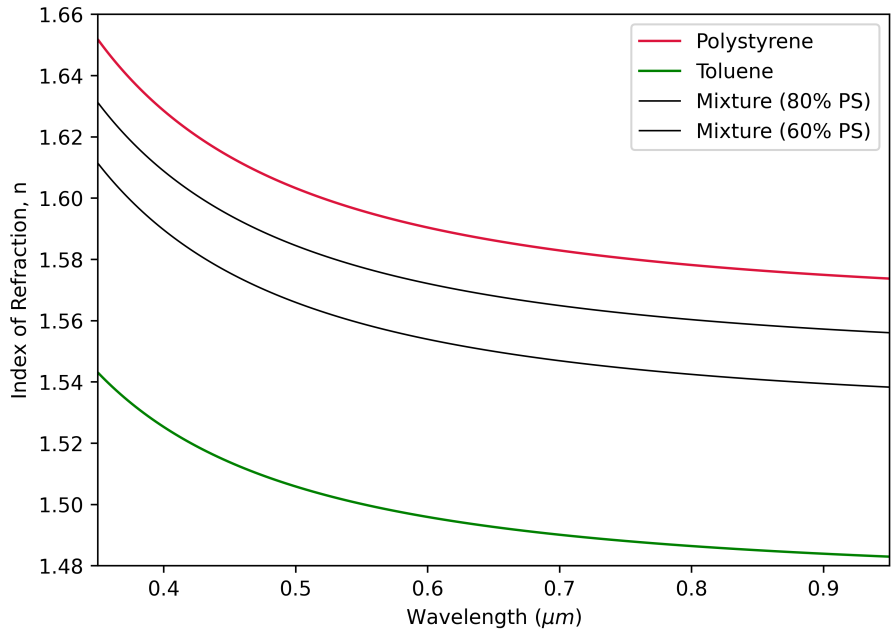

Figure 5.24: Plot of single term Sellmeier model of Chromatic dispersion of Polystyrene and Toluene. Also included are 2 examples of the responsive index of refraction functions, meant to approximate the dispersion of the thin film as it swells.

I will use the term "Responsive refraction index" to refer to this method of updating the index of refraction as the thin film swells. I have applied this to the SVA data obtained from sample J20 (PS 6000 kg/mol). The result can be seen in Figure 5.25, and the responsive refraction index clearly results in an increase in the fitted values of the swelling ratio.

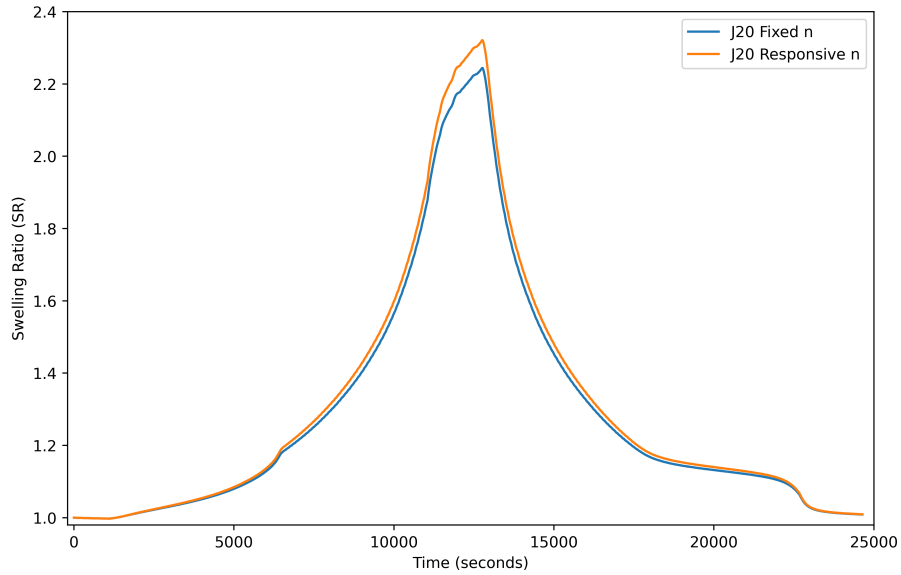

Figure 5.25: Plots of Swelling Ratio from SVA of sample J20, (PS 6000kg/mol), for both the fixed and the responsive Sellmeier models of index of refraction.

More importantly, the fitness parameter determining the accuracy of the fit (Sum of Squared Residuals between the reflectance data and reflectance model), is significantly improved for the Responsive refraction index method. The fitness parameters are plotted in Figure 5.26 below. With the fixed Sellmeier model of index of refraction, the fitness parameter increases each time that a new maxima/minima is present in the reflectance ratio curve. (The reason for this is explained in Section 4.1.) The responsive refraction index method actually improves the fit behavior as the film swells.

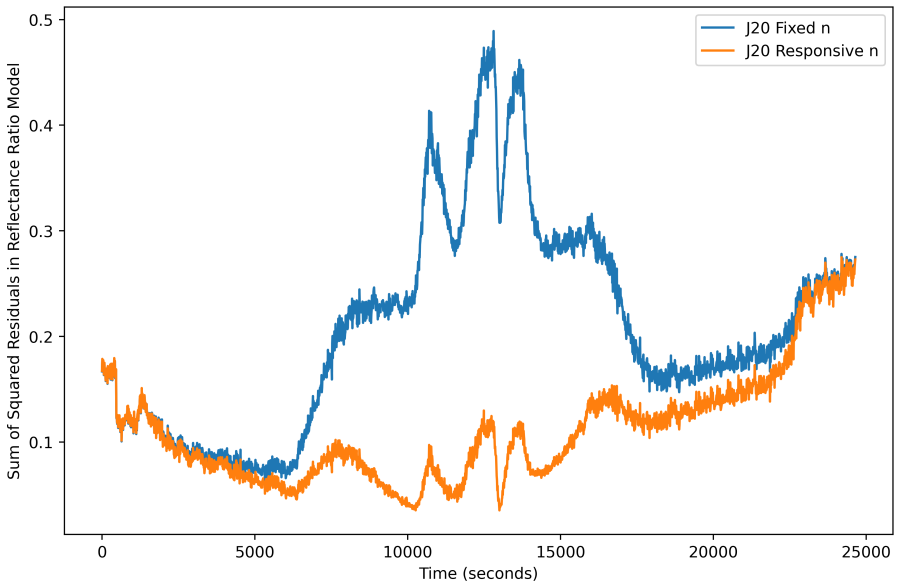

Figure 5.26: Plots of fitness parameter (sum of squared residuals from the reflectance ratio measurement and model) from SVA of sample J20, (PS 6000kg/mol), for both the fixed and the responsive Sellmeier models of index of refraction.

This is a great result in favor of implementing the Responsive Refraction Index method for all SVA data. Even a simplistic, weighted average implementation of variable index of refraction is able to improve the goodness of fit by a significant factor. I strongly encourage future researchers to use responsive r.i. fitting exclusively. At this point in the report, for the sake of readability and time constraints, I will not able to replace the previously analyzed data with this new fitting method. While this likely means that the real swelling ratios of the SVA tests are slightly larger than I have listed, the improvement in the fitting accuracy is slight, and I am certain that I have not missed any of the significant swelling behavior.

Now let's turn our attention to the variable index of refraction of the N_2 gas which carries the solvent vapor. Below are two plots of the reflectance ratio measured during an SVA test. In this test the sample was a blank wafer, with no polymer film. As the SVA progresses, there is no film for the solvent vapor to adsorb into, and the only reason for the reflectance to change is from the varying solvent content in the carrier gas. The model expects a reflectance ratio of 1, because the reference wafer and the sample wafer are identical. However, if the index of refraction of the

carrier gas changes, then the reflected light will be less.

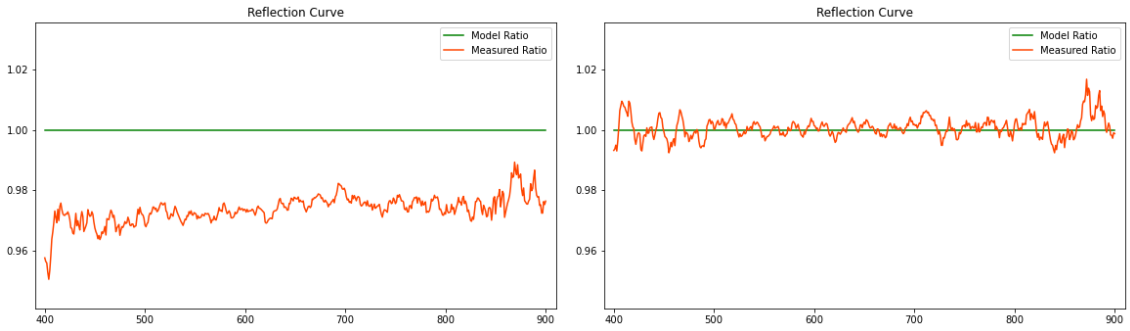

Figure 5.27: Plots of the reflectance ratio during SVA of a blank wafer. On the left, the reflectance ratio at maximum solvent concentration. On the right, the reflectance ratio after the SVA chamber has been quenched. The horizontal axis the wavelength measured by the spectrometer. The green line is the expectation of the model: a constant value of 1

Figure 5.27 shows that the reflected light was reduced by about 2 percent at the maximum solvent concentration. Once the chamber begins to quench, the reflectance ratio immediately returns to the the model prediction. A fitting procedure was made to estimate the index of refraction of the gas, and the result is shown in Figure 5.28 below. The estimated index of refraction is clearly changing, but not with linear correlation to the Absorbance. The index of refraction increases to a maximum of 1.025.

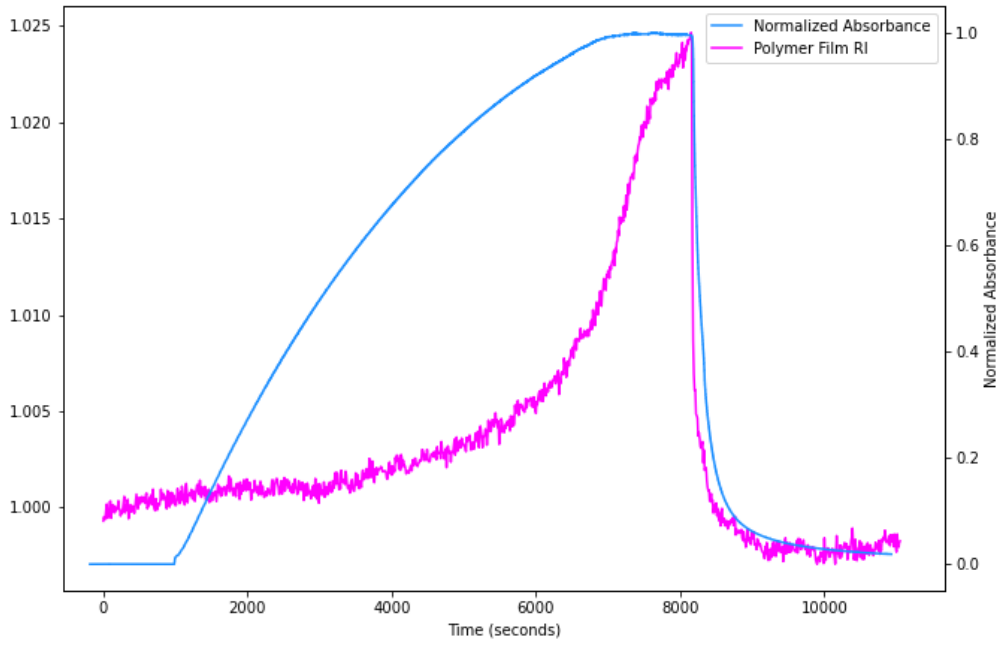

Figure 5.28: Plot of the fitted values for the index of refraction of the carrier gas (purple), and the Normalized Absorbance (blue). Please Notice: the legend says Polymer R.I., but is meant to say ”Gas refractive index”. The left vertical axis shows the values for the changing index of refraction

Intuition would say that the index of refraction for the gas should be linearly correlated to the volume fraction of solvent present. For gasses with diffused dielectric molecules, the usual method of calculation of index of refraction is the Lorentz Lorentz equation (Equation 5.8), but for small densities this is approximately a linear relationship [Wanstall et al., 2020].

$$\frac{n^2 - 1}{n^2 + 2} = K\rho \tag{5.8}$$

The results from the test of the blank wafer SVA suggest that the index of refraction of the gas has increased by 2.5%, which is a significant, but not an alarming amount. However, the non-linear dependence between the value of n and the absorbance is really surprising.

The change in the value of the index of refraction is small enough that, on its own, it will not have a very large impact on the outcome of other testing. But I think that the strange very large increase in n over such a small change in solvent concentration is hinting at something else occurring inside the SVA chamber which is not accounted for. For instance, if an small amount of solvent condenses either on the wafer surface, or alternatively on the illumination window of the optical path, then the reflectance would certainly be affected.

My best guess about this is that small dust particles or other defects on the wafer surface serve as nucleation sites for growth of small droplets of solvent. The droplets aren't able to cover the wafer because of the surface energy requirements, but can still form small droplets which surround these pieces of dust. At maximum size, these droplets reduce the the reflected light intensity by 1 or 2 percent. On a blank wafer, the solvent forms small droplet and goes no further, and when the gas is quenched of solvent vapor the droplets dissipate entirely. In wafers with a film however, these nucleation sites eventually collect enough solvent that the nearby polymer is de-wetted from the wafer surface. De-wetting is dealt with is Section 6.3, and includes some microscope images

6 Discussion

A few topics from this report deserve additional discussion.

6.1 Flory Huggins

With the Flory-Huggins estimations, it was clear that with the 2 free parameters that I added to Equation 5.5, the predicted swelling/deswelling curves still deviated from the SVA data. I have tried to add an additional third free parameter in a few different ways to improve this fitness. Usually, the result was a large deviation between the swelling and de-swelling predictions, which seems completely non-physical.

One of the parameters that I tried implementing was a sort of 'packing fraction', which scales the SR variable. With this additional parameter, the prediction and the SVA data have almost no deviation at all. However, the packing fraction for the swelling curve was 0.709, while for the de-swelling curve was 0.741. This is a nearly 5% difference in packing fraction, for the same sample, in the same state, barely an hour apart. I cant think of a reason for this difference in parameter besides noise/improper correlation of the SVA data. Rather than being an actual effect of the physics, it seems like the value of the parameter is being chosen based on inconsistencies in the measurement system. Additionally, if the interpretation of this parameter is as a 'packing fraction', surely it should depend on the volume fraction of the constituent particles, rather than be a fixed value for a polymer melt of arbitrary solvent volume fraction. Any physical interpretation of this parameter would suggest it should not be a single fixed value throughout the SVA. As a side-note, those values are quite close to the packing fractions for Cubic Close Packing (CCP) and Hexagonal Close Packing (HCP), but I can only image that is coincidental.

I think that including a scaling parameter for the Swelling Ratio is likely the most correct method for obtaining better agreement between the FH prediction and the SVA data. However, I can't meaningfully study the parameter dependence on the molar mass of the polymer, or initial thickness, without a physical reasoning for its independence on solvent volume fraction. Instead, if this is a real phenomena, it should be studied as a bulk-matter property of the polymer and solvent, and included as a the FH equation in a more intricate manner. I chose not to include any such scaling parameter for SR in this project for 2 reasons. First, I am worried about providing the model with too many degrees of freedom, such that tiny changes in the data result in large changes in the parameters. And second, the physical interpretation of the parameter as packing fraction suggests a more complex relationship than simple linear scaling.

6.2 Data Collection and Equipment

A frequent problem in several aspects of the SVA tests is that the data collection is not centralized. Because each device has been developed separately, it makes sense that the need to work independently. But aggregating the data, and re-synchronizing the data sets is not only tedious but it leads to a lot of errors and uncertainty in measurement results. Future researchers should make attempts to collect data from each piece of equipment simultaneously. This would avoid timing errors.

6.3 De-Wetting and Surface Energy

The polymer thin-films are bound to the silicon wafer substrate, generally remain that way even when in a rubbery state because the surface energy of the wafer is high, and the polymer prefers a 'wetted' configuration. However, given enough mobility the polymers can begin to move and form clumps which minimize surface area. This de-wetting process is complicated and rather slow, (just like most other polymer dynamics).

Because de-wetting is not a central part of the investigation of the project, I will only briefly mention some of the observations I have made over the course of the SVA tests.

The nucleation and growth of the de-wetting sections of the film almost always have internal patterning with some regular spacing. This is seen in Figure 6.1, where the film is seen in dark blue, and the de-wetting ring has been halted in its expansion by quenching the solvent from the film. This article by Lin Xiu, suggests that the growth rate of the de-wetting regions depends on the molar mass of the polymers [Xu et al., 2008]. This makes sense because the molar mass determines the viscosity, and the growth of these rings must depend on the polymer viscosity. An interesting point for future research would be to investigate further regarding the internal (and external) pattern structures of the rings.

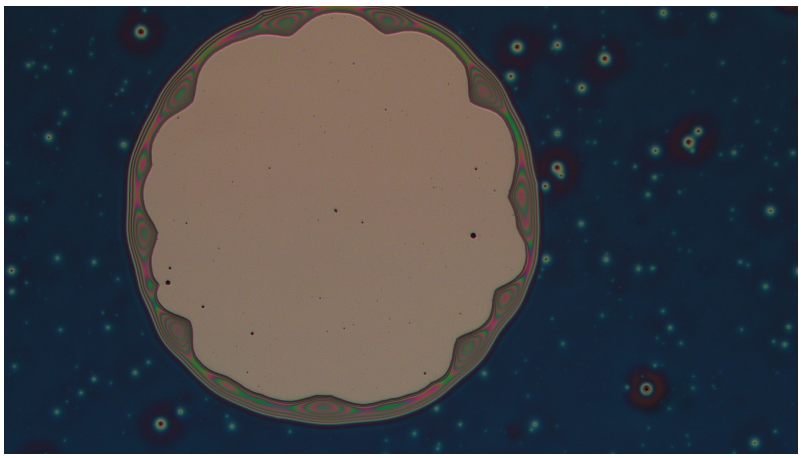

Figure 6.1: Figure showing de-wetting site, centered on a small defect in the surface. This is evidence that the surface energy of the substrate plays a role in initiating de-wetting.

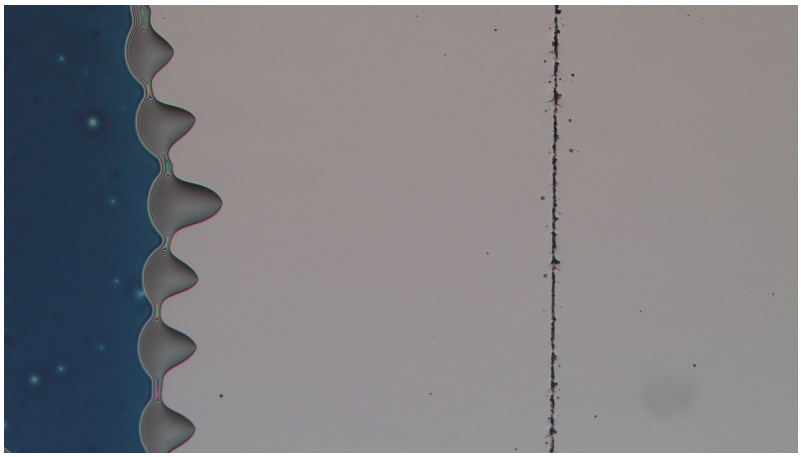

Figure 6.2: Figure showing a nearly linear de-wetting which is emanating from a scoring mark for dicing. In this image the de-wetting front extends both into the film and back over the substrate.

Figure 6.3: Figure showing a blob of de-wetted polymer, with strange shape. If given the mobility, the polymer would continue to break up into smaller (rounder) pieces.

Figure 6.4 show a stunning piece of interrupted de-wetting. The left side of the polymer has nearly completely de-wet, but the right side remains intact. Because the illumination of the wafer was slightly offset to the right, I did not even notice the de-wetting until the SVA was finished and I was removing the wafer from the chamber. I am not sure what caused this to happen. The solvent concentration is well dispersed within the SVA chamber. The only explanation that I can come up with is that the wafer was made partially dirty before spin coating. Possibly a spray of dust from a certain angle, which fell only onto one half of the wafer. Study of this sample, or others like it may help to uncover clever methods for keeping the thin films wetted.

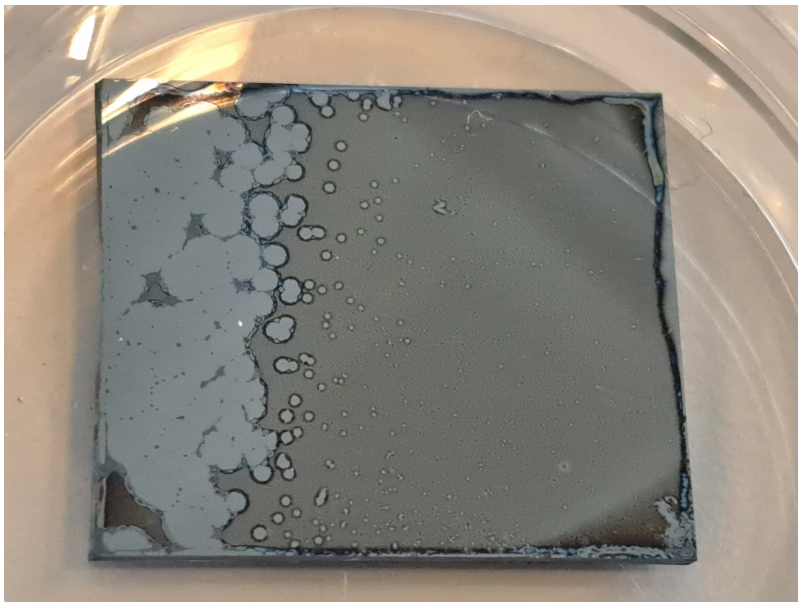

Figure 6.4: Figure showing a polymer wafer with directional de-wetting.

Lastly, I wanted to include this image of a wafer that had almost completely de-wetted. The angle of the illumination makes it east to see the thickness of the de-wetted rings. The silicon substrate is perfectly bare, and the edges of the de-wetting rings tower above the nano-meter thick film.

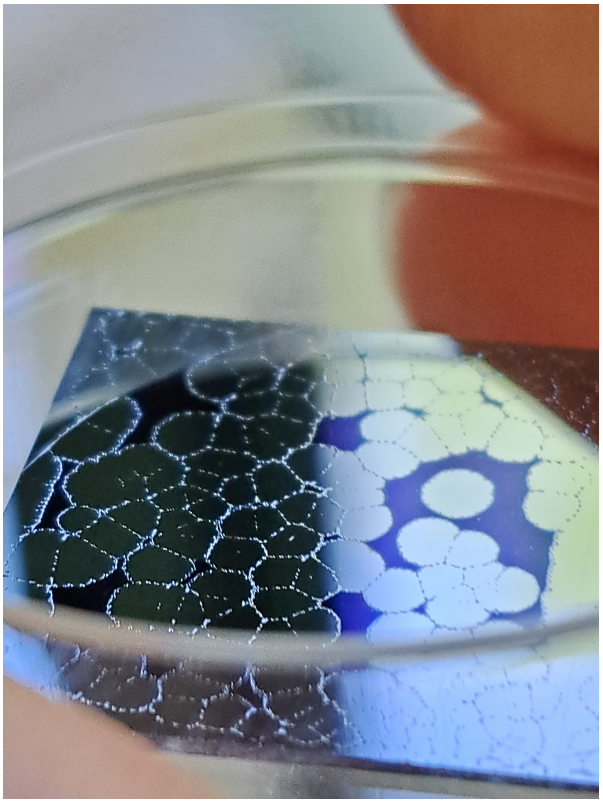

Figure 6.5: Figure showing a polymer wafer with a several de-wetting locations.

7 Conclusion

The use of smaller increments of solvent vapor concentration in SVA provided better understanding of the thickness response variation. Critical features of the SVA process like the Glass Transition and the extended de-swelling hysteresis are able to be characterized for any thin film. Also, the ability to anticipate and prevent de-wetting from destroying large parts of the film was discovered. Distinguishing these features reliably was a challenge both procedurally, and also in terms of the fitting procedure. Many variations of modelling functions were attempted to try to improve the accuracy of the thickness fitting. However, the role of the Silicon Oxide layer is still not well determined.

The Fresnel reflectance equations for multi-layer thin films can be challenging to make reliable. Due to the wide range of thicknesses of films, some have a very different dependence on the silicon oxide layer thickness than others. With the Responsive index of refraction method, a much closer agreement between the model and measured reflectance ratios is achieved. The improvement was shown to decrease the RSS value by a factor of 4, and is demonstrated over an equally large range of thicknesses. Additional improvements might yet be made with the data collected on the carrier gas index of refraction. Although the result was surprising in its form, there is a definite change in the reflected intensity of light at maximum solvent concentration. From the data collected, this has been quantified as an increase of 2.5% to the index of refraction. Additional study of this value and the apparently non-linear dependence on solvent concentration is needed before it is recommended for fitting procedures.

The Flory Huggins model of polymer melts showed only qualitative agreement with the measured SVA data. Attempts to use free parameters to match the F-H predictions to the data had limited success. The dependence on the bubbler efficiency is recognized, and the parameter of 90% efficiency roughly agrees with the relationship found in Section 5.5 regarding depletion of the solvent within the bubbler tank. The parameter for hole volume estimated more than 10% of the thin film is free space, and this result seems quite high but still possible. Even with these parameters, the agreement of the F-H model with measured SVA data is tenuous. The parameters estimated in this project are not corroborated by additional data, and should be reconsidered. The best agreement seems to come from implementing a scale parameter for the Swelling Ratio, but a realistic physical interpretation of this parameter is not obvious.

The glass transition temperature is a bulk property of the polymer, and this suggests that it should not depend on the quantity of polymer present (i.e. the initial thickness of the thin film). However, it was thought that especially thick or thin films might be impacted by the interaction energies of the substrate and air interface in such a way that the glass transition was shifted. From the data seen in Figure 5.8, and Table 5.3, there does not appear to be any correlation between film thickness and the swelling ratio at the point of Glass Transition.

The glass transition based on molar mass of the polymer is shown to agree with the theoretical

values provided by the Fox equation. Again, the constraint of the polymers to a thin film could possibly induce chain entanglement, which would be thought to increase the temperature of the glass transition [Wang et al., 2021]. From the data collected in Table 5.5, and presented in Figure 5.11, there are no outliers and all data seems to agree nicely with the Fox Equation.

References

Abiad, M., Carvajal, M., & Campanella, O. (2009). A review on methods and theories to describe the glass transition phenomenon: Applications in food and pharmaceutical products. *Food Engineering Reviews*, *1*, 105–132. https://doi.org/10.1007/s12393-009-9009-1

Alvarez-Fernandez, A., Cummins, C., Saba, M., Steiner, U., Fleury, G., Ponsinet, V., & Guldin, S. (2021). Block copolymer directed metamaterials and metasurfaces for novel optical devices. *Advanced Optical Materials*, *9*(16), 2100175. https://doi.org/https://doi.org/10.1002/adom.202100175

Angell, C. A., Sare, J. M., & Sare, E. J. (1978). Glass transition temperatures for simple molecular liquids and their binary solutions. *The Journal of Physical Chemistry*, *82*, 2622–2629.

Beer. (1852). Bestimmung der absorption des rothen lichts in farbigen flüssigkeiten. *Annalen der Physik*, *162*(5), 78–88. https://doi.org/https://doi.org/10.1002/andp.18521620505

Bhadauriya, S., Wang, X., Pitliya, P., Zhang, J., Raghavan, D., Bockstaller, M. R., Stafford, C. M., Douglas, J. F., & Karim, A. (2018). Tuning the relaxation of nanopatterned polymer films with polymer-grafted nanoparticles: Observation of entropy–enthalpy compensation [PMID: 30398875]. *Nano Letters*, *18*(12), 7441–7447. https://doi.org/10.1021/acs.nanolett.8b02514

Brandrup, J., Immergut, E. H., & Grulke, E. A. (1999). *Polymer handbook* (4th ed). Wiley.

Castel, A., Gutfreund, P., Cabane, B., & Rharbi, Y. (2020). Swelling, dewetting and breakup in thin polymer films for cultural heritage. *Soft Matter*, *16*, 1485–1497. https://doi.org/10.1039/C9SM01976F

Ciddor, P. E. (1996). Refractive index of air: New equations for the visible and near infrared. *Appl. Opt.*, *35*(9), 1566–1573. https://doi.org/10.1364/AO.35.001566

Cummins, C., Lundy, R., Walsh, J. J., Ponsinet, V., Fleury, G., & Morris, M. A. (2020). Enabling future nanomanufacturing through block copolymer self-assembly: A review. *Nano Today*, *35*, 100936. https://doi.org/https://doi.org/10.1016/j.nantod.2020.100936

Efremov, M. Y., & Nealey, P. F. (2022). Residual changes and thickness effects in glass-forming polymer thin films after solvent vapor annealing. *Polymer*, *238*, 124417. https://doi.org/https://doi.org/10.1016/j.polymer.2021.124417

Emad, N., El-Hiti, G. A., Yousif, E., & Kariuki, B. M. (2023). Metal oxide nanoparticles containing clotrimazole to suppress photodegradation of poly(vinyl chloride) thin films. *Polymers*, *15*(7). https://doi.org/10.3390/polym15071632

Flory, P. J. (1953). *Principles of polymer chemistry*. Ithaca : Cornell University Press, 1953. https://search.library.wisc.edu/catalog/999474843502121

Fox, T. G., & Loshaek, S. (1955). Influence of molecular weight and degree of crosslinking on the specific volume and glass temperature of polymers. *Journal of Polymer Science*, *15*(80), 371–390. https://doi.org/https://doi.org/10.1002/pol.1955.120158006

Gao, L., Lemarchand, F., & Lequime, M. (2013). Refractive index determination of sio2 layer in the uv/vis/nir range: Spectrophotometric reverse engineering on single and bi-layer designs. *Journal of the European Optical Society - Rapid publications*, *8*(0). https://www.jeos.org/index.php/jeos_rp/article/view/13010

Ghori, M. U., & Conway, B. R. (2015). Hydrophilic matrices for oral control drug delivery. *American Journal of Pharmacological Sciences*, *3*(5), 103–109. https://doi.org/10.12691/ajps-3-5-1

Hinze, G., Sillescu, H., & Fujara, F. (1995). Anisotropic motion of toluene above and below the glass transition studied by 2h nmr. *Chemical Physics Letters*, *232*(1), 154–158. https://doi.org/https://doi.org/10.1016/0009-2614(94)01322-M

Hulkkonen, H., Salminen, T., & Niemi, T. (2019). Automated solvent vapor annealing with nanometer scale control of film swelling for block copolymer thin films. *Soft Matter*, *15*, 7909–7917. https://doi.org/10.1039/C9SM01322A

Immergut, E. H., & Mark, H. F. (1965). Principles of plasticization. In *<bold>plasticization</bold> and plasticizer processes* (pp. 1–26). https://doi.org/10.1021/ba-1965-0048.ch001

Karlsson, O., Stubbs, J., Karlsson, L., & Sundberg, D. (2001). Estimating diffusion coefficients for small molecules in polymers and polymer solutions. *Polymer*, *42*(11), 4915–4923. https://doi.org/https://doi.org/10.1016/S0032-3861(00)00765-5

Kedenburg, S., Vieweg, M., Gissibl, T., & Giessen, H. (2012). Linear refractive index and absorption measurements of nonlinear optical liquids in the visible and near-infrared spectral region. *Opt. Mater. Express*, *2*(11), 1588–1611. https://doi.org/10.1364/OME.2.001588

Kim, H.-C., Park, S.-M., & Hinsberg, W. D. (2010). Block copolymer based nanostructures: Materials, processes, and applications to electronics [PMID: 19950962]. *Chemical Reviews*, *110*(1), 146–177. https://doi.org/10.1021/cr900159v

Laschitsch, A., Bouchard, C., Habicht, J., Schimmel, M., Rühe, J., & Johannsmann, D. (1999). Thickness dependence of the solvent-induced glass transition in polymer brushes. *Macromolecules*, *32*(4), 1244–1251. https://doi.org/10.1021/ma980743t

Lee, J., & Jin, J. (2022). A novel method to design and evaluate artificial neural network for thin film thickness measurement traceable to the length standard. *Scientific Reports*, *12*(1), 2212. https://doi.org/10.1038/s41598-022-06247-y

Li, H., & Xiao, R. (2021). Glass transition behavior of wet polymers. *Materials*, *14*(4). https://doi.org/10.3390/ma14040730

Lin, H.-M., & Nash, R. A. (1993). An experimental method for determining the hildebrand solubility parameter of organic nonelectrolytes. *Journal of Pharmaceutical Sciences*, *82*(10), 1018–1026. https://doi.org/https://doi.org/10.1002/jps.2600821001

Mark, J. E. (2007). *Physical properties of polymers handbook [electronic resource]* (2nd ed. 2007.). Springer New York. https://doi.org/10.1007/978-0-387-69002-5

Minco Products, Inc. (n.d.). *Polyimide Thermofoil - Minco*. Retrieved May 28, 2023, from https://www.minco.com/products/flexible-heaters/polyimide-thermofoil/

Miyazaki, H. (2010). Refractive index and dielectric constant of siox films deposited by reactive sputtering. *Physics and Chemistry of Glasses - European Journal of Glass Science and Technology Part B*, *51*.

Nelson, G., Drapes, C. S., Grant, M. A., Gnabasik, R., Wong, J., & Baruth, A. (2018). High-precision solvent vapor annealing for block copolymer thin films. *Micromachines*, *9*(6). https://doi.org/10.3390/mi9060271

Nistane, J., Chen, L., Lee, Y., Lively, R., & Ramprasad, R. (2022). Estimation of the flory-huggins interaction parameter of polymer-solvent mixtures using machine learning. *MRS Communications*, *12*(6), 1096–1102. https://doi.org/10.1557/s43579-022-00237-x

Ocean Insight. (n.d.). *Spectrometers | Ocean Insight*. Retrieved May 28, 2023, from https://www.oceaninsight.com/products/spectrometers/

Plastic Technology. (n.d.). *Interaction Parameter*. Retrieved May 30, 2023, from https://polymerdatabase.com/polymer

Polyanskiy, M. N. (n.d.). *Refractive index database*. Retrieved May 27, 2023, from https://refractiveindex.info

Polymer Source, Inc. (n.d.). *Polystyrene, Certified Reference Material*. Retrieved May 22, 2023, from https://www.polymersource.ca/index.php?route=product/category&path=2543_2544&category=catalogA&subtract=1&categorystart=B-4

Salazar, D., Soto-Molina, R., Lizarraga-Medina, E., Felix, M., Radnev, N., & Márquez, H. (2016). Ellipsometric study of siox thin films by thermal evaporation. *Open Journal of Inorganic Chemistry*, *6*, 8.

Schinke, C., Christian Peest, P., Schmidt, J., Brendel, R., Bothe, K., Vogt, M. R., Kröger, I., Winter, S., Schirmacher, A., Lim, S., Nguyen, H. T., & MacDonald, D. (2015). Uncertainty analysis for the coefficient of band-to-band absorption of crystalline silicon [067168]. *AIP Advances*, *5*(6). https://doi.org/10.1063/1.4923379

Sheehan, C. J., & Bisio, A. L. (1966). Polymer/Solvent Interaction Parameters. *Rubber Chemistry and Technology*, *39*(1), 149–192. https://doi.org/10.5254/1.3544827

Singh, M. K., Hu, M., Cang, Y., Hsu, H.-P., Therien-Aubin, H., Koynov, K., Fytas, G., Landfester, K., & Kremer, K. (2020). Glass transition of disentangled and entangled polymer melts: Single-chain-nanoparticles approach [PMID: 32921812]. *Macromolecules*, *53*(17), 7312–7321. https://doi.org/10.1021/acs.macromol.0c00550

Sultanova, N., Kasarova, S., & Nikolov, I. (2009). Dispersion properties of optical polymers. *ACTA PHYSICA POLONICA A*, *116*, 585–587. https://doi.org/10.12693/APhysPolA.116.585

Venkatram, S., Kim, C., Chandrasekaran, A., & Ramprasad, R. (2019). Critical assessment of the hildebrand and hansen solubility parameters for polymers. *Journal of Chemical Information and Modeling*, *59*(10), 4188–4194. https://doi.org/10.1021/acs.jcim.9b00656

Wang, F., Jiang, Z., Lin, X., Zhang, C., Tanaka, K., Zuo, B., Zhang, W., & Wang, X. (2021). Suppressed chain entanglement induced by thickness of ultrathin polystyrene films. *Macromolecules*, *54*(8), 3735–3743. https://doi.org/10.1021/acs.macromol.1c00224

Wanstall, C. T., Agrawal, A. K., & Bittle, J. A. (2020). Implications of real-gas behavior on refractive index calculations for optical diagnostics of fuel–air mixing at high pressures. *Combustion and Flame*, *214*, 47–56. https://doi.org/https://doi.org/10.1016/j.combustflame.2019.12.023

Xu, L., Shi, T., & An, L. (2008). The dewetting dynamics of the polymer thin film by solvent annealing [044904]. *The Journal of Chemical Physics*, *129*(4). https://doi.org/10.1063/1.2918734

Yang, G. G., Choi, H. J., Han, K. H., Kim, J. H., Lee, C. W., Jung, E. I., Jin, H. M., & Kim, S. O. (2022). Block copolymer nanopatterning for nonsemiconductor device applications [PMID: 35230079]. *ACS Applied Materials & Interfaces*, *14*(10), 12011–12037. https://doi.org/10.1021/acsami.1c22836

Yoshioka, A., & Tashiro, K. (2003). Solvent effect on the glass transition temperature of syndiotactic polystyrene viewed from time-resolved measurements of infrared spectra at the various temperatures and its simulation by molecular dynamics calculation. *Macromolecules*, *37*. https://doi.org/10.1021/ma035505z

Zha, H., Wang, Q., Wang, X., Cangialosi, D., & Zuo, B. (2021). Enhanced free surface mobility facilitates the release of free-volume holes in thin-film polymer glasses. *Macromolecules*, *54*(4), 2022–2028. https://doi.org/10.1021/acs.macromol.0c02887

Zhang, X., Qiu, J., Li, X., Zhao, J., & Liu, L. H. (2020). Complex refractive indices measurements of polymers in visible and near-infrared bands. *Applied Optics*, *59*. https://doi.org/10.1364/AO.383831

Appendix A Flow Scripts

```
[Generator]
Application=FlowPlot
Version=V3.34
[Script]
Repeat=1
SendSetpointAfter=false
001="1000.0; 50.0;  1;  9"
002="1.0;    49.5;  1;  9"
003="100.0;  01.0;  3;  9"
004="1.0;    49.0;  1;  9"
005="100.0;  02.0;  3;  9"
006="1.0;    48.5;  1;  9"

....

195="100.0;  97.0;  3;  9"
196="1.0;    01.0;  1;  9"
197="100.0;  98.0;  3;  9"
198="1.0;    00.5;  1;  9"
199="100.0;  99.0;  3;  9"
200="1.0;    00.0;  1;  9"
201="1500.0; 100.0; 3;  9"
202="1.0;    00.5;  1;  9"
203="100.0;  99.0;  3;  9"
204="1.0;    01.0;  1;  9"
205="100.0;  98.0;  3;  9"
206="1.0;    01.5;  1;  9"

....

396="1.0;    49.0;  1;  9"
397="100.0;  02.0;  3;  9"
398="1.0;    49.5;  1;  9"
399="100.0;  01.0;  3;  9"
400="1.0;    50.0;  1;  9"
401="1500.0; 00.0;  3;  9"
```

Appendix B Code for Fitting Methods

```
def reflection(n1,n2):
    num = n1 - n2
    den = n2 + n1
    r = num/den
    return r

def reflection_Cauchy(n1,n2):
    # Here, n1 and n2 are lists corresponding to the r.i. at each wavelength
    r = np.zeros(len(n1))
    for i in range(len(n1)):
        num = n1[i] - n2[i]
        den = n1[i] + n2[i]
        r[i] = num/den
    return r

def phase(d,N,Lambda):
    # Also a cosine term here, which is assumed to be 1 for normal incidence
    # Could be interesting to investigate slight deviations from normal.
    beta = 2*np.pi*d*N/Lambda
    return beta

def fresnel_reflection(Lambdas,N,D):
    # N is array (read: list) of refractive indices (complex) ordered as n1,n2,n3,...
    # D is array (read: list) of layer thickness ordered as d2,d3,...
    # d1 is assumed to be infinite (ambient), and n1 is usually 1. (Air)
    # In all cases, n1 must be real (no absorption).
    # final layer is assumed infinite thickness (complete absorption)
    # Therefore, len(N) = len(D) + 2
    # Minimum is 3 layer model (air, thin-layer, substrate)
    # Lambdas is either wavelength or range of wavelengths. (Same units as thickness)
    r_interfaces = np.zeros(len(N)-1,dtype=np.cdouble)
    betas = np.zeros([len(D),len(Lambdas)],dtype=np.cdouble)
    r_interfaces[0] = reflection(N[0],N[1])
    for i in range(len(N)-2):
        r_interfaces[i+1] = reflection(N[i+1],N[i+2])
        betas[i,:] = phase(D[i],N[i+1],Lambdas)
        # Note that index 0 of 'betas'/'D' corresponds to the first layer thickness
```

```
    R = np.zeros(len(Lambdas),dtype=np.cdouble)
    R[:] = r_interfaces[-1]
    r_interfaces = r_interfaces[:-1]
    while len(r_interfaces)>0:
        R[:] = (r_interfaces[-1] + (R[:]*np.exp(-2j*betas[-1,:])))\
        /(1 + r_interfaces[-1]*R[:]*np.exp(-2j*betas[-1,:]))
        r_interfaces = r_interfaces[:-1]
        betas = betas[:-1,:]
    R = np.real_if_close(R*np.conj(R),tol=1000)
    return R

def Sellmeier_formula(coefficient_list, Lambdas):
    # first argument is list of Sellmeier coefficients, A and B
    # First order Sellmeier equation
    # Values for Lambdas are in nanometers, but coefficients assume micrometer
    Lambdas = Lambdas/1000
    A = float(coefficient_list[0])
    B = float(coefficient_list[1])
    N_squared = 1 + (A*np.square(Lambdas)/(np.square(Lambdas)-B))
    return np.sqrt(N_squared)

def fresnel_reflection_Cauchy(Lambdas, N, D):
    # N is array of refractive indices (complex) ordered as n1,n2,n3,...
    # each n is list of Cauchy Dispersion constants.
    # D is array (read: list) of layer thickness ordered as d2,d3,...
    # d1 is assumed to be infinite (ambient), and n1 is usually 1. (Air)
    # In all cases, n1 must be real (no absorption).
    # final layer is assumed infinite thickness (complete absorption)
    # Therefore, len(N) = len(D) + 2
    # Minimum is 3 layer model (air, thin-layer, substrate)
    # Lambdas is either wavelength or range of wavelengths. (Same units as thickness)
    all_r_i = np.zeros([len(N),len(Lambdas)],dtype=np.double)
    # This array will be the conversion of list coefficients to r.i. list by wavelength
    for i in range(len(N)):
        all_r_i[i,:] = Sellmeier_formula(N[i],Lambdas)
    r_interfaces = np.zeros([len(N)-1,len(Lambdas)],dtype=np.double)
    betas = np.zeros([len(D),len(Lambdas)],dtype=np.cdouble)
    r_interfaces[0] = reflection_Cauchy(all_r_i[0],all_r_i[1])
    for i in range(len(N)-2):
```

```
    r_interfaces[i+1] = reflection_Cauchy(all_r_i[i+1],all_r_i[i+2])
    betas[i,:] = phase(D[i],all_r_i[i+1],Lambdas)
    # Note that index 0 of 'betas'/'D' corresponds to the first layer thickness
R = np.zeros(len(Lambdas),dtype=np.cdouble)
R[:] = r_interfaces[-1]
r_interfaces = r_interfaces[:-1]
while len(r_interfaces)>0:
    R[:] = (r_interfaces[-1] + (R[:]*np.exp(-2j*betas[-1,:])))\
    /(1 + r_interfaces[-1]*R[:]*np.exp(-2j*betas[-1,:]))
    r_interfaces = r_interfaces[:-1]
    betas = betas[:-1,:]
R = np.real_if_close(R*np.conj(R),tol=1000)
R = np.real(R) # I want to remove the complex datatype
return R
```